Stony Brook University

Synaptic Vesicle Dynamics at Retinal Ribbon Synapses

A Dissertation Presented

by

Lisamarie LoGiudice

to

The Graduate School

in Partial Fulfillment of the

Requirements

for the Degree of

Doctor of Philosophy

in

Neuroscience

Stony Brook University

August 2009

Stony Brook University

The Graduate School

Lisamarie LoGiudice

We, the dissertation committee for the above candidate
for the Doctor of Philosophy degree, hereby recommend
acceptance of this dissertation.

Gary G. Matthews, Ph.D., Professor,
Department of Neurobiology and Behavior

Lonnie Wollmuth, Ph.D., Associate Professor,
Department of Neurobiology and Behavior

Stephen Yazulla, Ph.D., Professor,
Department of Neurobiology and Behavior

David Zenisek, Ph.D., Associate Professor,
Department of Cellular and Molecular Physiology, Yale School of Medicine

This dissertation is accepted by the Graduate School

Lawrence Martin
Dean of the Graduate School

Abstract of the Dissertation

Synaptic Vesicle Dynamics at Retinal Ribbon Synapses

by

Lisamarie LoGiudice

Doctor of Philosophy

in

Neuroscience

Stony Brook University

2009

Synaptic ribbons are vesicle-tethering organelles found at the active zones of sensory synapses in the visual, auditory and vestibular systems. Their close proximity to distinctive calcium channels, the reservoir of vesicles they immobilize pending release, and their spatial relationship with sites of compensatory retrieval are essential elements of the vesicle cycle at ribbon synapses.

Glutamate release from retinal bipolar terminals is driven by calcium influx through L-type calcium channels situated along docking sites beneath synaptic ribbons. Using single cell RT-PCR, we identified the pore-forming $\alpha 1$ subunits responsible for the unusual properties exhibited by the calcium channels at ribbon synapses. Our results indicate that ON-type goldfish bipolar cells express transcripts of $Ca_v1.3a$ and/or $Ca_v1.3b$. The endogenous expression of only one or both subunits in a single cell raises the possibility of functionally distinct classes of bipolar cells that differ in calcium current properties.

Since synaptic ribbons and calcium channels are tightly correlated in space, it is assumed that vesicles tethered to ribbons participate in neurotransmitter release. To determine if tethered vesicles are released, we tracked vesicles labeled with FM4-64 dye in mouse bipolar cells whose ribbons had been labeled with a fluorescent peptide with affinity to RIBEYE. We photobleached vesicles in regions with and without ribbons and then followed fluorescence recovery as bleached regions were repopulated by labeled vesicles.

Our results indicate that vesicles immobilized at synaptic ribbons participate in the readily releasable pool that is tapped rapidly during depolarization.

Exocytosis must be balanced by endocytosis to maintain neurotransmission. Previously, the location of compensatory retrieval and the mechanism(s) of membrane recovery in ribbon-containing neurons were uncertain. EM observations of clathrin-coated invaginations in rapidly fixed bipolar neurons, in conjunction with experiments employing a dynamin inhibitor, indicate that endocytosis occurs largely via a clathrin-mediated pathway in mouse bipolar cells. Furthermore, by labeling ribbons in cells exposed to FM4-64, we show that stimulus-triggered endocytosis occurs at "hot spots" that spatially coincide with fusion sites. We conclude that ribbon-type active zones, and their flanking membrane regions, serve as substrates for the exocytotic and endocytotic limbs of the vesicle cycle.

Table of Contents

List of Figures

Acknowledgements

I would like to express my sincere thanks to those who have supported me during my time at Stony Brook University. First, I would like to thank my advisor, Dr. Gary Matthews, for sharing with me his expertise and insight. He has been supportive and patient, and I will miss being a member of his laboratory. I would also like to thank George Zanazzi, Diane Henry-Vanisko, and Karen Wexler. Besides being indispensable to my academic success, they have become my great friends. I will miss each of them dearly. Furthermore, I would like to acknowledge the friends and faculty members that I have interacted with over the last several years. They have positively influenced my life, and will continue to do so for many years to come.

I would like to extend my gratitude to my committee members, Dr. Stephen Yazulla, Dr. Lonnie Wollmuth, and Dr. David Zenisek, for their helpful discussions and advice. I am indebted to Dr. Zenisek for the generous gift of the RIBEYE-binding peptide, without which much of this project would not have been possible. In addition, I would like to thank Dr. Peter Sterling and Dr. Jian Li from the University of Pennsylvania. Dr. Sterling's comments helped to elevate the quality of my work, and Dr. Li's electron microscopy expertise has been paramount to my studies.

Finally, I would like to thank my family and friends for their unwavering love and support. And to my husband, I dedicate this work. His faith in my decisions and venturesome spirit encourages me to carve a unique path.

The text of this dissertation in part is a reprint of the materials as it appears in:

LoGiudice, L., D. Henry, et al. (2006). "Identification of calcium channel alpha1 subunit mRNA expressed in retinal bipolar neurons." Molecular Vision **12**: 184-9.

LoGiudice, L. and G. Matthews (2007). "Endocytosis at ribbon synapses." Traffic **8**(9): 1123-8.

LoGiudice, L., P. Sterling, et al. (2008). "Mobility and turnover of vesicles at the synaptic ribbon." Journal of Neuroscience **28**(12): 3150-8.

LoGiudice, L. and G. Matthews (2009). "The role of ribbons at sensory synapses." Neuroscientist.

Chapter I
Introduction

The primary receptor cells of the visual, auditory, and vestibular systems generate graded changes in membrane potential in response to sensory stimuli. To faithfully transmit these signals, their synapses must be capable of releasing quanta of neurotransmitter at a high rate for sustained periods. The active zone of these specialized synapses bears an electron-dense structure called the synaptic ribbon, which positions an abundance of synaptic vesicles close to release sites, within nanometers of calcium channels and directly across from postsynaptic glutamate receptors (Matsubara et al., 1996; Morigiwa and Vardi, 1999; Khimich et al., 2005). This dissertation will focus on several aspects of the synaptic vesicle cycle in ribbon-containing retinal bipolar neurons. In particular, this work considers the function of synaptic ribbons in vesicle exocytosis, the identity of the calcium channels that drive release, and the location and mechanisms of compensatory vesicle retrieval.

Morphology of synaptic ribbons

Synaptic ribbons are proteinaceous organelles that are anchored to the plasma membrane at the active zone and extend into the cytoplasm, perpendicular to the membrane (Fig. 1A). In addition to the large cytoplasmic population of synaptic vesicles in the terminal, a sizeable pool of vesicles is tethered to the surface of the ribbon via fine filaments of unknown composition. Across cell types and species, ribbons are anatomically diverse, varying in size, shape, and capacity to tether vesicles (see Fig. 1). Photoreceptor ribbons (Fig. 1A,B) are typically planar, ~30 nm thick, and vertically extend ~200 nm into the cytoplasm. Their length, parallel to the membrane, can vary from 0.2–1.0 μm. In a typical cone terminal, ribbons tether ~3000 vesicles and dock ~600 at the plasma membrane (Sterling and Matthews, 2005). Rod photoreceptor ribbons, of which there is usually one per terminal, are crescent-shaped sheets that dock ~130

vesicles (green subset of vesicles in Fig. 1) and tether ~640 vesicles (Rao-Mirotznik et al., 1995). Like photoreceptors, the second-order bipolar cells of the retina produce graded changes in membrane potential and have ribbon synapses. Generally, photoreceptor ribbons tend to be larger and less numerous than bipolar cell synaptic ribbons, which appear as spheres or flattened ellipsoids and can tether ~110 vesicles. Hair-cell synaptic ribbons—also called dense bodies—are among the most morphologically diverse. Depending on the cell type, they range from ~0.1 to ~0.4 μm in length and can be ellipsoidal, plate-like, barrel-shaped, or spherical (e.g., Fig. 1C,D). Accordingly, their vesicle capacities are quite varied, with the smallest ribbon tethering 20 vesicles and the largest tethering up to 400 vesicles (Moser et al., 2006). In the chick cochlea, hair cell ribbons vary in size along the tonotopic axis, with cells in high-frequency regions having larger ribbons that tether more vesicles (Martinez-Dunst et al., 1997). Interestingly, synapses in many parts of arthropod nervous systems commonly have a T-shaped structure at the active zone (Prokop and Meinertzhagen, 2006; Fig. 1E,F), which may be similar in function to ribbons of vertebrate sensory synapses.

Molecular composition of the synaptic ribbon complex

The only known component exclusive to synaptic ribbons is RIBEYE, a protein composed of a novel N-terminal A-domain that is unique to ribbons and a C-terminal B-domain that is identical to all but the N-terminal 20 amino acids of the transcriptional co-repressor CtBP2 (Schmitz et al., 2000). RIBEYE self-assembles into complexes and accounts for most of the mass of the ribbon (Zenisek et al., 2004). Therefore, it is thought to form the structural backbone of the ribbon (Fig. 2A). Both A- and B-domains contain sites for RIBEYE-RIBEYE interactions that potentially construct and stabilize synaptic ribbons (Magupalli et al., 2008). In addition to RIBEYE, several proteins first identified as part of the cytomatrix at the active zone (CAZ) of conventional synapses are also present at ribbon synapses, including CtBP1 (Fig. 2B), RIM1 (Fig. 2C), RIM2, Bassoon (Fig. 2D), and Piccolo (tom Dieck et al., 2005). Bassoon is located at the boundary between the ribbon and the plasma membrane (Fig. 2D; Brandstätter et al., 1999; tom

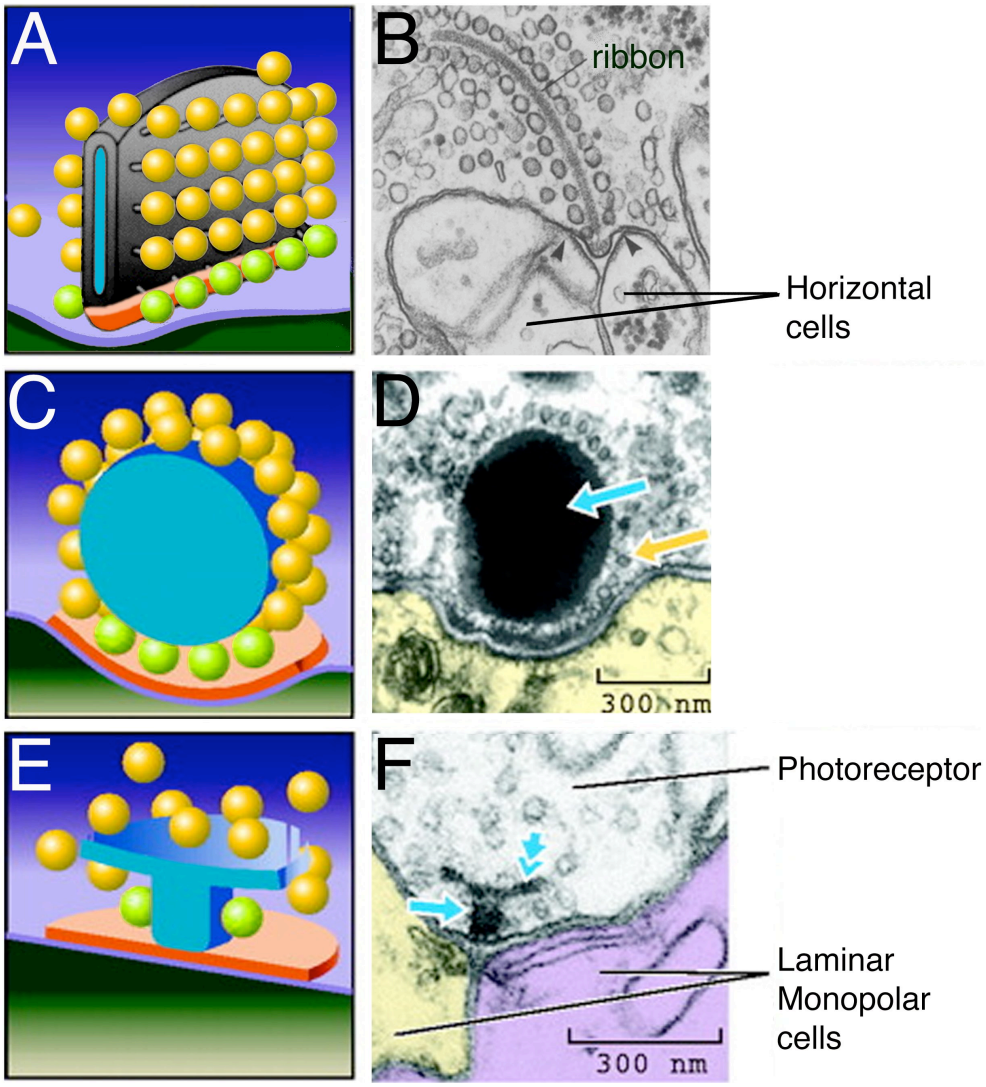

Figure 1. Synaptic ribbons are morphologically diverse organelles. A, C, E, Schematic representations of the electron micrographs shown to their right. Green vesicles represent the docked, ribbon-associated pool. Modified from Zhai and Bellen (2005) with permission of the American Physiology Society. B, Electron micrograph showing a ribbon-like projection surrounded by synaptic vesicles in a salamander rod photoreceptor terminal. Modified from Townes-Anderson and others (1985) with permission of the Rockefeller University Press. D, Electron micrograph showing a spherical synaptic body in a frog saccular hair cell. Yellow arrow points to vesicles tethered to the synaptic body (blue arrow). Modified from Lenzi and von Gersdorff (2001) with permission from John Wiley & Sons, Inc. F, Electron micrograph showing a T-bar shaped "ribbon" in a drosophila photoreceptor terminal. The T-bar is made up of a platform (double arrow) and a pedestal (single arrow). Modified from Meinertzhagen (1996) with permission of Elsevier Inc.

Dieck et al., 2005; Deguchi-Tawarada et al., 2006), and a direct interaction between Bassoon and RIBEYE is necessary for anchoring of the ribbon at the active zone (tom Dieck et al., 2005). Another protein localized to ribbons is KIF3A (Fig. 2E; Muresan et al., 1999), which is a component of the ATP-dependent kinesin II motor that moves cargo along microtubules. This led to the idea that vesicles might actively move down the ribbon, using a kinesin-like motor, to fuse at the plasma membrane. However, other kinesin II components, KIF3B and KAP3, and components of microtubules have not been detected at ribbons (Muresan et al., 1999), and turnover of the releasable pool has been shown not to require ATP hydrolysis, which would be necessary for the function of a kinesin motor complex. Therefore, the possible function of KIF3A at ribbons remains uncertain.

The monoclonal antibody B16 was the first to specifically label ribbons (Balkema, 1991), and its antigen has been shown to exhibit homology to the m chain of an adaptor protein that facilitates the binding of clathrin to vesicles during endocytosis (Nguyen and Balkema, 1999). This suggests that adaptor proteins may be distributed along the ribbon—perhaps to mediate vesicle binding—or that the ribbon may be involved in the endocytic limb of the vesicle cycle. When ribbons are absent from inner hair cells of Bassoon knockout mice, large tubular structures accumulate at the active zones, similar to the large endosomes observed at ribbon synapses of goldfish bipolar cells and frog saccular hair cells (Lenzi et al., 2002; Paillart et al., 2003; Holt et al., 2003). This might be another indication that the ribbon facilitates membrane turnover at the active zone by clearing endocytosed material.

Disruption of synaptic ribbons

Knockout of the CAZ protein Bassoon in mice causes dislocation of synaptic ribbons from their normal position at the active zone in photoreceptors (Dick et al., 2003) and cochlear inner hair cells (Khimich et al., 2005). Ribbons are still present, but they float free in the cytoplasm of the terminal. The amplitude of the b-wave of the electroretinogram—an index of synaptic transmission from photoreceptors to bipolar cells—is reduced in these mice, indicating impaired efficiency of photoreceptor synaptic transmission. However, dendrites of postsynaptic bipolar cells branch abnormally and

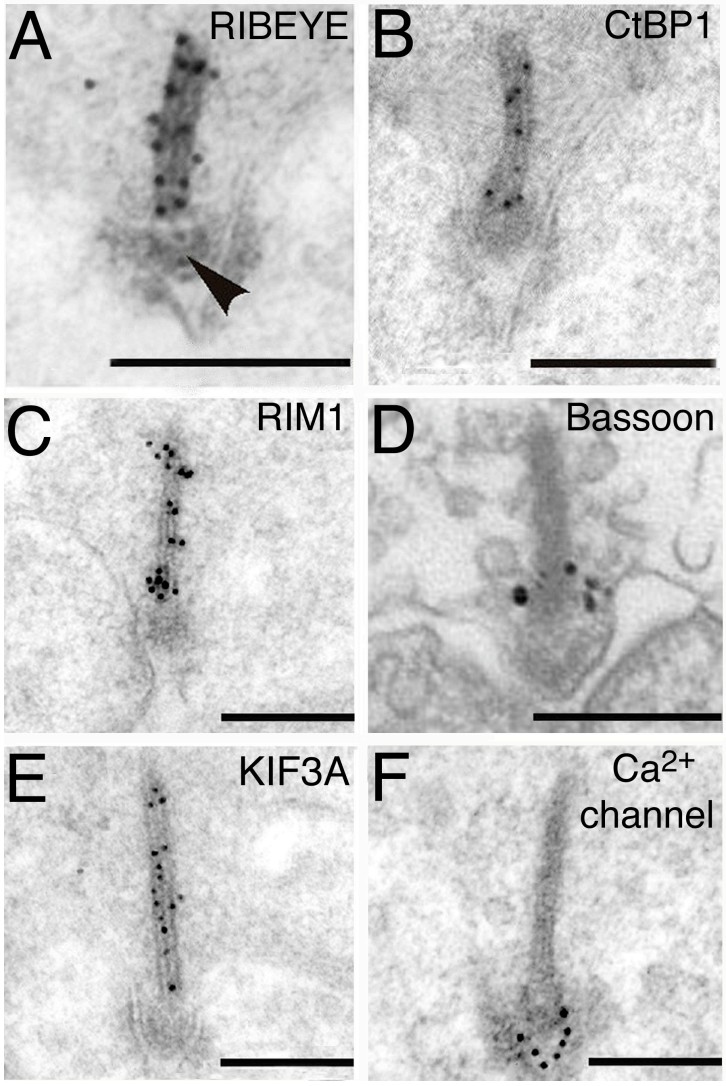

Figure 2. Electron micrographs showing the ultrastructural localization of photoreceptor synaptic ribbon-complex proteins. A-C, E, F, Postembedding immunogold labeling. A, RIBEYE labeling decorates the ribbon but is absent from the arciform density (arrow). B, CtBP1 is found along the length of the ribbon. C, RIM1 is found along the length of the ribbon. D, Immunolabeling reveals that Bassoon is located at the base of the ribbon but not along its length. Modified from Deguchi-Tawarada and others (2006) with permission of John Wiley & Sons, Inc., (E) KIF3A is found along the length of the ribbon. (F) Ca^{2+} channel a1 subunits are located beneath the ribbon at the active zone. Scale bars in A-F represent 200 nm. A-C, E, F, modified from tom Dieck and others (2005), with permission of the Rockefeller University Press.

extend past the terminal to the photoreceptor cell body, where they form ectopic synapses, complete with anchored ribbons on the presynaptic side and postsynaptic glutamate receptors (Dick et al., 2003). Also, ribbons in bipolar cell terminals remain anchored at active zones in Bassoon knockout retina. Since anchored ribbons still occur at ectopic photoreceptor synapses and bipolar cell synapses, alternative mechanisms for ribbon attachment must exist that do not involve Bassoon. It is not clear why this alternative mechanism is able to anchor ribbons at the plasma membrane in the photoreceptor soma, but not at their proper location in the synaptic terminal.

In inner hair cells lacking Bassoon, few anchored ribbons are observed, although active zones still formed, and synchronous afferent transmission to second-order neurons is impaired (Khimich et al., 2005; Fig. 3A). Interestingly, the fast component of exocytosis triggered by brief depolarization is strongly reduced without ribbons, but the slower, sustained response to longer depolarizations is largely unaffected (Fig. 3B). This result is surprising, because the canonical view is that ribbons support sustained release, whereas the mutant synaptic phenotype indicates that hair cell ribbons are essential for fast vesicle fusion but are less critical for sustained release. Perhaps this indicates that the primary purpose of ribbons in inner hair cells is to coordinate the release of multiple vesicles during the initial response to sound onset, and that other mechanisms can apparently compensate for the absence of ribbons and support sustained release. However, this does not necessarily mean that ribbons play no role in sustained neurotransmitter release when they are present.

Synaptic ribbons are dynamic organelles whose size, shape, and number change on a circadian cycle. These cyclical changes in ribbon number and morphology provide a way to examine ribbon function without altering the cell's native protein components. For instance, in goldfish bipolar cells, the number of ribbons is reduced by ~65% at night, yet the number of active zones remains constant, and many active zones therefore lack ribbons at night (Hull et al., 2006). Recordings of membrane capacitance revealed a correlation between ribbon number and the fast component of exocytosis (Hull et al., 2006). At night, exocytosis in response to a 20-ms depolarization is reduced compared to evoked release during the day, when ribbons occupy the active zones. However, the

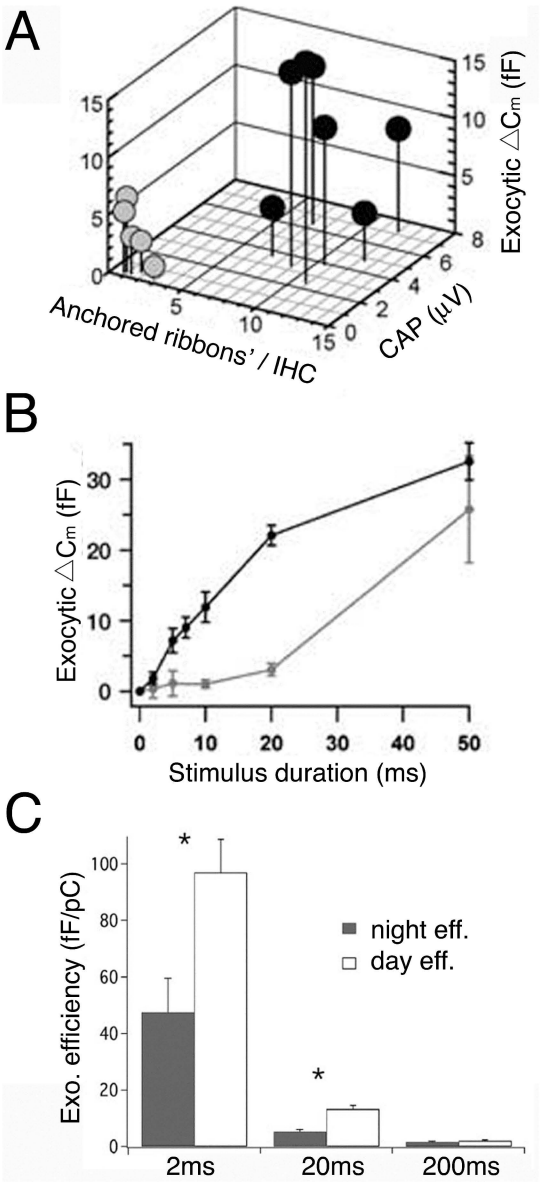

Figure 3. Synaptic ribbons are essential for fast, synchronous release. A, Bassoon mutant mice (grey) have impaired fast exocytosis and synchronous release compared to wild type mice (black). The diagram correlates the mean number of anchored synaptic ribbons per inner hair cell (IHC), fast exocytosis in response to 10-ms depolarizations measured by a change in IHC membrane capacitance (DC_m), and spiral ganglion neuron compound action potential amplitude. B, Graph showing the kinetics of exocytosis assembled from DC_m of the same inner hair cells in response to depolarization of varying lengths. Mutant mice DC_m was significantly different for 5, 10 and 20 ms depolarizations compared to wild-type mice. Modified from Khimich and others (2005) with permission of the Nature Publishing Group. C, Bar graph illustrating the efficiency of exocytosis per pC of calcium entry. Exocytosis is significantly more efficient during the daytime for short depolarizations. The efficiency of exocytosis in response to longer depolarizations was not significantly different from day to night. Modified from Hull and others (2006) with permission of the American Physiology Society.

exocytic response to a 200-ms depolarization was the same in day or night (Fig. 3C). As with the results from inner hair cells lacking Bassoon discussed above (Khimich et al., 2005), this surprising result again suggests that ribbons are more important for fast, synchronous release than for sustained release.

Calcium channels at ribbon type synapses

Glutamate release from bipolar cell terminals is driven by L-type calcium channels with uncommon biophysical properties (Heidelberger and Matthews, 1992). The Ca^{2+} current in these cells activates rapidly and at unusually negative voltages for L-type channels, deactivates rapidly, and exhibits unusually slow calcium-dependent inactivation. These features, shaped by the $\alpha 1$ and auxiliary subunits, allow the synaptic L-type channels to rapidly modulate sustained neurotransmitter release. Unlike conventional synapses, ribbon-containing synapses express the L-type $Ca_V1.3$ (Kollmar et al., 1997; Sidi et al., 2004; Brandt et al., 2005) or $Ca_V1.4$ isoforms (Bech-Hansen et al., 1998; Strom et al., 1998). Using single cell RT-PCR, we have found that goldfish ON-type bipolar cells express transcripts of $Ca_V1.3a$ and/or $Ca_V1.3b$.

Synaptic ribbons and calcium channels are tightly correlated in space, with the channels situated along docking sites beneath the ribbon (Fig. 2F) (Roberts et al., 1990; Issa and Hudspeth, 1994; Llobet et al., 2003; Zenisek et al., 2003, 2004; Midorikawa et al., 2007). Consequently, the vesicles docked at the base of the ribbon are poised for rapid release when calcium channels open. The functional significance of the ribbon is further indicated by its direct apposition to dense clusters of postsynaptic glutamate receptors (Matsubara et al., 1996; Morigiwa and Vardi 1999; Khimich et al., 2005).

The synaptic ribbon as a scaffold for releasable vesicles

The mobility of reserve vesicles at conventional synapses is highly constrained (Henkel et al., 1996; Kraszewski et al., 1996), most likely because vesicles bind to proteins such as synapsin (Hilfiker et al., 1999), which is not expressed at ribbon-type synapses (Mandell et al., 1990). Perhaps because of the absence of synapsin, cytoplasmic vesicles in ribbon-type terminals are more mobile than in conventional boutons. In cone

photoreceptor terminals, for example, ~85% of vesicles are mobile, which may contribute to the fast replenishment of vesicles at tonically active release sites (Rea et al., 2004). Vesicles in goldfish bipolar cell terminals diffuse freely in regions both proximal and distal to the plasma membrane, and random collision of cytoplasmic vesicles is considered sufficient to refill the synaptic ribbon after depletion (Holt et al., 2004). We have found that in terminals of mouse bipolar cells, approximately half of the cytoplasmic vesicles are mobile in the resting state (LoGiudice et al., 2008). Therefore, a large pool of cytoplasmic vesicles is freely mobile within ribbon-containing terminals. How, then, are these mobile vesicles stabilized near the active zone? A variety of lines of evidence indicate that the ribbon carries out this job, acting as a trap or "safety belt" for releasable vesicles (Parsons and Sterling, 2003).

In the static snapshot provided by EM, a halo of vesicles is attached to the surface of the ribbon, and it is natural to suppose that these ribbon-tethered vesicles are immobile. Indeed, measurements in living neurons provide solid evidence that this pool is in fact stationary in the resting cell. Total internal reflection fluorescence microscopy (TIRFM) shows that vesicles labeled with fluorescent FM dye in bipolar cell terminals preferentially reside at "hot spots" near the plasma membrane, where they appear to be spatially fixed (Zenisek et al., 2000). Resident vesicles at these sites rarely disappeared without undergoing exocytosis and releasing their dye, unlike vesicles at other locations, which often left the membrane without fusing. The presumed substrate for vesicle immobilization and preferential fusion at these hot spots is the synaptic ribbon. To determine directly the mobility of vesicles associated with ribbons in mouse bipolar cell terminals, we used a fluorescent peptide that labels ribbons (Zenisek et al., 2004), in conjunction with FM dye to label vesicles. Fluorescence recovery after photobleaching revealed that only ~20% of vesicles at ribbons are mobile, compared with ~50% of cytoplasmic vesicles. Therefore, ribbon-tethered vesicles are not in dynamic equilibrium with cytoplasmic vesicles and are tightly bound to the ribbon in the resting neuron. TIRFM in goldfish bipolar neurons corroborate this conclusion. Single synaptic vesicles were preferentially captured and locked into position at the base of fluorescently labeled ribbons, whereas vesicles at non-ribbon locations were less stable (Zenisek, 2008). These

studies provide compelling evidence that ribbons execute at least one key task at the synapse: to immobilize a pool of vesicles at the active zone.

Ribbon-associated vesicles contribute to the releasable pool

Several lines of evidence indicate that the vesicles immobilized on synaptic ribbons participate in neurotransmitter release. First, EM images of photoreceptors, bipolar cells, and hair cells reveal that ribbon-bound vesicles can contain extracellular markers such as horseradish peroxidase (Fig. 4A) and in our experiments, photoconverted FM dye (Fig. 4B), clearly demonstrating turnover of at least some of the ribbon-associated pool (Schaeffer and Raviola, 1978; Siegel and Brownell, 1986; LoGiudice et al., 2008). Second, EM reveals that in stimulated goldfish bipolar cells, ribbons are significantly denuded of their vesicles compared to ribbons in inhibited neurons (Figure 4 D-F; Holt et al., 2004; Matthews and Sterling, 2008). Third, in frog saccular hair cells, vesicles associated with synaptic ribbons are depleted in response to strong stimulation, with depletion being strongest on the part of the ribbon nearest the plasma membrane (Figure 4 G, H; Lenzi et al., 2002). Finally, we have directly observed turnover of ribbon-associated vesicles in response to depolarization in living mouse bipolar neurons (LoGiudice et al., 2008). Photobleached vesicles immobilized at ribbons were released upon stimulation and replaced by unbleached labeled vesicles, resulting in an increase in FM dye fluorescence specifically at the ribbon location (Fig. 4C; LoGiudice et al., 2008). Thus, it seems clear that vesicles on ribbons contribute to the pool of vesicles that are released upon depolarization.

When synaptic vesicles fuse with the plasma membrane, the resulting increase in surface area can be monitored using membrane capacitance, allowing the kinetics of fusion and retrieval to be observed with fine temporal resolution at living synapses. Capacitance measurements in several sensory neurons, including retinal bipolar cells, rod and cone photoreceptors, cochlear hair cells, and frog saccular hair cells, indicate the presence of at least two kinetically distinct components of release (Parsons et al., 1994; Spassova et al., 2004; Mennerick and Matthews 1996; von Gersdorff et al., 1998; Moser and Beutner, 2000; Thoreson et al., 2004; Khimich et al., 2005; Innocenti and Heidelberger, 2008). The first component reflects a rapidly depleted vesicle pool that is

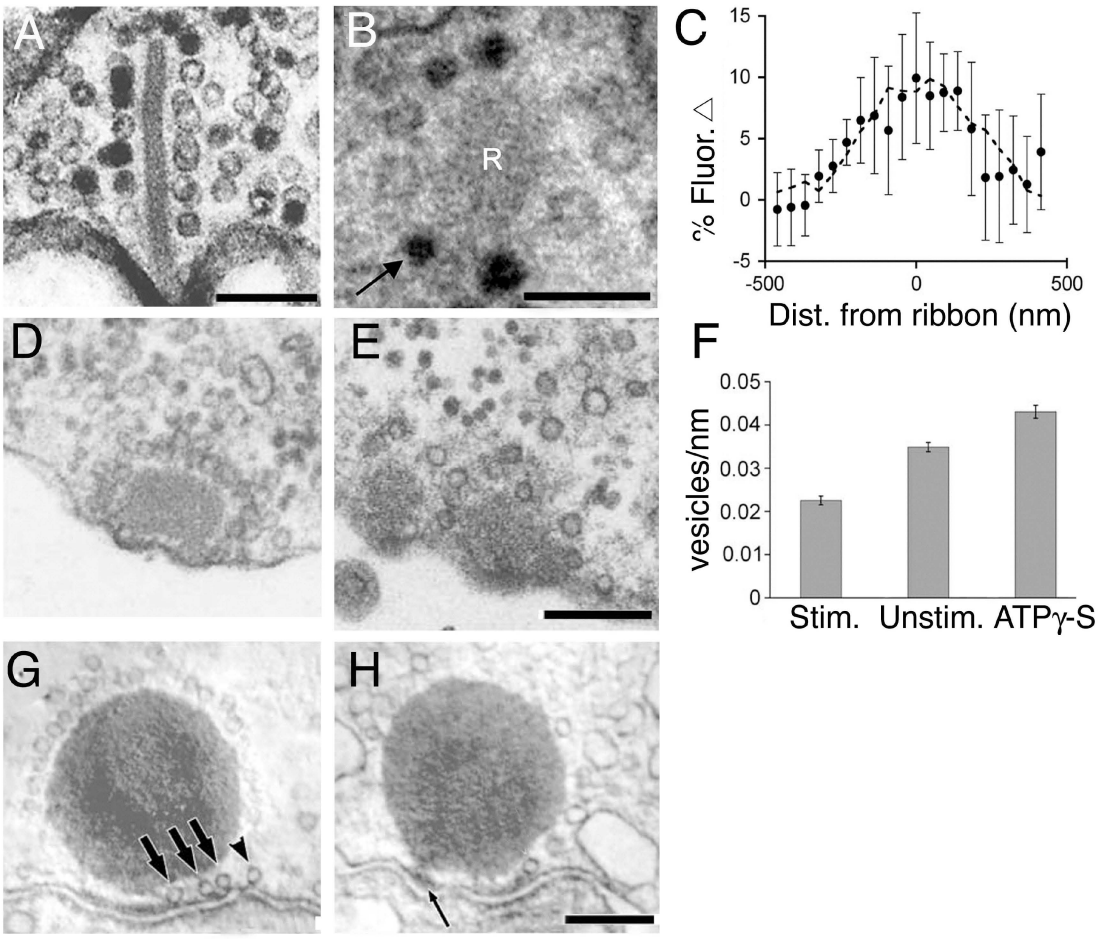

Figure 4. Synaptic ribbons release and recapture vesicles in response to stimulation. A, Electron micrograph of the turtle cone synapse reveals that horseradish peroxidase (HRP) labeled vesicles appear on the ribbon after a 1.0 hr. HRP incubation in the dark. Scale bar represents ~125 nm. Modified from Schaeffer and Raviola (1978) with permission of the Rockefeller University Press. B, Electron micrograph reveals that photoconverted FM1-43 labeled vesicles (arrow) appear on the mouse bipolar cell synaptic ribbon after a 5 min. of repetitive high K^+ stimulation (3 sec puff/15 sec). Scale bar represents 125 nm. R denotes the ribbon. C, Fluorescence profile of the change in previously bleached FM4-64 fluorescence (filled circles) with respect to ribbon position (dashed line) in response to a 250ms pulse from –60mV to 0mV (mouse bipolar cells). Modified from LoGiudice and others (2008) with permission of the Society for Neuroscience. D and E, Electron micrographs of goldfish bipolar cells reveal that calcium spiking reduces the number of vesicles attached to synaptic ribbons (E) compared to cells inhibited by muscimol (D). Scale bar in E represents 200nm and is applicable to D as well. F, Bar graph showing the density of vesicles attached to a ribbon in a single EM slice. ATPγ-S further inhibits cells from releasing vesicles. Modified from Matthews and Sterling (2008) with permission of the Society for Neuroscience. G. Transmission electron micrographs of frog saccular hair cells exposed to 0 Ca^{2+} saline. Long arrows indicate vesicles that are docked beneath the synaptic body and arrowhead marks a vesicles that is docked nearby. H, Transmission electron micrographs of frog saccular hair cells exposed to high K^+. Thin arrow points to a region of presynaptic density. Scale bar in H represents 200 nm and is applicable to G as well. Modified from Lenzi and others (2002) with permission of Elsevier, Inc.

released within milliseconds, while the second component is delayed and can last for several hundred milliseconds or more. What are the morphological correlates of the fast and slow components and to what extent do ribbon-associated vesicles contribute to each? In a variety of cell types, there is good agreement between the size of the fast component and the number of synaptic vesicles at the base of the ribbon, in close proximity to the plasma membrane (the docked pool; green vesicles in Fig. 1). Therefore, the conclusion seems reasonable that these docked vesicles likely account for the very rapid, synchronous burst of exocytosis when calcium channels open.

But what about the correspondence between the slower component of release and the non-docked vesicles in higher rows on the ribbon? Here, things get murkier. On the one hand, in rod photoreceptors (Thoreson et al., 2004), goldfish bipolar cells (von Gersdorff et al., 1996), and chick cochlear hair cells (Spassova et al., 2004), the total population of ribbon-attached vesicles corresponds well with the size of the entire releasable pool. This would be consistent with a "ribbon hypothesis" that attributes the majority of functional vesicle release to the ribbon. On the other hand, in other instances the anatomically defined, ribbon-tethered pool is either smaller than the physiologically defined releasable pool (saccular hair cells; Lenzi et al., 1999) or larger (mouse cochlear hair cells; Khimich et al., 2005). Also, as discussed earlier, disruption of ribbons suggests a more important role for the ribbon in fast, synchronous release than in sustained, slower release.

As an alternative, the “docked outlier hypothesis” offers a less ribbon-centric point of view with regard to sustained vesicle release. This idea similarly attributes the fast component to the fusion of vesicles docked near synaptic ribbons, but credits the delayed component to the fusion of outlier vesicles positioned at a distance from synaptic ribbons (e.g., Midorikawa et al., 2007). In goldfish bipolar cells, TIRF imaging reveals that stimulation evokes the fast, reliable fusion of vesicles docked beneath synaptic ribbons, as well as delayed vesicle release at outlying sites, perhaps uncovering the physiological correlates of the fast and slow components of exocytosis in the bipolar cell (Zenisek et al., 2000; Midorikawa et al., 2007; Zenisek 2008). While fast transient events predominantly occurred in ribbon-containing regions, both ribbon-associated and ribbon-free zones maintained a low rate of vesicle fusion during prolonged depolarization

(Midorikawa et al., 2007). Furthermore, activation of protein kinase C, which is known to selectively increase the size of the slowly released component (Minami et al., 1998; Berglund et al., 2002), significantly enhanced the number of fusion events outside of the ribbon region (Midorikawa et al., 2007), which is again consistent with the delayed component being partially due to the fusion of outliers. Are some of these outlier sites authentic ribbon-free active zones? In support of this possibility, Midorikawa et al. (2007) showed EM images documenting the presence of two different types of active zone in goldfish bipolar neurons: ribbon-associated synapses with dyad processes, and ribbon-free synapses contacted by single postsynaptic processes. However, given the plasticity of ribbons described above, it is unclear whether ribbons once occupied these active zones, or if these non-ribbon vesicles actually contribute to functional neurotransmission.

The physiological relevance of glutamate release from sites distal to postsynaptic receptors is a potential issue for the docked outlier hypothesis. AMPA receptors are selectively apposed to synaptic ribbons (Matsubara et al., 1996; Morigiwa and Vardi, 1999; Qin and Pourcho 1999; Khimich et al., 2005), but extrasynaptic receptors may participate in sensory transmission as well. For instance, immunogold labeling of retinal ganglion cells confirms that NMDA receptors are located perisynaptically, ~100-300nm from the postsynaptic density (Chen and Diamond, 2002; Zhang and Diamond, 2006), and NMDA receptors may also be located extrasynaptically on AII amacrine cell dendrites (Matsui et al., 2001; Zhou and Dacheux, 2004). Therefore, release events hundreds of nanometers away from synaptic ribbons may have postsynaptic targets. In bipolar cells and frog saccular hair cells, synaptic vesicles dock at the plasma membrane peripheral to the central ribbon region and so may sense incoming calcium, albeit less rapidly than those docked beneath the ribbon (Roberts et al., 1990; Burrone et al., 2002). In addition to these docked vesicles, cytoplasmic vesicles appear to cluster near synaptic ribbons in mouse and goldfish bipolar cells and in frog saccular hair cells (Lenzi et al., 1999; LoGiudice et al., 2008; Matthews and Sterling, 2008). These non-docked vesicle clusters may provide a mechanism to quickly refill the ribbon (Spassova et al., 2004) or perhaps they are directly released at the active zone and contribute to the sustained component without ever contacting the ribbon itself.

Mechanisms of release from the ribbon: The synaptic ribbon as a conveyor belt

The ribbon is often likened to a conveyor belt, dynamically moving vesicles toward the active zone in response to a depolarizing stimulus (Parsons and Sterling, 2003). In this context, the presence on ribbons of the kinesin motor protein KIF3A is of interest. Additionally, the actin-based motor molecule Myosin Va (Mehta et al., 1999) is found in photoreceptors, and mutation of this protein leads to abnormal visual function, malformed ribbons, and ectopic vesicle clustering (Libby et al., 2004). Myosin VIIa is also found in photoreceptors (Liu et al., 1997) and has been implicated in Usher Syndrome type 1, a heritable condition that causes deafness, balance problems, and visual defects (Weil et al., 1995). However, while the presence of both microtubule- and actin-based motor proteins is suggestive, actin and components of microtubules, though present within the terminal, are believed to be absent from synaptic ribbons. Furthermore, using TIRFM, Zenisek et al. (2000) showed that vesicles at active zones and at outlying positions approach the membrane at the same speed (~0.8 $\mu m\ s^{-1}$). This suggests that a ribbon-based motor, if it exists, does not deliver vesicles any faster than the means of delivery (most likely diffusion) used by ribbon-free vesicles. By tethering vesicles on its surface, the synaptic ribbon effectively constrains vesicle movement to two dimensions, thus increasing their probability of docking at the active zone. Therefore, diffusion may be a viable mechanism for delivering vesicles to the active zone. It is unclear how vesicles would diffuse on the ribbon, however. Do tethered vesicles diffuse freely on the ribbon or are they fixed in place until a release-triggering event? Precise optical measurements of fluorescent vesicles on ribbons could potentially resolve this question.

Mechanisms of release from the ribbon: Coordinated release

Several lines of evidence indicate that ribbon synapses are able to coordinate the simultaneous fusion of multiple synaptic vesicles. Recordings from afferent boutons postsynaptic to cochlear hair cells show that multiquantal release occurs from single presynaptic active zones (Glowatzki and Fuchs, 2002). Also, analysis of fluctuations in capacitance responses of cochlear inner hair cells suggests that elementary fusion events

are often larger than predicted for single synaptic vesicles (Neef et al., 2007), which is also consistent with synchronized fusion of multiple vesicles. In the auditory system, this synchronized release by cochlear hair cells requires ribbons and is the basis for precisely timed activation of the postsynaptic neuron (Khimich et al., 2005). Such precision is in turn necessary for brainstem auditory neurons to detect slight differences in interaural arrival time of acoustic stimuli. Large postsynaptic events consistent with synchronized release of multiple quanta have also been reported at the ribbon synapse between bipolar neurons and AII amacrine cells in the retina (Singer et al., 2004), but the functional requirement for such synchrony is not as readily apparent in this system.

What mechanisms might account for synchronized fusion of multiple vesicles? If multivesicular events reflect the coordinated release of multiple docked vesicles (Glowatzki and Fuchs, 2002), then vesicles may be coupled in some manner, enabling them to fuse in unison as suggested by Singer et al. (2004). (Figure 5A, synchronized fusion). One could imagine this to be the case if the filamentous tethers of distinct vesicles were physically coupled, or if the synaptic ribbon somehow coordinated the fusion machinery of separate vesicles. Alternatively, multivesicular release may occur via the homotypic "compound" fusion of several vesicles associated with the same release site (Heidelberger et al., 1994; Parsons and Sterling, 2003; Edmonds et al., 2004; Matthews and Sterling, 2008). Compound fusion could be a cumulative event triggered by depolarization, in which a docked ribbon-associated vesicle fuses with the membrane and other vesicles sequentially fuse with the one below (Figure 5A, sequential compound fusion). This type of mechanism was proposed by Edmonds et al. (2004) to explain their observation that a brief depolarization of frog saccular hair cells releases ~10 times more vesicles than are docked at the active zone. Alternatively, vesicles could fuse with each other either in the cytoplasm or on the ribbon prior to their contact with the plasma membrane (Figure 5A, Compound fusion). Such homotypic fusion could then result in larger quantal events like those reported by Glowatzki and Fuchs (2002) and Singer et al. (2004).

Recently, Matthews and Sterling (2008) reported two types of ultrastructural evidence favoring compound fusion at ribbons of goldfish bipolar cells. First, depolarization increased the percentage of unusually large vesicles attached to ribbons

(Fig. 5B), consistent with possible calcium-dependent fusion among non-docked vesicles tethered to the face of the ribbon. Second, in cells fixed during repetitive stimulation, large, cistern-like membrane structures were observed at the base of the ribbon, attached by tethers like those that bind synaptic vesicles to the ribbon (Fig. 5C,D). Moreover, the attached cisternal structures were continuous with the plasma membrane, as if in the process of fusing with the membrane. A simple interpretation is that the cisterns arise from exocytosis rather than endocytosis, because 1) they occupy the base of the ribbon, where synaptic vesicles are found in unstimulated terminals, 2) they are continuous with the plasma membrane at a location where exocytosis is thought to occur, and 3) they are attached to the ribbon by filaments like those that tether normal synaptic vesicles. Therefore, these structures may represent compound fusion of synaptic vesicles during neurotransmitter release. Although the evidence for vesicle-vesicle fusion at synaptic ribbons is by no means conclusive, compound fusion would neatly account for the functional characteristics of transmitter release at ribbons, including the rapid, synchronous release of multiple vesicles and, to the degree it occurs at ribbon vs. non-ribbon sites, the slower sustained release during prolonged depolarization.

Endocytosis at ribbon synapses

To maintain the fidelity of synaptic transmission, exocytosis must be balanced by high-capacity endocytosis, to retrieve excess membrane inserted during vesicle fusion. Capacitance measurements following vesicle release in ribbon-type neurons indicate two kinetically distinct phases of compensatory endocytosis, whose relative contributions vary with stimulus intensity. The two phases can be independently regulated and may reflect different underlying mechanisms operating on separate pools of recycling vesicles. Electron microscopy reveals diversity among ribbon-type synapses in the relative importance of clathrin-mediated endocytosis vs. bulk membrane retrieval as mechanisms of compensatory endocytosis. Ribbon synapses, like conventional synapses, make use of multiple endocytosis pathways to replenish synaptic vesicle pools, depending on the physiological needs of the particular cell type.

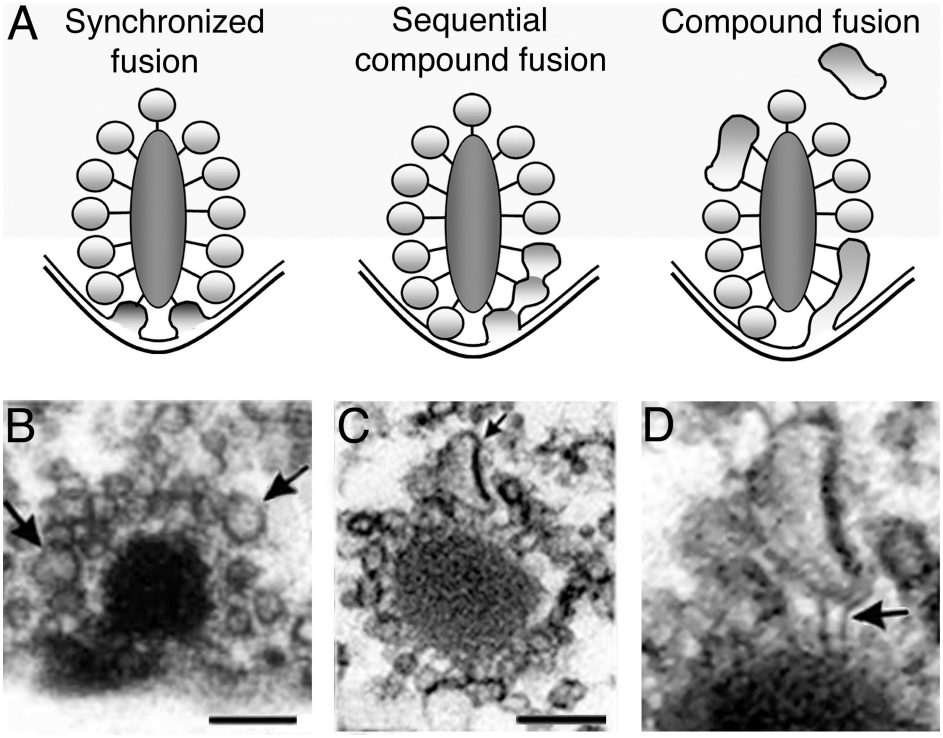

Figure 5. Multivesicular release at ribbon-type synapse. A, Schematic representation of three different scenarios where the contents of multiple vesicles are released in a highly synchronized manner. B-D, Electron micrographs of goldfish bipolar cell synaptic ribbons. Large vesicles are often seen attached to synaptic ribbons (arrows, B). C, Large pleomorphic structures appear to be attached by tether-like filaments to the base of the ribbon in repetitively stimulated neurons. Scale bars represent 100nm. D, Magnified view of cistern-like structure in C. Arrow points at the electron dense filaments that contact the ribbon and the structure. Modified from Matthews and Sterling (2008) with permission of the Society for Neuroscience.

Bulk-membrane retrieval

In goldfish bipolar cell and frog saccular hair cells, EM images confirm that the principle means of compensatory endocytosis involves the retrieval of large bites of membrane that later give rise to synaptic vesicles (Lenzi et al., 2002; Paillart et al., 2003; Holt et al., 2003). Examples of this bulk retrieval are shown in Fig. 6. Clathrin-mediated endocytosis (CME) is important in conventional synapses (Heuser and Lennon 1973; Takei et al. 1996; Shupliakov et al. 1997; Granseth et al. 2006), but EM observations of compensatory endocytosis at ribbon synapses of goldfish bipolar cells and frog saccular hair cells have revealed little or no evidence for major involvement of CME (Lenzi et al. 2002; Holt et al. 2003; Paillart et al. 2003). In spite of this, endocytic proteins, including clathrin, dynamin, AP180, and amphiphysin, are expressed in ribbon-containing neurons (von Kriegstein et al., 1999; Park et al., 2008; Hosoya and Tsutsui, 2004; Sherry and Heidelberger, 2005; Ullrich and Sudhof, 1994; Yao et al., 2002), and perturbation of essential elements in the clathrin-mediated pathway blocks the slow mode of retrieval in goldfish retinal bipolar cells (Jochkusch et al., 2005).

The molecular basis for bulk retrieval is not yet known, although it does share some features with forms of endocytosis such as macropinocytosis, which also retrieves large chunks of membrane without involvement of clathrin. Compensatory endocytosis in bipolar cell synaptic terminals is blocked by inhibition of ATP hydrolysis with ATP-γS (Heidelberger 2001; Heidelberger et al. 2002) but not by GTP-γS or GDP-βS (Heidelberger 2001), both of which would inhibit dynamin-dependent endocytosis such as CME. It should be noted, however, that this conclusion has been challenged by Jockusch et al. (Jockusch et al. 2005), who reported that the slow phase of endocytosis but not the fast phase in bipolar cell terminals was indeed blocked by GTP-γS, as well as by other manipulations that interfere with the clathrin pathway. In goldfish bipolar neurons, however, clathrin coated vesicles are rarely observed by EM, including vesicles arising from large cytoplasmic structures.

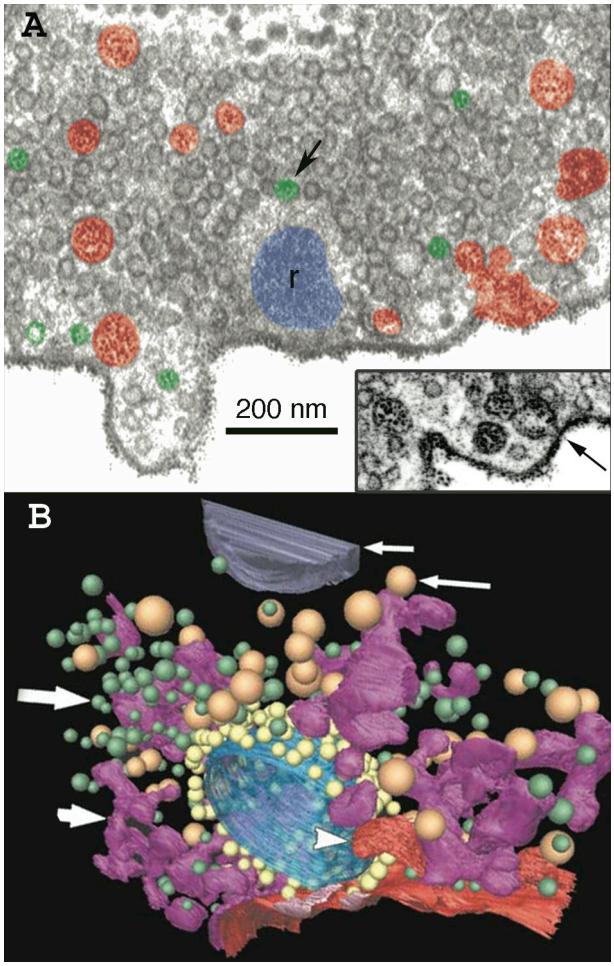

Figure 6. Bulk membrane retrieval is the principal mechanism of endocytosis in stimulated goldfish retinal bipolar and frog saccular hair cells. A, Electron micrograph of goldfish bipolar cell ribbon synapse that fired spontaneous calcium action potentials in the presence of cationized ferritin. Membrane was predominantly retrieved into large cytoplasmic structures (red). Several vesicles were also labeled with ferritin (green) and one vesicle associated with the synaptic ribbon (arrow). Blue structure represents the synaptic ribbon (r). Inset shows a ferritin labeled structure budding from the plasma membrane (arrow). Figure modified from Paillart et al. (23). Reproduced with permission (copyright 2003 by the Society for Neuroscience). B, Electron tomographic reconstruction of frog saccular hair cells stimulated with high K^+. Coated (gold) and uncoated (green) vesicles and large cisterns (purple) are apparent after stimulation. Yellow structures represent vesicles that are associated with the synaptic body. A tubular invagination (arrowhead) arising from plasma membrane (red) can be seen. Large endocytic structures account for 75% of membrane area lost in response to prolonged depolarization. Figure reprinted from Lenzi et al. (21), with permission of Elsevier (copyright 2002).

Clathrin-mediated endocytosis

Ultrastructural analysis of photoreceptor synapses shows that endocytosis markers are localized principally in synaptic vesicles, some of which bear clathrin coats (Schacher et al. 1976; Cooper and McLaughlin 1983; Townes-Anderson et al. 1985; Rea et al. 2004). Although bulk retrieval is also used to some extent, this suggests a major contribution of CME to compensatory endocytosis in photoreceptors. Figure 7 illustrates extensive labeling of coated and uncoated synaptic vesicles, but not large endocytic structures, at the ribbon synapse of a cone photoreceptor in goldfish retina, after incubation with microperoxidase for 2 minutes in the dark. Labeled vesicles are also associated with the synaptic ribbon, indicating rapid entry of recycled vesicles into the releasable pool. Similarly, we show that in mouse bipolar cell terminals, almost all of the photoconverted FM dye was contained within vesicles ~30 nm in diameter. Clathrin-coated vesicles are commonly observed budding from the plasma membrane and within the cytosol, and application of dynasore, a dynamin inhibitor, arrested membrane retrieval at the budding stage. This pattern contrasts sharply with the bulk membrane retrieval observed in goldfish bipolar cell synapses, shown in Fig. 6A.

Location of compensatory retrieval

Electron microscopy images of photoreceptor cell and hair cell ribbon-synapses reveal endocytotic structures budding laterally to synaptic ribbons, suggesting that compensatory retrieval occurs locally near active zones (Gray and Pease, 1971 ; Lenzi et al., 1999). In photoreceptors, coated vesicles appeared to form on the membrane located lateral to synaptic ribbons (Gray and Pease, 1971), and in frog hair cells, elongated omega profiles and clathrin-coated pits were observed adjacent to synaptic bodies (Lenzi et al., 1999). By concurrently visualizing fluorescently labeled synaptic ribbons and FM4-64 uptake in living neurons, we show that mouse bipolar cell terminals recover excess membrane at distinct sites that correlate with the position of synaptic ribbons in the axon and terminals.

Figure 7. Cone photoreceptors retrieve membrane via synaptic vesicles, not large endosomes. Electron micrograph of a cone photoreceptor terminal in goldfish retina after incubation with external microperoxidase for 2 min in the dark. Recently endocytosed structures are discernible by the dark reaction product (e.g., thin arrow). Labeling is localized to coated and uncoated synaptic vesicles but not large endocytic structures. Both labeled (thin arrow) and unlabeled (thick arrow) vesicles are associated with the synaptic ribbon (C. Paillart, G. Matthews, and P. Sterling, unpublished data).

Chapter II
Methods

Cloning $Ca_v1.3$ and $Ca_v1.3b$ from goldfish retina using RT-PCR

All animal procedures were carried out in accordance with National Institutes of Health guidelines under protocols approved by the Institutional Animal Care and Use Committee. Initial a1 sequences were generated by RT-PCR from goldfish retina total RNA using random hexamers (Invitrogen) for reverse transcription. Goldfish equivalents of $Ca_v1.3a$ and $Ca_v1.3b$ were amplified with degenerate primers designed against known zebrafish and mammalian sequences. The first round primers used to detect $Ca_v1.3a$ were
5' AYTTGGCWGACGCWGARAG 3' and
5' GAARAARATGGAGATSWCCAC 3'. The second round primers were
5' TCTTCTTGGCCATYGCTGTRG 3' and 5' CGAARTTGAAATCACTRTTYTSCC 3'. The first round primers used to detect $Ca_v1.3b$ were
5' CTTGGMATGCAGCTSTTTGG 3' and
5' GTTRAARTCACTGTTSWCCCAG 3'. The second round primers used were
5' GTCTTTCAGATYYTGACNGGWGAGG 3' and
5'CTGMACCACATGYTTGAGKCC 3'.
Subsequently, subunit-specific primer sets were designed to extend the sequences 5'. The $Ca_v1.3a$ primers were 5' CGTCGCTGGAACCGGTTG 3' and
5' CTCGTCTCCAGCCTTGGCAT 3'.The $Ca_v1.3b$ primers were
5' CAGAAGCTTCGRGAGAARCAGCAG 3' and
5' CAGATGCCTTGACGTCTCCAT 3'. The GenBank accession numbers of the corresponding goldfish $Ca_v1.3a$ and $Ca_v1.3b$ sequences are DQ314779 and DQ314780, respectively. The goldfish sequences were then used to design primers for single-cell RT-PCR.

Single-cell RT-PCR

For single-cell RT-PCR, goldfish retinal cells were dissociated by mechanical trituration after papain digestion, as described in the literature (Heidelberger and Matthews, 1992). Cells were plated on flamed polished glass coverslips and washed thoroughly with goldfish Ringer's solution to eliminate debris. For each experiment, several negative controls were collected to assess the possibility of false positives. To test for contamination in the bath, one or two samples of bath fluid were collected near live cells and designated "no cell" controls. In addition, two bipolar cells per experiment were collected and processed normally, except that reverse transcriptase was omitted. These "-RT" cells test that detected transcripts were derived from cellular mRNA. To check for possible contamination in reagents, one water–only sample underwent PCR and was designated "no DNA". The contents of single bipolar cells and controls were aspirated into a whole-cell patch pipette containing approximately 1 μl RNase-free solution. The contents of the pipette were then expelled into a siliconized 0.5 ml microfuge tube containing 10.5 μl Nuclease-free water (Ambion). We immediately added 4 μl 5x first strand buffer, 0.5 μl 0.1 M DTT, 2 μl RNAsin (2 units/ μl), 1μl dNTPs (10mM each), and 1 μl random hexamer primers (3 mg/ml). All reagents were obtained from Invitrogen. Following a 10 min incubation at room temperature, 1 μl (200 units) of Superscript II reverse transcriptase was added, and cDNA synthesis was carried out at 42 ^{o}C for 1 h. Amplification of a region of a specific subunit was achieved with two rounds of PCR using Platinum Taq DNA polymerase and 2 μl reverse-transcribed cDNA in 50 μl PCR buffer and reactants (Invitrogen). The PCR protocol was as follows: 95^{o} C for 5 min, 40 cycles of 95, 55, and 72 ^{o} C for 1 min each, and 72 ^{o}C for 4 min at completion. The first round primers were degenerate and designed to span Domain II, the II-III linker, and a piece of Domain III. This region was chosen based on the high degree of homology across subunits and species, thus allowing the 1st-round primers to effectively amplify both Ca_v1.3a and Ca_v1.3b. The degenerate forward primer was 5' GKCTGCAGGCMTAYTTTGTGTC 3' and the degenerate reverse primer was 5' GAGGATGAGRTTGGTGAAGATSTGRTG 3' (expected size of Ca_v1.3b 896 bp, Ca_v1.3a 830 bp). The 2nd-round specific primers were designed to span the II-III linker

region of a specific target gene and nest within the first round primers. This region was chosen for the high degree of divergence between $Ca_v1.3a$ and $Ca_v1.3b$ while preserving homology within a subunit across species. The specific forward primer designed to target $Ca_v1.3b$ was 5' TTGCTTGGCATGCAGCTC 3' and the specific reverse primer was 5' AGGCTCAGCTCTGACAGCCT 3' (512 bp). The specific forward primer designed to target $Ca_v1.3a$ was 5' GTGGTGTGTGGAGGCATCAC 3', and the specific reverse primer was 5' CGTCTCCAGCCTTGGCAT 3' (577 bp). All 1st and 2nd round primer sets are predicted to span introns based on the mammalian $Ca_v1.3$ genomic sequence. PCR products of the correct size were gel-purified, subcloned in pGEM-T Easy, and sequenced to verify their identity.

Mouse bipolar cell isolation

We used adult male mice of strain C57BL/6J. A mouse was killed by CO_2 inhalation, and both eyes were removed and hemisected. Neural retinas were detached and cut into 6 pieces. To isolate bipolar cells, retinal pieces were dissociated by mechanical trituration after papain digestion (Fluka) for 28 min at RT (Heidelberger and Matthews, 1992). Cells were plated on flame-polished glass coverslips in a solution containing 135 mM NaCl, 5 mM KCl, 1 mM $MgCl_2$, 2.5 mM $CaCl_2$, and 10 mM Hepes and briefly washed with the same solution prior to recording.

Electrophysiology for vesicle mobility experiments

Isolated bipolar cells were identified as rod bipolar cells based on their distinctive morphology (Ghosh et al., 2004). Cells were voltage clamped using an EPC-9 amplifier controlled by Pulse software. Bipolar cell bodies were patch clamped, held at –60 mV, and dialyzed with a Cs-gluconate solution (120 mM Cs-gluconate, 10 mM TEA-Cl, 20 mM Hepes, 0.2 mM NMDG–EGTA, 3 mM $MgCl_2$, 2 mM Na_2ATP, 0.5 mM GTP) containing 35 µM fluorescent peptide (fluor-EQTVPVDLSVARPR-COOH; kind gift of Dr. David Zenisek, Yale Medical School) with affinity for the CtBP2 domain of the synaptic ribbon protein RIBEYE (Zenisek et al., 2004). Glutathione (2 mM) was added to the solution to reduce photodamage (Meister and Anderson, 1983). The extracellular bath

solution contained 135 mM NaCl, 5 mM KCl, 1 mM $MgCl_2$, 2.5 mM $CaCl_2$, and 10 mM Hepes. The pH of the solution was adjusted to ~7.4 with NaOH. To load vesicles, cells were either bathed in a solution of high K^+ containing FM4-64 (15 μM) for 90 s, or repetitively stimulated with focal application of the same solution for 5 minutes with a 50% duty cycle. All experiments were done at room temperature.

Confocal imaging

All fluorescence images were acquired using an Olympus FV-300 laser-scanning confocal microscope and Fluoview software (Olympus America, Center Valley, PA). The fluorescein-tagged peptide and FM4-64 labeling were sequentially scanned to reduce channel cross-talk. Coordination with the patch-clamp amplifier and programming of sequences of image acquisitions were accomplished using Tiempo software extension to Fluoview. Subsequent analysis and processing of images was carried out in Fluoview, Image J, or Igor Pro software.

Electron microscopy

Cells were plated on Aclar instead of glass coverslips and were stimulated with high K^+ in the presence of FM1-43 (5 μM). They were then washed and lightly fixed in 4% paraformaldehyde and 0.2% glutaraldehyde in 0.13 M PB at room temperature for 25 min, washed, and bathed in DAB. Photoconversion was achieved by illumination with high intensity blue light through a 50x objective for 20 min. The cells were washed once again in a 0.13 M PB solution and fixed with 2.5% paraformaldehyde and 2.5% glutaraldehyde for 30 min at RT, then processed for EM as previously described (Paillart et al., 2003). Uranyl acetate and lead, typically used to stain the sections, were omitted to preserve the contrast between labeled and unlabeled vesicles (Brumback et al., 2004).

Fluorescence recovery after photobleaching

Bleached regions of interest (ROI) were ~1.0 μm x 0.5 μm in size and contained at least one synaptic ribbon and a cytoplasmic region of similar FM4-64 fluorescence intensity. The standard FRAP protocol involved 5 pre-bleach images at 2 s intervals (5%

laser intensity, 543 nm), 5 bleach iterations (100% intensity, 543 nm, 0 interval, ~1 s), and 30-40 post-bleach images at 2 s intervals (5% intensity, 543 nm). Recovery curves at the ribbon and at a non-ribbon location were acquired simultaneously by measuring average fluorescence intensity in two 0.5-μm-square boxes centered on the ribbon and displaced 0.5 μm to the side. Curves were fit with a single exponential equation to determine the time constant and asymptotic level of recovery. Fluorescence during recovery was also corrected for the bleaching produced by the 5%-intensity acquisition illumination, which was measured in control experiments using the same imaging protocol but omitting the intense bleaching stimulus.

Estimation of mobile fraction

We estimated the mobile fraction of vesicles (m) from the asymptotic fluorescence intensity (f_∞; normalized by dividing by pre-bleach intensity) achieved at steady state after recovery from bleaching of FM4-64-labeled synaptic vesicles in a subregion of the synaptic terminal. If all vesicles in the terminal were mobile, the dim vesicles from the bleached region and the bright vesicles from the unbleached region would distribute equally throughout the terminal, and at each location bleached and unbleached labeled vesicles would be present in proportions reflecting their overall proportions in the terminal as a whole. Thus, the normalized fluorescence in the bleached region would equilibrate at f_{tot}, where f_{tot} is the proportion of the total initial fluorescence of the entire terminal remaining after bleaching the targeted subregion. In our experiments, f_{tot} was typically 0.6 to 0.75, which sets the maximum normalized intensity that would be achieved in the bleached region after full recovery, if m = 1.0. Conversely, if m were 0 (no mobile vesicles), there would be no recovery in the bleached region, and the normalized intensity in the bleached region would remain at its value immediately after the bleach, f_b. In our experiments, $f_b \approx 0.2$. Therefore, m is given by the fractional recovery of normalized fluorescence between these two extremes:

$$m = \frac{f_\infty - f_b}{f_{tot} - f_b}$$

In the figures presenting FRAP data, fluorescence recovery is plotted directly in units of

m, ranging from 0 to 1.0, which was calculated for each terminal based on the individual values for f_{tot}, f_{∞}, and f_b.

Measuring stimulation-induced changes in FM4-64 fluorescence

A portion of a synaptic terminal containing one or more ribbons was photobleached as described for FRAP measurements and allowed to recover fully. Series of 2-5 images were then taken before and after a 500-ms depolarization from –60 mV to 0 mV to trigger exocytosis. To measure the fluorescence change at ribbon locations in bleached and unbleached subregions, a 0.5 μm x 0.5 μm box was centered on each ribbon, defined by fluorescent peptide labeling, and the average FM4-64 fluorescence in the box before and after stimulation was measured using ImageJ software. Fluorescence at non-ribbon locations was measured similarly by moving the box to 2-4 surrounding positions that lacked punctate fluorescence of RIBEYE-binding peptide. The difference between pre- and post-stimulus fluorescence was then expressed as a percentage of the pre-stimulus fluorescence. The spatial profile of the fluorescence change at ribbons was measured using the Plot Profile function of ImageJ within a 0.5 μm x 1.5 μm box centered on each ribbon, with the long axis parallel to the plasma membrane.

Electrophysiology and vesicle loading for endocytosis experiments

A fluorescent peptide (fluor-EQTVPVDLSVARPR-COOH) with affinity for the synaptic ribbon protein RIBEYE (Zenisek et al., 2004) was introduced into the cell via a whole-cell patch pipette. To label recycling vesicles, FM4-64 (20 μM) was focally applied to the voltage-clamped cells and a 250 ms depolarizing stimulus was given after achieving asymptotic intensity of FM4-64 fluorescence in the membrane. Approximately 10 s after stimulation, Advasep-7 was puffed onto the cell to remove plasma membrane fluorescence, leaving behind trapped dye only. Localization analysis was done in NIH image. Dynasore, when used, was diluted to 80-90 μM in 0.16% DMSO. Cells were exposed to dynasore for ~ 5 minutes prior to stimulating cells with high K^+ in the presence of FM4-64 or AM1-43. Labeled ribbons and FM dye was visualized by CLSM. All confocal imaging was done with Olympus Fluoview software.

Fixation and photoconversion for endocytosis experiments

After loading with AM1-43, cells were washed and lightly fixed in 4% paraformaldehyde (PAF) and 0.2% glutaraldehyde at RT. Photoconversion was achieved by illuminating with high intensity blue light through a 50x objective for 20 min in the presence of DAB. Cells were washed and fixed with 2.5% paraformaldehyde and 2.5% glutaraldehyde for 30 min at RT. Cells were processed for electron microscopy as previously described by Paillart et al. (2003).

Antibodies and immunofluorescence

Cells were isolated as usual and plated on glass coverslips. They were fixed with 4% PAF for 15 min at RT then bathed in 0.3% Triton X-100 for 30 min. at RT. Cells were subsequently incubated in primary antibody for 1 hr 15 min. and then in secondary antibody for 1.0 hr at RT. Primary antibody: Mouse monoclonal against dynamin-1 (1:250), BD Biosciences, Franklin Lakes, NJ. Secondary antibody: Goat Anti-Mouse conjugated to AlexaFluor 546 (1:200), Jackson ImmunoResearch, West Grove, PA.

Chapter III

Identification Of Calcium Channel α1 Subunit mRNA Expressed in Retinal Bipolar Neurons

Introduction

Glutamate release from goldfish bipolar cell terminals is driven by L-type calcium channels with uncommon biophysical properties (Heidelberger and Matthews, 1992). The Ca^{2+} current in these cells activates rapidly and at unusually negative voltages for L-type channels, deactivates rapidly, and exhibits unusually slow calcium-dependent inactivation (von Gersdorff and Matthews, 1996 ; Mennerick and Matthews, 1998). These features, shaped by the α1 and auxiliary subunits, allow the cell to drive sustained neurotransmitter release, a requirement at the bipolar cell terminal. Although the synaptic terminal of the goldfish bipolar cell is a widely used model for neurotransmitter release at ribbon synapses, the molecular composition of the calcium channels that drive release is unknown.

The α1 subunit is the largest and most significant among the calcium channel subunits. Each of its four repetitive domains is comprised of six transmembrane segments. Together, the α1 subunit domains give rise to the pore-forming region, selectivity filter, voltage sensor, gating apparatus, and the channel's functional binding sites. Therefore, the α1 subunit shapes the channel's primary biophysical characteristics and is sufficient to form a functional calcium channel (Zhang et al., 1993). To date, there are 10 known α1 subunits in mammals. $Ca_v3.1$ (α1G), $Ca_v3.2$ (α1H), and $Ca_v3.3$ (α1I) form T-type channels, and $Ca_v2.1$ (α1A), $Ca_v2.2$ (α1B) and $Ca_v2.3$ (α1E) are present at P/Q, N, or R-type channels. The remaining 4 subunits, $Ca_v1.1$ (α1S), $Ca_v1.2$ (α1C), $Ca_v1.3$ (α1D) and $Ca_v1.4$ (α1F), form the L-type calcium channels. One or more of the L-type subunits may be expressed in the bipolar cell.

Based on the observed properties of heterologously expressed $Ca_v1.2$ (Bourinet et al., 1994 ; Charnet et al., 1994), all L-type calcium channels had been thought to share the distinctive properties of the native cardiac calcium current, including activation at high voltages, high sensitivity to dihydropyridines (DHPs), slow activation and deactivation kinetics, and calcium-dependent inactivation (Ertel et al., 2000). Calcium currents mediated by $Ca_v1.1$ and $Ca_v1.2$ exhibit many of the classic L-type current characteristics. Compared to the native bipolar cell current, both channels are highly sensitive to DHPs, activate more slowly and at potentials 20-25 mV more depolarized, deactivate more slowly, and show strong calcium-dependent inactivation (Libscombe et al., 2004). These properties make both $Ca_v1.1$ and $Ca_v1.2$ unlikely candidates for the presynaptic calcium channels at the bipolar cell synapse.

On the other hand, $Ca_v1.4$, found at the rod photoreceptor ribbon synapse, does not exhibit the classic kinetic or pharmacological profile of the L-type channel and has similar kinetics and DHP sensitivity to the bipolar terminal calcium current. Heterologous expression of $Ca_v1.4$ indicates however, that the channel's inactivation is insensitive to calcium (McRory et al., 2004 ; Koschak et al., 2003). This is unlike the bipolar cell calcium current, which inactivates in a calcium-dependent manner, albeit slowly. Most similar to the native calcium current observed in bipolar cells is $Ca_v1.3$. It is less sensitive to DHPs than classic L-type channels, has a threshold of activation that is physiologically relevant in the retina, and shows little calcium-dependent inactivation when depolarized (Xu and Libscombe, 2001 ; Libscombe et al., 2004). The kinetic profile permits the channel to activate at subthreshold voltages and to mediate sustained calcium entry when the cell is depolarized. As the bipolar cell pre-synaptic terminal requires a similar kinetic and pharmacological profile to sustain rapid and long-lasting release, it is likely that $Ca_v1.3$ is the primary channel found in this cell type.

Previously detected in neuronal and endocrine cells (Catterall et al., 2003), $Ca_v1.3$ has been shown by immunostaining to be present in the outer and in the inner plexiform layers of the retina, where photoreceptor and bipolar cell terminals are located respectively (Morgans, 1999). $Ca_v1.3$ expression has also been shown at the chick hair cell ribbon synapse, where mounting evidence suggests it is responsible for sustained neurotransmitter release (Kollmar et al., 1997). Furthermore, studies in zebrafish hair

cells have revealed that a $Ca_v1.3$-like channel mediates release at the hair cell ribbon synapse. While the mammalian and avian genomes contain only one copy of the $Ca_v1.3$ gene, the zebrafish genome contains two genes both belonging to the 1.3 class, $Ca_v1.3a$ and Ca_v 1.3b (Sidi et al., 2004). As part of the extensive gene duplication in teleosts (Nordström et al., 2004), $Ca_v1.3$ apparently underwent duplication and subsequently diverged, giving rise to the paralogs $Ca_v1.3a$ and $Ca_v1.3b$. The zebrafish mutant Gem is deaf and imbalanced as a result of a loss of calcium influx at hair cell ribbon synapses. The mutated gene giving rise to the phenotype, Gemini, was shown to encode $Ca_v1.3a$, thus supporting this channel's role in sustained neurotransmission at the hair-cell ribbon synapse (Sidi et al., 2004). In the same study, $Ca_v1.3a$ expression was localized to the inner plexiform, inner nuclear and ganglion cell layers of the retina, whereas $Ca_v1.3b$ was localized to the outer plexiform and photoreceptor layers (Sidi et al., 2004). It is unclear, however, which of these paralogs might be expressed in the bipolar cell.

We used single-cell RT-PCR to determine if $Ca_v1.3a$ and/or $Ca_v1.3b$ transcripts are expressed in individual morphologically distinct bipolar neurons enzymatically dissociated from goldfish retina. We show that single bipolar cells express transcripts of the L-type calcium channel pore-forming subunits $Ca_v1.3a$ and/or $Ca_v1.3b$. Different combinations of $\alpha 1$ subtype expression may alter the specific function of the cell within the network.

Results

To characterize the molecular identity of the partial cDNAs obtained from goldfish retina, the predicted amino acid sequences were aligned with known zebrafish and mammalian sequences (Clustalw). The percent identity, based on the partial sequence, between goldfish $Ca_v1.3a$ and zebrafish $Ca_v1.3a$ is 95% and the percent identity to human $Ca_v1.3$ is 82%. The percent identity between goldfish $Ca_v1.3b$ and zebrafish $Ca_v1.3b$ is 82% and the percent identity to human $Ca_v1.3$ is 71% (NCBI BLAST). Figure 8 is an alignment across subunits and species of the II-III linker amino acid sequences (Clustalw). The shaded regions highlight amino acid motifs that are highly conserved in $Ca_v1.3a$ and $Ca_v1.3b$ across species. Though $Ca_v1.2$ shares similar

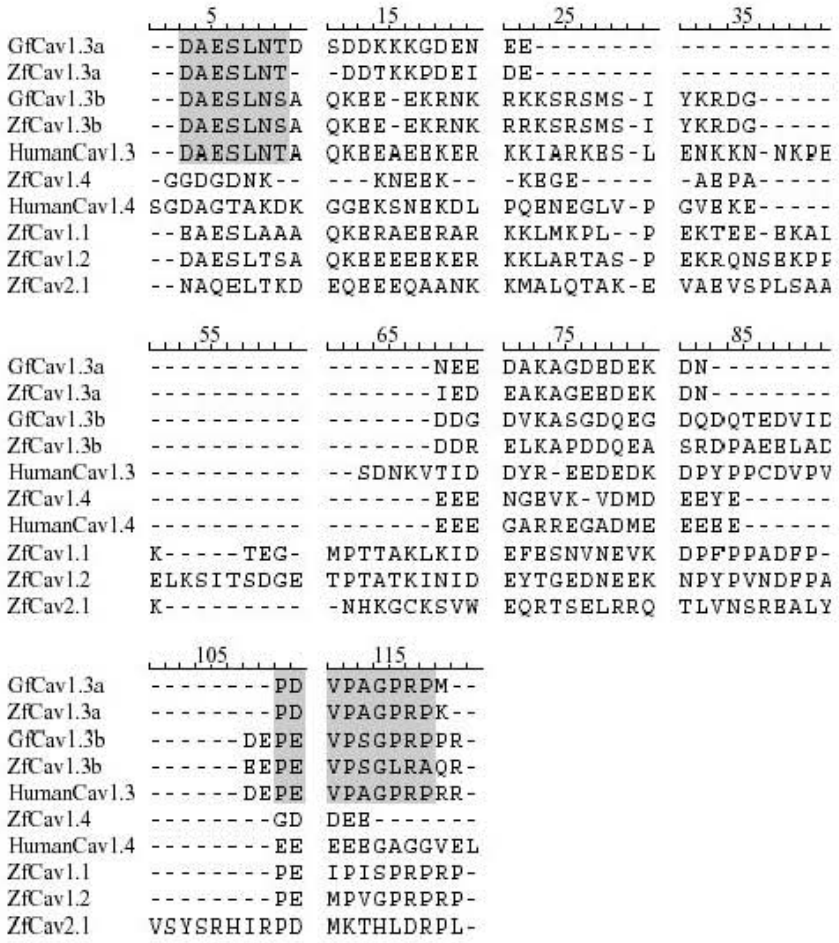

Figure 8. Alignment of II-III linker amino acid sequences across subunits and species (Clustalw). The shaded regions highlight amino acid motifs that are highly conserved amongst $Ca_v1.3a$ and $Ca_v1.3b$ across species. The zebrafish alpha1 subunits $Ca_v1.1$, 1.2, 1.4, 2.1 and human Ca_v 1.4 do not share the conserved motifs.

conserved motifs as $Ca_v1.3$, the overall homology between goldfish $Ca_v1.3a/b$ and zebrafish $Ca_v1.2$ is significantly lower compared to zebrafish $Ca_v1.3a/b$. Other $\alpha 1$ subunits such as $Ca_v1.1$, 1.4, 2.1 and 2.2 have low homology and do not share these conserved motifs. Therefore, we conclude that the subunits we have detected in goldfish are in fact orthologs of zebrafish $Ca_v1.3a$ and $Ca_v1.3b$.

To determine the subunits present in mixed bipolar cells, we utilized the single cell RT-PCR technique described in METHODS. Figure 9 shows an example of amplicons detected in the 2nd round of PCR for a single experiment. Each sample was collected in the order that it appears on the agarose gel. Lanes 1, 4, 6, 7, 9, and 10 are results from single bipolar cell cDNA synthesis. The remaining lanes show results of control experiments: lanes 2 and 11 are –RT control cells, lanes 3, 5, and 8 are bath-fluid +RT controls, and lane 12 is a no DNA (water) control. In this experiment, $Ca_v1.3a$ and $Ca_v1.3b$ were detected both individually and together in single cells. One bipolar cell expressed only $Ca_v1.3a$ (lane1), another expressed only $Ca_v1.3b$ (lane 7), and one cell expressed both $Ca_v1.3a$ and $Ca_v1.3b$ (lane 9). Experiments were included in the analysis only if all negative controls failed to yield PCR products and at least one sample was clearly positive for one or both subunits. PCR products of the correct size were gel-purified, subcloned in pGEM-T Easy, and sequenced, which confirmed the identity of the detected transcripts.

In 11 experiments that met the criteria, 25% of all cells collected were positive for $Ca_v1.3a$, $Ca_v1.3b$, or both. In 17 cells that were negative for both transcripts, the original RT sample was retested with another two rounds of PCR to determine if negative cells would become positive when retested. All 17 samples were again negative for both transcripts, which suggests that detection failure occurred at the RT stage.

Overall, $Ca_v1.3a$ or $Ca_v1.3b$ transcripts were detected in 18 bipolar cells. Figure 10 shows 16 of the 18 positive products, after two rounds of PCR. All amplicons were of the expected size except the $Ca_v1.3a$ amplicon detected in lane 11, which was smaller than the expected size of 577 bp. Sequencing revealed that the detected transcript in this case was in fact $Ca_v1.3a$, suggesting a possible splice variant. Figure 11A shows the percentage of the total number of positive cells expressing each $\alpha 1$ subunit: 33% expressed only $Ca_v1.3b$, 39% expressed only $Ca_v1.3a$, and 28% of cells expressed

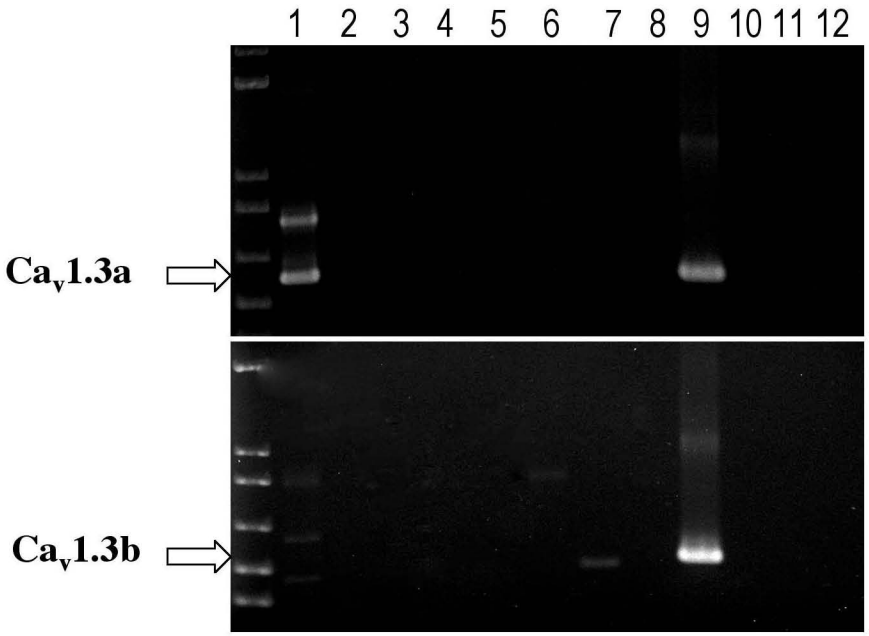

Figure 9. Calcium channel expression pattern in a single experiment. Gel electrophoresis of 2nd round RT-PCR products. 6 negative controls were included to eliminate the possibility of false positives (Lanes 2,3,5,8,11,12). Six bipolar cells were collected for subunit detection by RT-PCR (Lanes 1,4,6,7,9,10). Expected band sizes (indicated by arrows): $Ca_v1.3a$ - 577 bp, , $Ca_v1.3b$ - 512 bp. One cell expressed only $Ca_v1.3a$ (lane 1), one expressed only $Ca_v1.3b$ (lane 7), and one expressed both subunits (lane 9). On average across experiments, ~25% of all collected bipolar cells expressed one or more calcium-channel subunits.

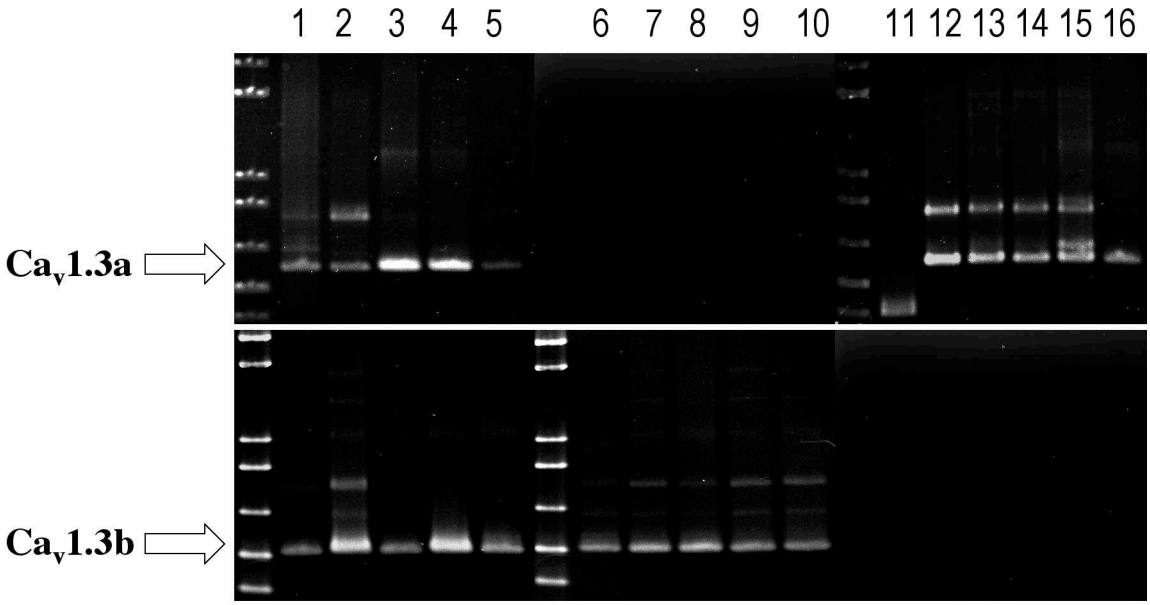

Figure 10. Bipolar cells express transcripts of Ca^{2+} channel subunits $Ca_v1.3a$, $Ca_v1.3b$, or both. Gel electrophoresis of RT-PCR products. cDNA from 16 of 18 positive cells are shown. Top panel shows $Ca_v1.3a$ PCR products. Bottom panel shows $Ca_v1.3b$ products. Bands that appear in the same lane in both the top and bottom panel indicate cells that express both subunits. Correct band size is indicated with an arrow. Sample number 11 is smaller in size than the rest of the $Ca_v1.3a$ products, but sequencing verified that this product is in fact $Ca_v1.3a$. It is unknown whether this represents a $Ca_v1.3a$ splice variant.

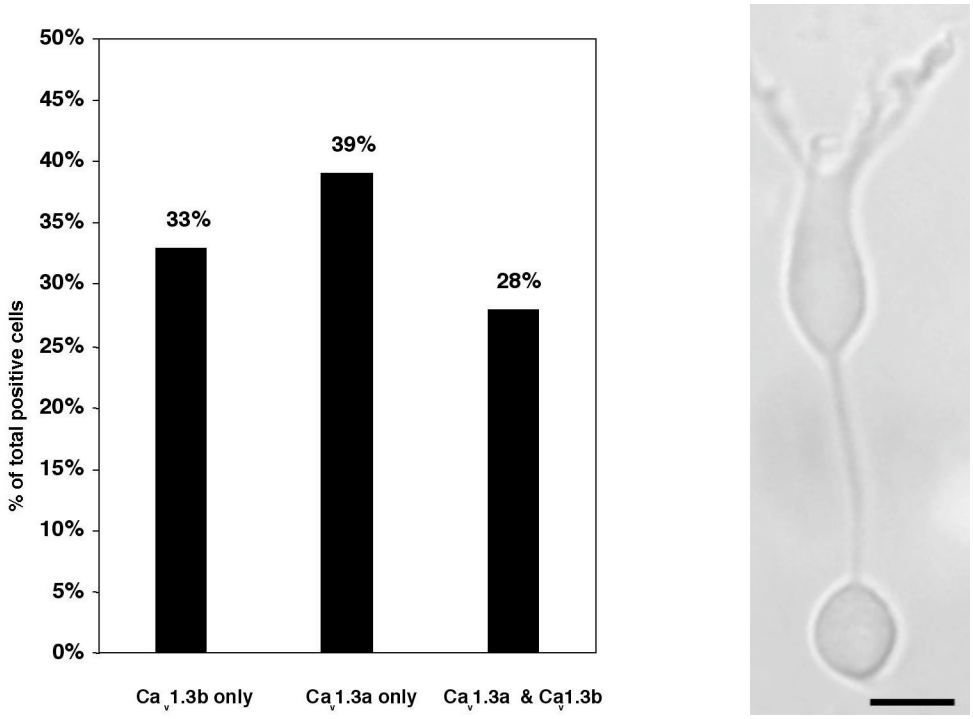

Figure 11. Goldfish bipolar cells form L-type Ca^{2+}channels composed of one or more subunits. A, Percentage of total positive cells expressing α1 subunits. Of the 18 cells positive for α1 subunits, 33% expressed only $Ca_v1.3b$, 39% expressed only $Ca_v1.3a$, and 28% expressed both subunits. B, Bright field image of an ON-type goldfish bipolar cell. Scale bar represents 10μm.

transcripts of both subunits. Figure 11B is a bright field image of an ON-type mixed bipolar cell harvested for single cell RT-PCR and treated as a –RT negative control. All of the cells sampled were large terminal mixed bipolars, and we did not examine small-terminal, presumptive cone bipolar cells.

Discussion

Using single cell RT-PCR, we have shown that mRNA transcripts of the L-type calcium channel subunits $Ca_v1.3a$ and/or $Ca_v1.3b$ are expressed in bipolar cells of the goldfish retina. Though mRNA expression does not always assure protein synthesis, the similarities between the bipolar calcium current and chick and mammalian IHC $Ca_v1.3$ currents support the conclusion that $Ca_v1.3a$ and/or $Ca_v1.3b$ are translated into functional proteins in bipolar cells. Whole-cell patch clamp experiments have revealed that the bipolar cell calcium current rapidly activates at low voltages and is less sensitive to DHPs compared to $Ca_v1.1$ and $Ca_v1.2$. Also, inactivation of the calcium current in bipolar cells occurs only after an extended depolarization and completes with a time course of several seconds, which is ~100-fold slower than in many other cells expressing L-type calcium channels (von Gersdorff and Matthews, 1996). Nonetheless, inactivation eventually takes place in a calcium-dependent manner, unlike heterologously expressed $Ca_v1.4$. These characteristics are most closely mimicked by the $Ca_v1.3$ - mediated calcium current recorded in mammalian and avian systems. Whole-cell patch clamp recordings of mouse IHCs reveal calcium currents reminiscent of the L-type current found in bipolar cells: rapidly activating at low voltages and slowly inactivating in a calcium-dependent manner (Platzer et al., 2000). In the same study, a $Ca_v1.3$ -/- mouse was generated to test the function of this L-type calcium channel subunit at the inner hair cell ribbon synapse. The null mouse lost 90% of its calcium current density, was resistant to DHPs and had congenital deafness (Brandt). In another study, $Ca_v1.3$ -/- mice exhibited reduced exocytosis in the organ of corti, indicating a direct role for $Ca_v1.3$ in neurotransmission (Brandt et al., 2003). These experiments provide evidence that $Ca_v1.3$ is the primary L-type calcium channel mediating neurotransmitter release at the IHC ribbon synapse. The

resemblance of calcium current characteristics among ribbon synapses of the cochlea and of the retina lends credence to the idea that $Ca_v1.3a$ and/or $Ca_v1.3b$ mRNA expression predicts functional protein expression in the goldfish bipolar cell.

In goldfish bipolar cells, approximately 90% of the whole-cell calcium current is generated by calcium channels residing in the synaptic terminal, and the remaining 10% arises from the soma (Heidelberger and Matthews, 1992). We found that at least some bipolar cells express transcripts for both $Ca_v1.3a$ and $Ca_v1.3b$ calcium channels, and it is possible that the two channel subtypes differ in subcellular localization, and thus in function. For instance, $Ca_v1.3a$ may be associated with synaptic ribbons and drive transmitter release, whereas $Ca_v1.3b$ may represent the somatic calcium current. However, the specific properties of $Ca_v1.3b$ are unknown, as is whether the two genes encode channels with functionally distinct properties. Our results suggest that subsets of bipolar cells may express either $Ca_v1.3a$ or $Ca_v1.3b$ alone, which raises the possibility of functionally distinct classes of bipolar cells that may differ slightly in calcium current characteristics. Clarification of these issues of isoform distribution both within and across cells awaits the availability of subtype-specific antibodies to localize the $Ca_v1.3a$ and $Ca_v1.3b$ alpha subunits in fish retina.

Chapter IV
Mobility and Turnover of Vesicles at the Synaptic Ribbon

Introduction

The ribbon synapse releases neurotransmitter continuously and at high rates (Sterling and Matthews, 2005; Moser et al., 2006). The ribbon itself is necessary for this process, as evidenced by severe disruption of neurotransmission at ribbon synapses in mutant animals whose ribbons do not localize properly at the active zone (Allwardt et al., 2001; Dick et al., 2003; Van Epps et al., 2004). The static snapshot provided by electron microscopy shows the ribbon surrounded by a halo of vesicles that are tethered by fine filaments to its surface, and at retinal ribbon synapses, these tethered vesicles may constitute the readily releasable pool that supports prolonged release (von Gersdorff et al., 1996; Mennerick and Matthews, 1996; Thoreson et al., 2004; however, see Midorikawa et al., 2007 for a contrary view). Despite their presumed importance in ribbon synapse function, however, the dynamics of these ribbon-associated vesicles have not been examined directly in living cells, leaving some basic questions unanswered. First, are vesicles associated with the ribbon truly immobile, or are they in dynamic equilibrium with vesicles in the cytoplasm? Second, can vesicles on the ribbon be released during depolarization? Third, once released, are ribbon-associated vesicles replenished from mobile cytoplasmic pools, or by local recycling of recently endocytosed vesicles? Fourth, to what extent is depolarization-triggered vesicle turnover spatially localized to the vicinity of the ribbon?

To approach these questions regarding vesicle dynamics, we labeled vesicles and ribbons in mouse retinal bipolar neurons with different fluorescent tags, whose specificity was confirmed by electron microscopy (EM). Then we photobleached vesicles in a subregion of a terminal and measured their mobility at two locations: near the ribbon and away from it. We found that the immobile fraction of vesicles is larger at ribbons than at

non-ribbon locations. Using EM, we observed photobleached vesicles attached to ribbons, which suggests that vesicles tethered to ribbons account for the excess immobile vesicles at ribbons compared to cytoplasmic locations. In the resting terminal, vesicles associated with the ribbon do not readily exchange with those in the cytoplasm, on a time scale of minutes. However, in the stimulated terminal, as vesicles leave the ribbon to fuse with the plasma membrane, they appear to be replenished with vesicles from the cytoplasm. Finally, turnover of photobleached vesicles triggered by depolarization occurred within an approximately diffraction-limited region around the ribbon location, which suggests that depolarization mobilized previously immobile vesicles that are very near, and probably attached to, synaptic ribbons. These experiments establish that vesicles are in fact immobilized near ribbons, from which they are released rapidly during depolarization.

Results

Visualizing synaptic ribbons

To label synaptic ribbons in the living neuron we used a fluorescent peptide that binds to RIBEYE (Zenisek et al., 2004), the main structural component of synaptic ribbons (Schmitz et al., 2000). Because previous experiments with the RIBEYE-binding peptide (Rpep) showed it to label ribbons in goldfish, we needed to determine if it also binds to ribbons in our experimental system, the mouse. Figure 12 shows that it does. When the peptide was introduced into a mouse bipolar cell via a whole-cell patch pipette placed on the cell body, it diffused down the axon and bound to synaptic ribbons, which were then seen as fluorescent spots in the terminals (Fig. 12). On average, there were 8 ± 0.6 fluorescent spots per terminal swelling (mean ± sem; N = 19) and 1-5 terminal swellings per cell (e.g., Figs. 12B-D). In addition, fluorescent spots were sometimes observed in the distal part of the axon. To confirm that the bright spots observed by confocal microscopy were in fact synaptic ribbons, we acquired confocal images of cells loaded with fluorescein-conjugated Rpep, then fixed and processed them for electron microscopy (EM). Figure 13 shows individual examples of the correspondence between

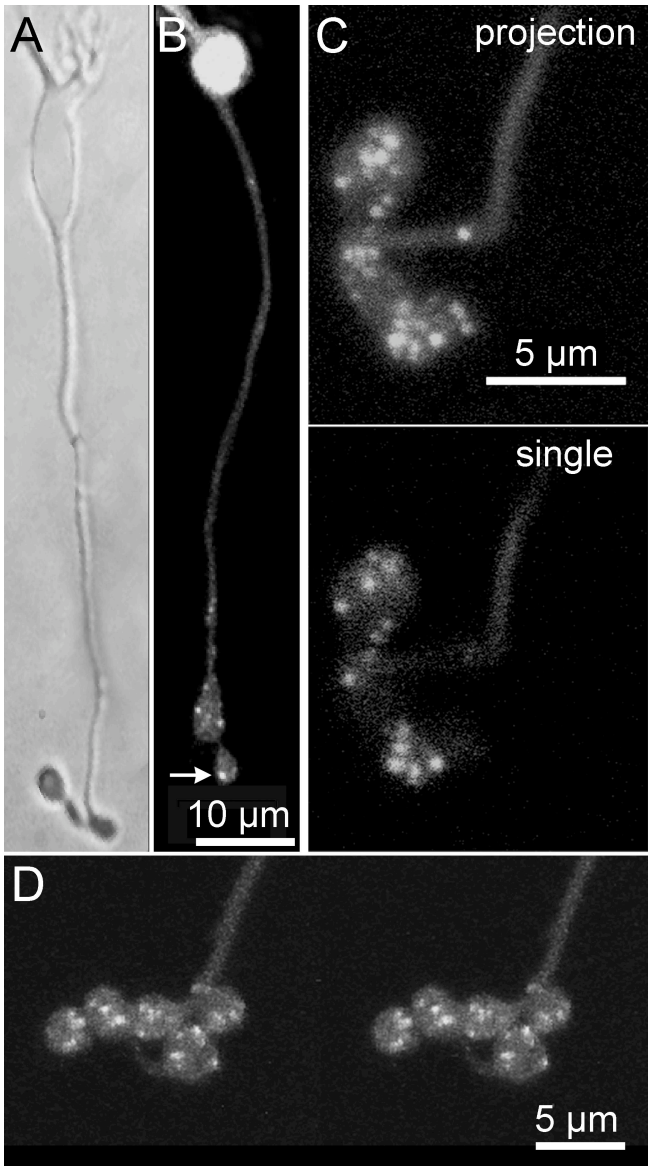

Figure 12. Fluorescent peptide with affinity for RIBEYE labels synaptic ribbons in live mouse bipolar cells. A, Bright-field image of an isolated mouse bipolar cell B, Confocal image of a different cell loaded with RIBEYE -binding peptide (Rpep). Bright spots (e.g., arrow) mark the positions of synaptic ribbons. C, Rpep-labeled bipolar cell terminal at higher magnification. Top panel shows a projection of a series of z-axis confocal optical sections through the depth of the terminal. Spots varied in size, suggesting that they might represent clusters with multiple ribbons. Bottom panel shows a single optical section of the same cell. D, A stereo pair showing a 3D reconstruction from optical sections through a bipolar cell synaptic terminal loaded with Rpep.

spots and ribbons. In Fig. 13A,B, a single thin section (~90 nm) for EM fortuitously caught three synaptic ribbons (black arrows, Fig. 13B) that were visible in the same locations in a single confocal optical section from the living cell (white arrows, Fig. 13A), despite the much greater thickness of the confocal section (~1.6 μm; Zenisek et al., 2004). Note that the more diffuse accumulations of Rpep fluorescence visible in Fig. 13A correspond to other ribbons located out of the focal plane (see full Z-axis projection in the inset). Figure 13C shows two additional fluorescent Rpep spots in the distal axon, with corresponding ribbons observed in EM below. In two cells, we obtained serial thin sections through the terminals and counted 11 and 23 unique ribbons visible by EM. In the same cells, the identical number of unique Rpep spots (11 and 23) were counted in 3D reconstructions from series of Z-axis optical sections through the terminals. Therefore, we conclude that in living mouse bipolar terminals (as in goldfish; Zenisek et al., 2004), Rpep fluorescent puncta accurately indicate the location and number of synaptic ribbons.

The number of ribbons counted by EM (maximum 23) in our experiments is lower than the 43 ribbons reported by Tsukamoto et al. (2001) in a mouse rod bipolar cell reconstructed by EM from serial sections of intact retina. In living cells, the maximum number of Rpep puncta we observed in a single cell (46) is similar to the EM count from intact retina (43), but ~20 puncta is more typical (e.g., Fig. 12C,D). Because the number of puncta per individual terminal bouton revealed by Rpep fluorescence (8 ± 0.6) is comparable to the number of ribbons per terminal swelling shown by Tsukamoto et al. (see Figure 2 of Tsukamoto et al., 2001), the reduced number of ribbons or Rpep spots in our cells likely arises from the typical loss of one or more distal terminal boutons during cell isolation.

Visualizing synaptic vesicles

To label synaptic vesicles we bathed bipolar cells in a solution of high K^+ plus the styryl dye, FM4-64 or FM1-43. After 90 seconds cells were washed in dye-free external solution containing Advasep-7 to destain the plasma membrane. Dye internalized during depolarization was restricted to the synaptic terminals and distal axon, and cells

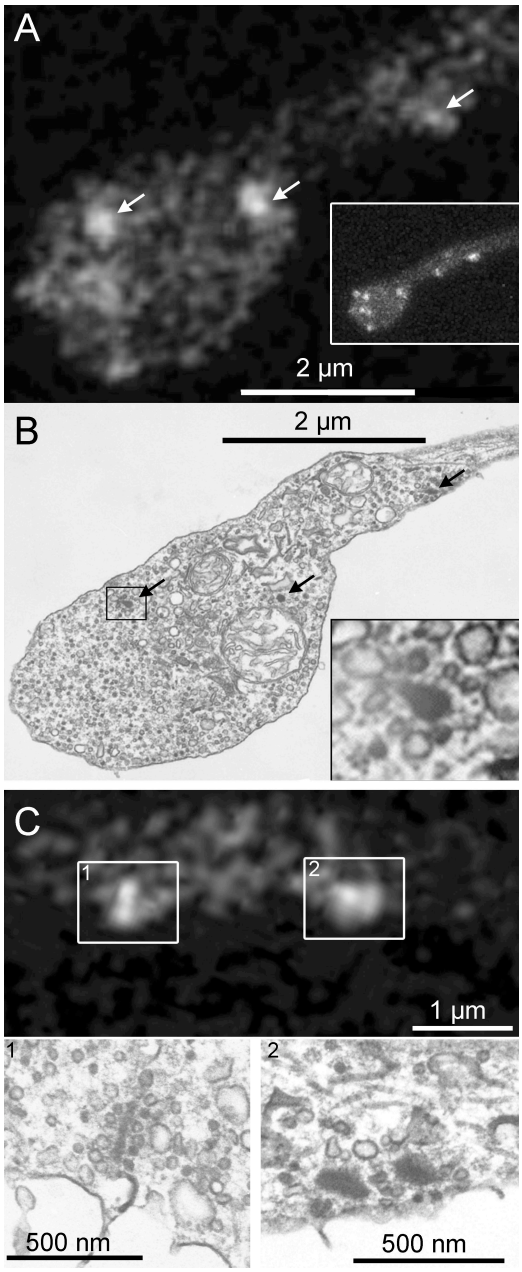

Figure 13. RIBEYE-binding peptide fluorescent puncta mark the location of synaptic ribbons in living mouse bipolar cells. A, Ribbon positions (arrows) in a live synaptic terminal revealed by fluorescein-Rpep labeling in a single confocal optical section. The inset shows a projection of a series of z-axis sections through the entire terminal to illustrate the positions of ribbons in other focal planes, which contribute some of the dimmer Rpep fluorescence in the single-section in the main panel. B, The same terminal fixed and photographed by EM. Arrows indicate ribbons, and the inset shows a magnified view of the ribbon marked by a rectangle. C, Top panel shows a single confocal section with labeled synaptic ribbons. Box 1 contains a labeled synaptic ribbon that appears elongated. The synaptic ribbon in the corresponding EM section, C1, also has an elongated, plate-like structure. Box 2 in the top panel contains a broad fluorescent spot, perhaps indicating the presence of two side-by-side synaptic ribbons. Indeed, the corresponding EM image (C2) shows two adjacent synaptic ribbons.

incubated in FM dyes without high K^+ did not accumulate dye, consistent with its activity-dependent uptake into recycling synaptic vesicles. However, it is possible that FM dye also accumulates in other endosomal structures. For instance, fused vesicle membrane in goldfish bipolar cell terminals is retrieved in large endosomes, which only later produce recycled synaptic vesicles (Paillart et al., 2003; Holt et al., 2003), and these large endosomes also take up and release FM dye upon stimulation (Coggins et al., 2007).

To identify the structures labeled by FM dye in our experiments, we photoconverted FM1-43 and examined the terminals by electron microscopy (Richards et al., 2000; Harata et al., 2001; Rea et al., 2004). The electron-dense photo-product marked structures that had accumulated FM1-43 during depolarization, and it was readily apparent that the dark structures resemble the surrounding unlabeled synaptic vesicles (Figs. 14A,B). Consistent with this visual impression, the size distributions of the labeled structures and unlabeled vesicles within a terminal were indistinguishable; mean diameter for both populations equaled ~33 nm (Figs. 14C,D). This confirms that FM dye fluorescence tracks the dynamics of synaptic vesicles and not large endosomes.

Because our goal was to measure the mobility of vesicles associated with the synaptic ribbon, we also examined whether recycled vesicles labeled with FM dye would re-enter the pool of vesicles attached to the ribbons. To preserve the contrast between labeled and unlabeled vesicles, lead and uranyl acetate staining of the ultrathin sections was omitted, leaving the ribbons pale but still distinguishable (Figs. 14E,F). Ribbons tethered mixtures of labeled and unlabeled vesicles, indicating that in these experiments labeled synaptic vesicles did indeed recycle back to the ribbons (Fig. 14F).

To examine explicitly the spatial relation between FM-labeled vesicles and synaptic ribbons, we introduced fluorescein-conjugated Rpep into cells via a whole-cell patch pipette (Fig. 15A) after loading cells with red-fluorescing FM4-64. Synaptic ribbons (green) and internalized FM4-64 (red) co-localized extensively in terminal boutons (Fig. 15B). Therefore, uptake of FM4-64 is associated with depolarization-triggered release and recycling of vesicles in the vicinity of ribbon-type active zones. The spatial profiles of ribbon and vesicle fluorescence, acquired approximately 10 min after activity-dependent loading with FM4-64, show that labeled vesicles remain closely

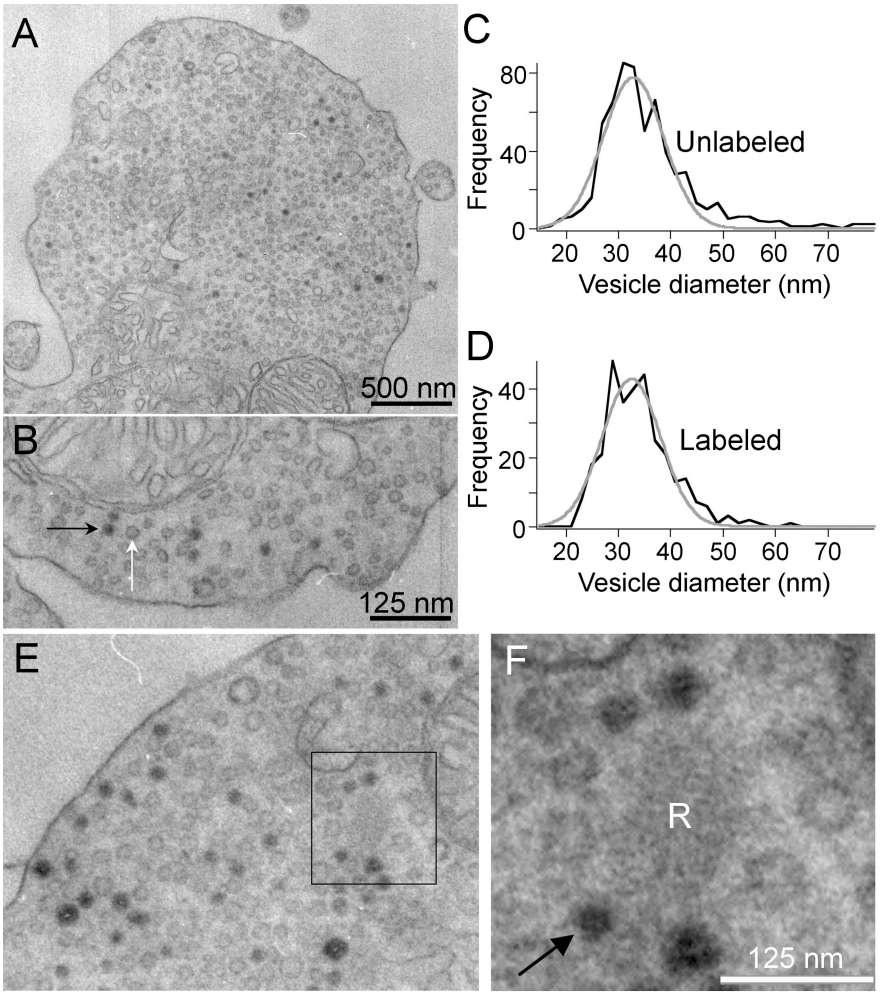

Figure 14. FM dyes taken up during synaptic activity label synaptic vesicles in mouse bipolar terminals. Depolarization-induced uptake of FM1-43 is visible in EM after photoconversion in synaptic vesicles. A, EM image of a synaptic terminal after photoconversion. Some vesicles are filled with dark reaction product. B, Higher magnification view of the same cell as A. Black and white arrows indicate labeled and unlabeled vesicles, respectively. Sections were not stained with uranyl acetate or lead. C, D, Size distributions of unlabeled and labeled vesicles were identical, with a mean diameter of 33 nm. E, F, Labeled vesicles recycle back to the synaptic ribbon. EM images of a mouse bipolar cell terminal after photoconversion of FM1-43. Black box identifies a synaptic ribbon shown at higher magnification in F. Sections were not stained with uranyl acetate or lead, and so ribbons are pale and filaments that tether vesicles to the ribbon surface are not visible.

associated with ribbons (Fig. 15B). Therefore, dye-labeled vesicles are spatially stable and do not readily diffuse along the terminal process. To determine directly the stability of synaptic ribbons and their associated FM-labeled vesicles, we imaged dual-labeled synapses at 10 min and again at 15 min after activity-dependent uptake of FM4-64 (Figs. 15C-E). Clusters of FM4-64 fluorescence (arrows, Fig. 15C) coincided with Rpep-labeled ribbons and remained at the same position over at least 5 min (compare red and black traces in Fig. 15D). Therefore, FM-labeled vesicles associate stably with synaptic ribbons on a time scale of several minutes.

We showed in Fig. 14 that some of the labeled vesicles are tethered to synaptic ribbons, which accounts in part for the stability of FM4-64 fluorescence at ribbon locations. However, the stable clusters of FM fluorescence were sometimes broader than the ribbon itself (e.g., Fig. 15E). The spatial extent of the ribbon (green trace, Fig. 15E) resembled the point spread function of the microscope, measured using 20-nm fluorescent beads, which is consistent with the submicroscopic size of ribbons in bipolar neurons. On the other hand, the full-width at half maximum of the ribbon-associated FM4-64 fluorescence was wider by ~1 μm than that of the ribbon fluorescence itself, which suggests that additional vesicles, beyond those attached to the ribbon, are stabilized in the vicinity of ribbons. In the next section, we describe experiments to examine the mobility of vesicles at both ribbon and non-ribbon locations within this stable cluster of ribbon-associated FM4-64 fluorescence.

The ribbon immobilizes vesicles

To measure the overall mobility of vesicles in the cytoplasm, we used FRAP. When fluorescent vesicles are bleached by focal application of intense excitation light, the bleached vesicles exchange with unbleached vesicles from surrounding regions, partially restoring the lost fluorescence (e.g., Gaffield et al., 2006; Rea et al 2004). The degree of recovery estimates the fraction of vesicles free to move, and the rate of recovery estimates vesicle mobility. We bleached a strip across part of a terminal bulb by scanning the subregion 5 times in 1 s with the exciting laser stepped up from its usual 5% of maximum intensity to 100%; then we tracked recovery of fluorescence in the bleached strip by re-imaging every 2 s. Recovery followed an exponential time course with a time

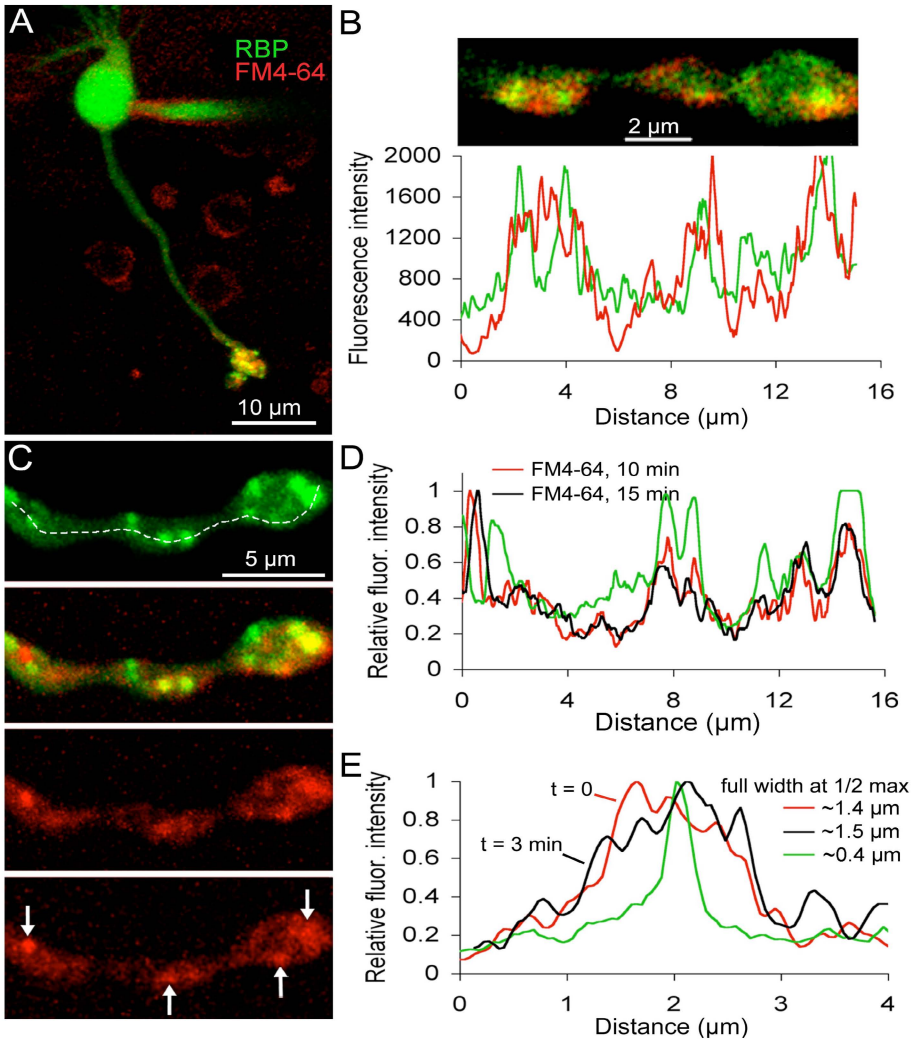

Figure 15. FM dyes taken up during synaptic activity concentrate near ribbons in live mouse bipolar terminals. A, Confocal image of a live bipolar cell loaded with FM4-64 (red) and RIBEYE-binding peptide (Rpep; green). The peptide was dialyzed via a whole-cell patch pipette visible on the cell body. The image is the z-axis projection of a series of confocal optical sections through the entire cell. B, Single confocal optical section of a live bipolar cell terminal loaded with FM4-64 (red) and Rpep (green). Cell was loaded with FM4-64 approximately 10 min before peptide dialysis and imaging. The graph below the image is the fluorescence intensity profile of the bottom half of the synaptic terminal (Fluoview software). The red trace indicates the fluorescence intensity of FM4-64 and the green trace indicates the fluorescence intensity of the peptide. C, Confocal image of a live bipolar cell axon and terminal loaded with FM4-64 (red) and Rpep (green). The top panel shows peptide labeling and the panel just below it shows the overlay of the peptide and FM4-64 fluorescence. The bottom two panels show FM4-64 labeling approximately 10 minutes and 15 minutes after activity-dependent loading with FM4-64, respectively. Arrows in the bottom panel indicate clusters of FM4-64 labeling that remained stable over time. D, Fluorescence intensity profile along the dashed line shown in panel C for Rpep (green trace) and FM4-64 10 minutes (red trace) and 15 minutes (black trace) after activity-dependent loading. E, Fluorescence intensity profile through a single synaptic ribbon (green) and FM4-64 labeling taken at t = 0 min (red) and t = 3 min (black). The full width at half maximum of the ribbon fluorescence is ~400 nm. The full width at half maximum of the cluster of FM4-64 fluorescence at 0 and 3 minutes is ~1.4 and 1.5 µm, respectively.

constant, t = 16.6 s in the example shown in Fig. 16A,B. This is similar to the FRAP time constant of ~20 s in similar experiments on goldfish bipolar cell synaptic terminals (Holt et al., 2004), but somewhat slower than in cone photoreceptor terminals (biexponential time constants ~2 s and 9 s; Rea et al., 2004). Taking into account the amount of total fluorescence lost during the bleach (see Methods), we estimated that ~50% of cytoplasmic vesicles were mobile. By comparison, the mobile fraction in cone photoreceptor synaptic terminals is estimated to be 87% (Rea et al., 2004), whereas it is ~0% at the neuromuscular junction (Henkel et al., 1996).

Next, we compared vesicle mobility in areas with a ribbon and without one, using cells loaded with FM4-64 and dialyzed with fluorescein-Rpep. A square region of interest (ROI), 0.5 μm x 0.5 μm, was centered on a well-isolated ribbon using Rpep fluorescence as a guide (Fig 16C; yellow square), and second ROI of the same size was placed in a neighboring ribbon-free zone (Fig. 16C; magenta square), with ~0.75 μm separating the centers of the two ROIs. The subregion containing the ROIs was then selectively bleached, and confocal scans were acquired every 2 s to simultaneously track the rate and fractional recovery in both the ribbon and non-ribbon ROI (Fig. 16D). Bleaching reduced fluorescence at both sites to ~20% of the pre-bleach intensity (12 cells), quenching the terminals' total fluorescence by an average of 38%. At the non-ribbon ROI, recovery was exponential (t =11.2 s), and the estimated mobile fraction, *m*, was 0.52 (Fig. 16D). Both measures from the small ROI are similar to the estimates of cytoplasmic vesicle mobility obtained when fluorescence in the entire bleached region was measured (Fig. 16B). At the ribbon ROI, recovery was similar in form (exponential) and time course (t = 13.5 s), but the estimated mobile fraction was significantly smaller (0.23; Fig. 16D).

The similar time constants at ribbon and non-ribbon ROIs suggest that both represent the mobility of free vesicles unattached to cytoskeletal elements. Because the effective voxel depth (~1.6 μm; Zenisek et al., 2004) is substantially larger than a ribbon, some of the fluorescence at a ribbon location comes from vesicles not associated with it, and we assume that this component has the same mobility as vesicles at non-ribbon sites. However, at ribbon sites, immobile vesicles represent ~80% of the vesicles *vs.* ~50% at non-ribbon sites. A simple interpretation is that the extra immobile vesicles at ribbon sites include those *attached* to the ribbon, like the labeled vesicles shown previously in Fig.

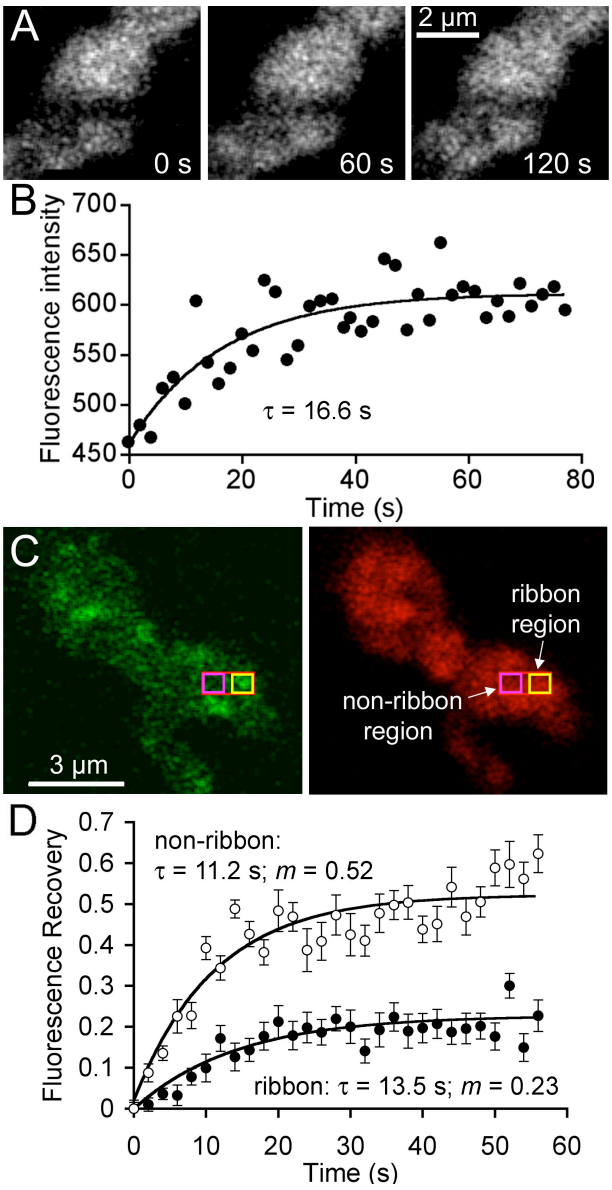

Figure 16. Vesicle mobility is reduced at synaptic ribbons. A, Confocal images of a terminal loaded with FM4-64 immediately after bleaching a stripe across the terminal (left), and after asymptotic recovery at 60 s (middle) and 120 s (right) after the bleach. B, Time course of fluorescence recovery in the bleached region shown in A. Curve indicates the best-fitting exponential rise. C, Terminal loaded with RIBEYE-binding peptide (left) and FM4-64 (right). Red rectangle indicates the photobleached region; yellow box shows where fluorescence was measured at a ribbon site; magenta box shows where fluorescence was measured at a non-ribbon site. D, Average fluorescence recovery at ribbon and non-ribbon sites in 12 cells. The mobile fraction of vesicles in the measured area surrounding the ribbon (filled circles) was 0.23, and the recovery t was 13.5 s. The mobile fraction at non-ribbon regions (open circles) was 0.52 and the recovery t was 11.2 s. On average, the initial bleach reduced fluorescence in the entire terminal by 38%. The recovery curves have been normalized accordingly (see Materials and Methods).

14F. Fluorescence recovery at ribbons remained steady at the asymptotic photobleached state for >60 s, indicating that the ribbon-tethered vesicles do not exchange with the cytoplasmic pool on a time scale of minutes, consistent with the stability of ribbon-associated FM4-64 fluorescence demonstrated in Fig. 15.

Stimulus-dependent changes in vesicle fluorescence at ribbons

What effect would depolarization have on the additional immobilized vesicles at photobleached ribbons (Fig. 16D)? If the releasable pool contains the ribbon-tethered vesicles (Mennerick and Matthews, 1996; von Gersdorff et al., 1996; Zhou et al., 2006), a depolarization sufficient to deplete the pool should cause bleached vesicles immobilized at ribbons to be replaced with some unbleached vesicles that entered the bleached zone during prior FRAP. This would stably increase fluorescence at sites with ribbons. To test this, we first needed to determine if ribbons remain competent for exocytosis after photobleaching of FM4-64 in a subregion of a terminal bouton. We bleached a ROI encompassing a ribbon and allowed asymptotic recovery. Then, after measuring fluorescence at ribbon sites in the bleached and unbleached region (see Methods), we briefly depolarized the cell under voltage-clamp to trigger exocytosis and re-measured the fluorescence. Figure 17A shows that bleaching did not affect the calcium current elicited by a 500-ms depolarization from –60 mV to 0 mV. Therefore, there was no detectable photodamage of the calcium channels that drive exocytosis. To monitor exocytosis, we measured the percentage of FM dye unloading triggered by the second of two post-bleach depolarizations at bleached and unbleached ribbons in the same terminal. In six cells, bleaching did not significantly affect the degree of stimulus-induced unloading in the bleached zone (bleached: -9.5 ± 2%, N = 11 ribbons; unbleached: -11.6 ± 1.7%, N = 19 ribbons; p=0.44 by two-tailed t-test). This suggests that bleaching FM4-64 to the degree used in our mobility measurements did not compromise the ability of ribbons in the bleached subregion to generate vesicle turnover in response to depolarization.

Armed with this information about the fusion competence of bleached ribbons, we returned to the question of the effect of the first post-bleach depolarization on the excess immobile vesicles at ribbon sites. A portion of a terminal loaded with FM4-64 was

photobleached, and after asymptotic recovery, 2-5 confocal images were acquired for measurement of FM4-64 fluorescence within 0.25-μm^2 ROIs centered on ribbons in both the bleached and unbleached subregions of the terminal. Then, we triggered release by a 500-ms depolarization and several seconds later measured the fluorescence at the same locations in 2-5 images. In the unbleached part of the terminal, FM-dye fluorescence at ribbons decreased after the stimulus (Fig. 17B), consistent with stimulation-dependent destaining (Betz and Bewick, 1993). However, in the bleached region, fluorescence at ribbons *increased* following the first post-bleach stimulus, which we interpret to indicate that bleached vesicles immobilized at ribbons were released during exocytosis and replaced by new vesicles that included fully fluorescent labeled vesicles.

To examine the stimulation-induced change in mobile fraction at ribbons, we measured the full FRAP time course at ribbons, in the same manner shown previously in Fig. 16C,D. In this set of experiments, summarized in Fig. 17C, the mobile fraction at the ribbon sites was 0.19, which is similar to the value estimated previously (see Fig. 16D). Subsequently, a 500-ms depolarizing stimulus (arrow, Fig. 17C) was given to trigger exocytosis, which caused a stable increase of normalized fluorescence intensity (from 0.19 to 0.36, on average) in the region containing the ribbon. Apparently, the stimulus released bleached vesicles immobilized at the ribbon — which were then replenished by a mix of labeled, unlabeled, and bleached vesicles from surrounding regions. This indicates that releasable vesicles are immobilized by the ribbon until depolarization triggers exocytosis.

Where with respect to ribbons does the stimulation-induced increase in FM4-64 fluorescence occur? To answer this, we examined the spatial profile of the increase in fluorescence triggered by the initial depolarization following asymptotic recovery from photobleaching. Figure 18A-B shows an example of the spatial pattern in an individual experiment in which 20 confocal images of FM4-64 fluorescence before stimulation were averaged (Fig. 18A) and compared with the average of 20 images at the same location after a 500-ms depolarization (Fig. 18B). After stimulation, fluorescence increased most

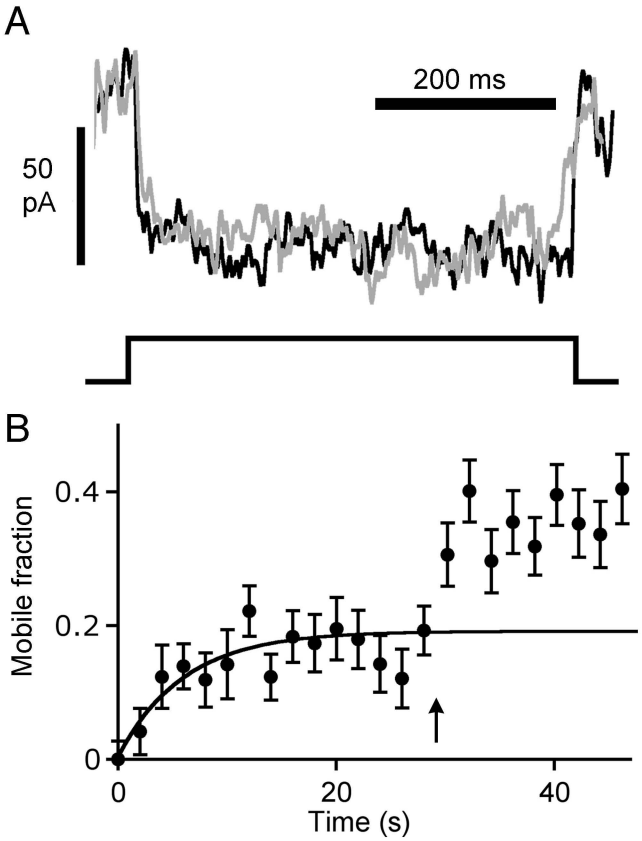

Figure 17. Effects of stimulation on FM4-64 fluorescence at synaptic ribbons. A, Voltage-dependent calcium current recorded from dissociated retinal bipolar cells before and after photobleaching. The gray trace is the average calcium current evoked by a 500-ms depolarizing pulse from –60mV to 0mV, recorded from five cells prior to photobleaching. The black trace is the average calcium current, recorded from the same five cells, after photobleaching FM4-64 fluorescence in a ribbon-containing region of the cell to ~ 25% of its initial intensity. Calcium current amplitude ranged from 40 pA to 100 pA, and bleaching had no effect on the current. B, At photobleached synaptic ribbons, the first post-bleach stimulus evoked an increase in FM4-64 fluorescence, but fluorescence decreased at unbleached ribbons. C, Recovery of fluorescence at ribbon locations after photobleaching at t = 0 (N = 8). The arrow marks timing of a 500-ms depolarizing pulse, which elicited a stable increase in mobile fraction from 0.19 to 0.36.

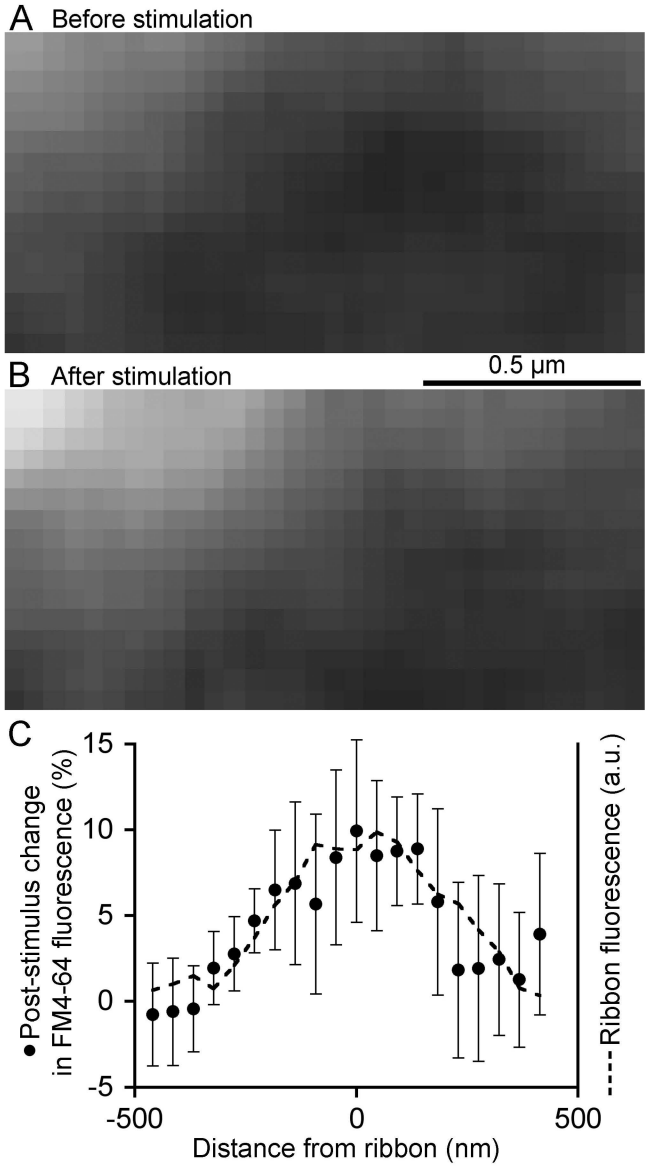

Figure 18. Bleached ribbon-associated vesicles are replaced after a depolarizing pulse. A, Confocal image of FM4-64 fluorescence near a ribbon, located at the upper left, after asymptotic recovery from a prior photobleach. B, Same region after a 500-ms depolarizing pulse. A and B are averages of 20 frames taken at 2-s intervals. C, Spatial profile of the average stimulation-induced change in FM4-64 fluorescence (filled circles) at 8 photobleached ribbons with respect to ribbon position. Dashed line shows the profile of the average Rpep fluorescence to mark the ribbon position. Distance is measured from the center of the Rpep fluorescence peak.

strongly at the ribbon position (upper left corner). Figure 18C presents the average spatial profile of the fluorescence change triggered by stimulation at 8 photobleached ribbons, measured parallel to plasma membrane. The stimulus-induced increase in FM4-64 fluorescence coincided with the ribbon location, which was marked by Rpep-fluorescein fluorescence (dashed line, Fig. 18C). This spatial pattern suggests that the bleached vesicles released upon depolarization reside at the same location as the ribbon, with both fluorescence profiles being limited by the point-spread function of the microscope. A simple interpretation is that the vesicles released by stimulation are the labeled vesicles observed to be attached to ribbons in EM (Fig. 14).

Discussion

The present experiments, by simultaneously visualizing both vesicles and ribbons in the living cell, have answered several basic questions about vesicle dynamics at ribbon synapses. First, absent a depolarizing stimulus, vesicles associated with the ribbon do not exchange dynamically with vesicles in the cytoplasm. Rather, they behave as though they are stuck firmly to the ribbon, like a tennis ball to Velcro, to be released only during exocytosis at the presynaptic active zone. Previous work on effects of the nonhydrolyzable ATP analog, ATP-gS, on capacitance responses in goldfish bipolar neurons (Heidelberger et al., 2002) suggested that vesicles in the releasable pool turn over slowly in the absence of stimulation, but did not directly connect the "releasable pool" with vesicles at ribbons. The present results explicitly establish that connection, by directly quantifying vesicle mobility and by relating reduced mobility selectively to visualized sites of ribbons.

Second, vesicles immobilized at ribbons do turn over during depolarization. Previously, an EM probe for release of ribbon-attached vesicles in the goldfish bipolar cell found no stimulus-induced change in overall vesicle density on ribbons and only partial depletion of vesicles near the plasma membrane (Holt et al., 2004), which calls into question whether vesicles on ribbons actually participate in release. Here, however, by photobleaching fluorescent vesicles at the ribbon and following their replacement

(during depolarization) with unbleached vesicles, we established that depolarization does in fact release immobilized vesicles at ribbon locations. This locus for vesicle fusion makes functional sense, given that the glutamate receptors mediating postsynaptic responses are located directly across the synapse from the ribbons (Brandstätter et al., 1996, 1997; Ghosh et al., 2001). Therefore, the ribbon ensures that release-ready vesicles will dock and fuse in the appropriate location relative to the postsynaptic receptors.

Third, we have shown that vesicles released at ribbons are replaced by vesicles from cytoplasmic pools, because fluorescence at ribbons *increases* after stimulation at photobleached ribbons, as bleached vesicles are replaced by fluorescent vesicles that entered the bleached area during recovery after photobleaching. The results also suggest that this stimulus-dependent turnover of immobile vesicles occurs at the ribbon (or very near it) because the increase in FM4-64 fluorescence elicited by depolarization at photobleached ribbon sites coincided with the diffraction-limited image of the ribbon itself (Fig. 18). EM analysis of FM-labeled synaptic terminals after photoconversion showed labeled vesicles immediately surrounding ribbons (Fig. 14), in position to be tethered to the surface of the ribbon. Plausibly, the release of this halo of ribbon-associated vesicles during depolarization accounts for the observed post-stimulus changes in FM4-64 fluorescence at ribbon sites, as shown schematically in Fig. 19. Prior to bleaching (Fig. 19A), mobile, labeled vesicles (red) and immobile, labeled vesicles (red, with anchor) are present in the cytoplasm surrounding the ribbon. Additional labeled vesicles are immobile because they are attached to the ribbon. At non-ribbon locations, the mobile fraction of vesicles is ~0.5, indicating that cytoplasmic mobile and immobile pools are approximately equal, whereas at ribbons the mobile fraction is ~0.2. Therefore, we conclude that mobile and immobile vesicles in the cytoplasm within 0.5 μm of the ribbon each constitute 20% of the labeled population. This leaves ~60% for the immobile vesicles attached to the ribbon.

Immediately after bleaching (Fig. 19B), most of the fluorescence is lost from the labeled vesicles (pink). With time, recovery from bleaching occurs as the mobile bleached and mobile unbleached vesicles equilibrate in proportion to their representation in the terminal as a whole. This is indicated in Fig. 19C by the appearance of two unbleached, labeled vesicles (red) and two bleached, labeled vesicles, accounting for the

recovery observed at ribbons. The immobile vesicles, both ribbon-attached and cytoplasmic, are fixed in place and make up ~80% of the total at the ribbon location. When depolarization evokes exocytosis (Fig. 19D), vesicles associated with the ribbon are released, allowing unbleached, labeled vesicles to attach to the ribbon. The result is what we observed: an increase in fluorescence after stimulation—as though the ribbon-attached vesicles were rendered "mobile" by the depolarization.

What does depolarization-triggered vesicle turnover at the ribbon imply about mechanisms of transmitter release at ribbon synapses? Following depolarization, the fractional recovery of fluorescence at ribbons increased by approximately 0.2, but this is only about one-third of the expected vesicles attached to ribbons (see above). This shortfall of stimulus-evoked increase in fluorescence has several possible interpretations: (i) repopulation occurs preferentially from the immobile, bleached vesicles near the ribbon, restricting the opportunity for repopulation by *un*bleached vesicles; (ii) unreleasable vesicles may be immobilized near the ribbon but not precisely coincide with it (e.g., Fig. 15E); (iii) some vesicles attached to the ribbon may be unreleasable. In support of the latter, Singer and Diamond (2006) also found the readily releasable pool in rat bipolar neurons was smaller than the expected number of vesicles per ribbon, consistent with partial participation of ribbon-attached vesicles in rapid release. If correct, this scenario would imply that the releasable pool includes a contribution from exocytosis at non-ribbon sites, as suggested for goldfish bipolar neurons (Zenisek et al., 2000; Coggins et al., 2007; Midorikawa et al., 2007). Our experiments were not designed to test for this possibility.

Our primary goal here was to determine if the vesicles attached to ribbons are stably immobile in the resting state and then released by stimulation. The results strongly support this conjecture: in mouse bipolar terminals, vesicles labeled with FM dye associate stably with synaptic ribbons and remain immobilized until released by depolarization. Furthermore, by directly visualizing the stimulus-induced turnover of ribbon-associated vesicles, we have established that the vesicles immobilized at the ribbon contribute a major fraction of the readily releasable pool.

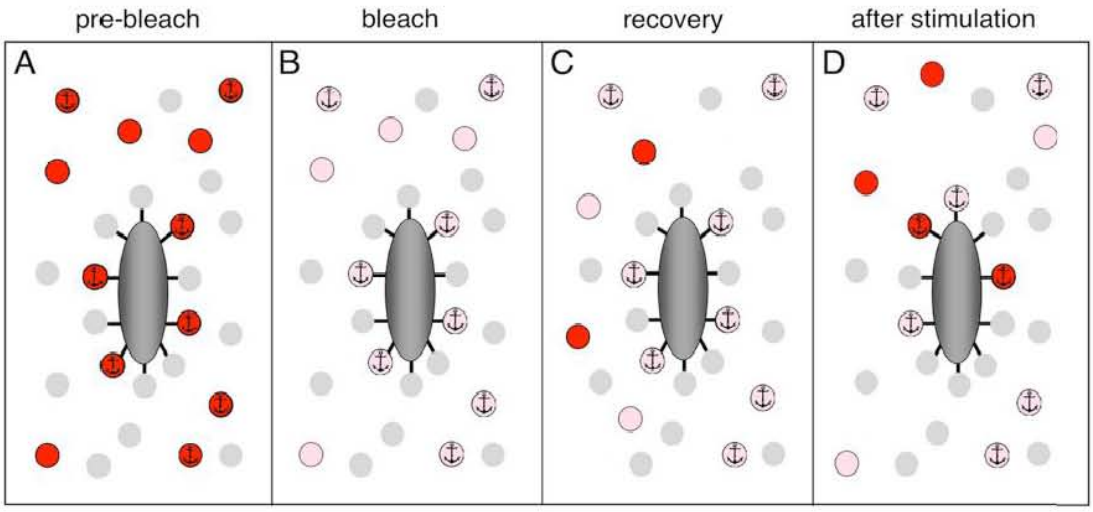

Figure 19. Schematic representation of fluorescence recovery after photobleaching and stimulation-induced recovery at a synaptic ribbon. A. The condition prior to photobleaching of vesicles labeled with FM4-64 (red). Immobile vesicles are marked with an anchor symbol. A subgroup of immobile vesicles is attached to the synaptic ribbon (dark gray). Unlabeled vesicles (light gray) are not visible in our experiments and are shown for completeness only. B. The condition immediately after photobleaching but before recovery. Pink indicates photobleached, labeled vesicles. C. After asymptotic recovery, mobile vesicles equilibrate between the bleached and unbleached regions of the terminal, restoring a fraction of the pre-bleach fluorescence intensity. D. After a depolarizing stimulus to release the vesicles attached to the ribbon, the bleached vesicles on the ribbon are replaced by a mixture of unbleached and bleached labeled vesicles, resulting in a further increase in fluorescence.

Chapter V
Vesicle Recycling at Ribbon Synapses in the Finely Branched Axon Terminals of Mouse Retinal Bipolar Neurons

Introduction

To conserve the readily releasable pool of vesicles in a presynaptic terminal, vesicle membrane inserted during exocytosis must be retrieved by compensatory endocytosis and then recycled to active zones as newly generated synaptic vesicles. Ribbon-type synapses in retina and inner ear, which are specialized for rapid and sustained exocytosis, might require specialized mechanisms of membrane retrieval to keep pace. Indeed, images from electron microscopy (EM) indicated that membrane recovery at ribbon synapses of goldfish bipolar neurons and frog saccular hair cells involves bulk endocytosis, where large endosomes pinch off from the plasma membrane and then produce synaptic vesicles (Lenzi et al., 2002; Paillart et al., 2003; Holt et al., 2003; LoGiudice and Matthews, 2007). This would be consistent with specialization of the endocytosis phase to match the high exocytotic load – quite different from the standard pathway of clathrin-mediated retrieval of single fused vesicles at conventional, non-ribbon synapses. The fish bipolar and frog hair cell showed no evidence for the canonical clathrin-mediated mechanism even though components of this pathway, including clathrin and dynamin, are expressed in some ribbon-containing neurons (Ullrich and Südhof, 1994; von Kriegstein et al., 1999, 2004; Sherry and Heidelberger, 2005).

But the goldfish bipolar neurons and frog hair cells were originally chosen for study because of their large size and huge reserve pools of synaptic vesicles (~900,000 in the goldfish terminal; von Gersdorff et al., 1996). So we wondered if these large reserves might allow bulk uptake to combine with leisurely replenishment of the releasable pool, whereas smaller terminals with smaller reserve pools might rely on the standard clathrin-

mediated mechanism. To answer this, we characterized compensatory endocytosis at a mammalian ribbon-containing neuron, the mouse retinal bipolar cell, whose terminal volume and reserve pool is more than 100-fold smaller than that of the goldfish. The small size led us to adopt a fluorescence imaging approach for physiological characterization of the vesicle cycle at individual ribbon-type active zones, using a fluorescent peptide to label ribbons and uptake of FM dyes to mark internalized vesicles. Then, we examined the same cell by EM after photoconversion of internalized dye to determine the ultrastructural basis of compensatory endocytosis.

In this way, we addressed several questions about the endocytotic limb of the vesicle cycle at mammalian ribbon-type synapses. First, is excess membrane retrieved at discrete locations within the terminal? If so, are these sites stable over multiple rounds of stimulation? Second, where is membrane recaptured with respect to ribbon-type active zones? Third, is membrane initially recovered in bulk or directly as single vesicles? Fourth, do new vesicles immediately enter the releasable pool? Fifth, does clathrin-mediated retrieval play a role in the vesicle cycle? If so, at what stage in the endocytotic pathway is it involved? We found that synaptic vesicles are retrieved near sites of vesicle fusion at least partly via a clathrin-mediated pathway. Thus, the size of the reserve pool may dictate whether compensatory endocytosis occurs in bulk or leads directly to production of new synaptic vesicles.

Results

"Hot spots" of membrane retrieval

To detect sites of membrane retrieval, we depolarized single bipolar cells by focally applying the styryl dye FM4-64 in high K^+ for several seconds. Approximately 12 s after the onset of stimulation, the cells were washed with a dye-free external solution containing Advasep-7 to eliminate plasma membrane fluorescence. Trapped FM4-64 was confined to the synaptic terminals and the adjacent axon (Fig. 20A), and was located discretely, suggesting that endocytosis occurred at distinct sites along the plasma membrane (Fig. 20B). To determine whether recovered membrane redistributes

throughout the cytosol or remains concentrated near the initial retrieval sites, we imaged the same terminals five minutes after application of Advasep-7 (Fig. 20B, right panel). The fluorescent spots were spatially stable over this interval, indicating that populations of recovered structures remained relatively close to their respective retrieval sites (Fig. 20C).

Are sites of endocytotic activity consistent over multiple stimuli? To address this question, we depolarized individual cells with focal superfusion of high K^+ plus FM4-64 and then washed with Advasep-7 to reveal the location of trapped fluorescence (Fig. 21A, top panel). Then, we bleached the FM4-64 fluorescence by exposing the cells to high intensity 543 nm laser light. The cells were then stimulated a second time with high K^+ plus FM4-64, and after 12 s, they were washed with Advasep-7 (Fig. 21A, bottom panel). The spatial fluorescence patterns produced by each stimulus were highly correlated, indicating that sites of activity-dependent endocytosis are consistent over at least two rounds of stimulation (Fig. 21B,C). Although the stimuli were separated by minutes, and the calcium currents remained comparable in amplitude, the increase in fluorescence after the second stimulus was on average ~ 30% less than after the first.

Membrane retrieval occurs near synaptic ribbons

In Figures 20 and 21, we showed that excess membrane inserted during exocytosis is retrieved at distinct sites along the membrane. Are these retrieval sites spatially related to "hot spots" of vesicle fusion? In retinal bipolar neurons, many of the exocytotic active zones are marked by the presence of synaptic ribbons (LoGiudice et al., 2008; Zenisek et al., 2008; Midorikawa et al., 2007). Therefore, by marking synaptic ribbons with a fluorescent peptide, and labeling recycling membrane with FM4-64, we could visualize the vesicle cycle with respect to individual active zones in the living cell (LoGiudice et al., 2008). To directly assess whether trapped dye concentrates near ribbons, cells were bathed in high K^+ and FM4-64 for 90 s and then washed with Advasep-7 to remove excess membrane staining. Subsequently, cells were dialyzed, via whole-cell patch pipette, with a fluorescent peptide that binds to the ribbon protein RIBEYE (RIBEYE-binding peptide, RBP). Sequential confocal scanning reveals that

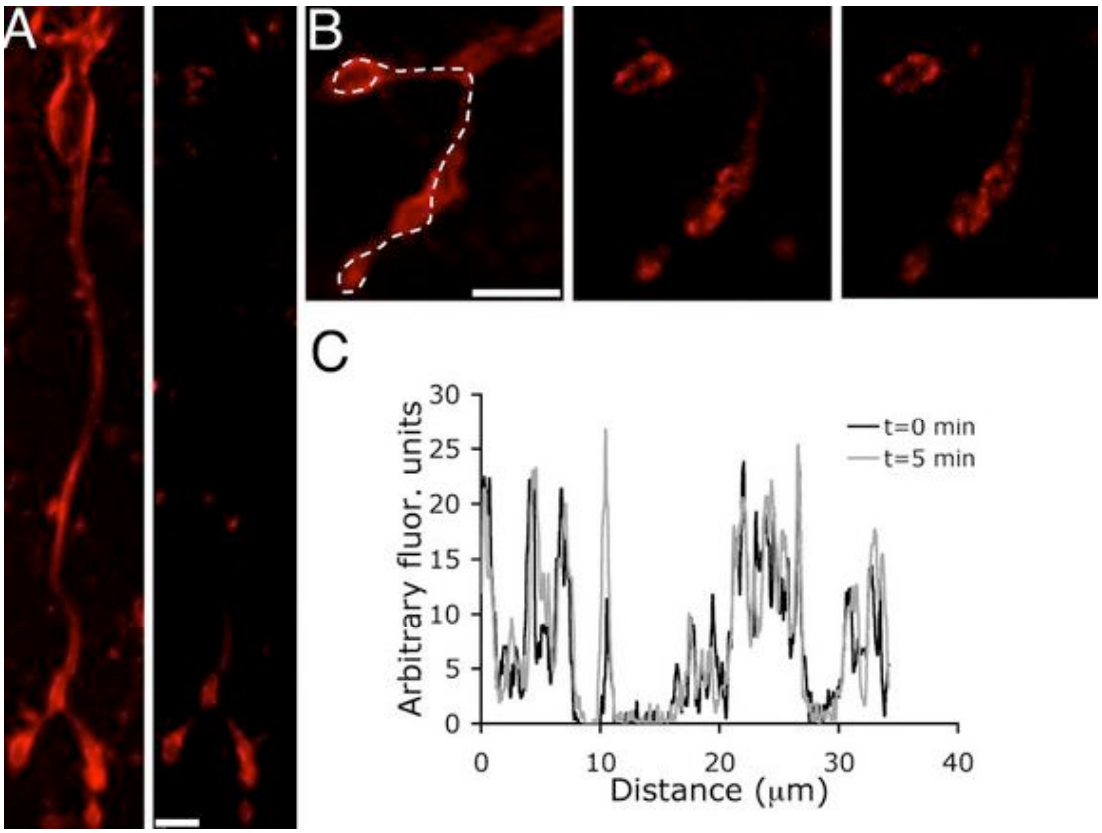

Figure 20. Activity-dependent membrane retrieval occurs at discrete locations within the terminal. The fluorescence profile remains stable over time. A, Confocal z-stack of a mouse bipolar cell that was stimulated with high K^+ plus FM4-64 (left panel). Cell was then washed with Advasep-7 to rapidly remove plasma membrane dye and expose trapped fluorescence (right panel). B, Zoomed-in images of the same terminals shown in A: before washing with Advasep-7 (left panel), immediately following Advasep-7 wash (middle panel), and five minutes later (right panel). C, Spatial profile under the dashed line in B of the fluorescence immediately following Advasep-7 (black trace) and five minutes later (gray trace).

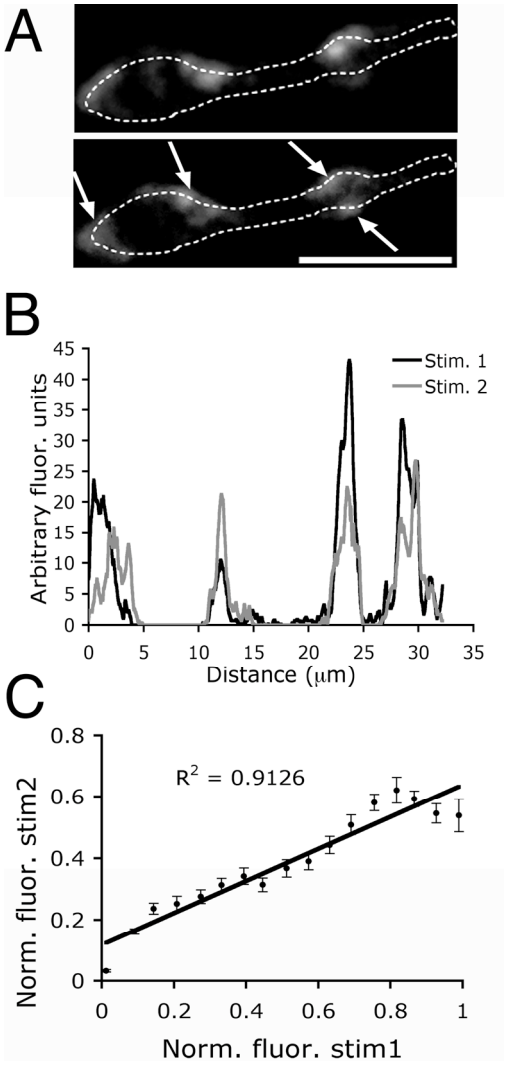

Figure 21. Membrane is retrieved at "hot spots" within the terminal. A, Terminals were briefly exposed to FM4-64 and high K^+ and then washed with Advasep-7 to reveal trapped dye (top panel). The dye was then bleached with 543-nm laser light. The cell was exposed to a second round of FM4-64 and high K^+ then washed with Advasep-7 (bottom panel). Scale bar represents 5.0 μm. B, Fluorescence intensity profile along the dashed line shown in A for the first (black) and second (gray) stimulus. Endocytosis occurs in similar positions after each stimulus. C, Graph illustrating the relationship between the fluorescence profiles after the first and second rounds of stimulation (total of 2042 points, n=4 cells).

trapped FM dye concentrates near synaptic ribbons within minutes of membrane recovery (Fig. 22A).

To resolve the position of retrieved membrane within ~15 sec of stimulus onset, cells were patch-clamped and dialyzed with the fluorescent peptide prior to introducing FM4-64 into the bath (Fig. 22B). The dye was then focally applied to a voltage-clamped neuron, and after achieving asymptotic intensity of FM4-64 in the membrane, the cell was presented with a 250-ms depolarizing pulse. FM4-64 was removed from the bath ~12 s after stimulation, and Advasep-7 was puffed onto the cell to remove residual external dye, leaving the fluorescence trapped in endosomes that were internalized during the post-stimulation interval (Fig. 22B,C). Similar to prolonged stimulation with high K^+, a single, short depolarization produced an increase in FM4-64 fluorescence at discrete locations within the synaptic terminals. The resulting spatial fluorescence profile of synaptic ribbons and FM4-64 fluorescence reveals that sites of membrane retrieval are highly correlated with the location of exocytotic active zones in the axon and axon terminals (Fig. 22D).

To compare the percent of the total fluorescence that is retrieved near and away from ribbons, the average FM4-64 fluorescence per pixel was measured within 750 nm of the plasma membrane in all regions of the terminal cluster, including ribbon and non-ribbon locations. This provided a normalization factor for the overall brightness of a particular cell. Then, the fluorescence per pixel was measured in a square 0.75 μm x 0.75 μm region of interest centered on a synaptic ribbon, defined by punctate RBP staining, and compared to the fluorescence per pixel at non-ribbon locations. The total area away from ribbons was approximately twice that of the area containing synaptic ribbons. The data graphed in Figure 22E show that across 10 cells containing 113 synaptic ribbons, the fluorescence per pixel at ribbons was 218 ± 18% of the average fluorescence per pixel for the entire terminal, but at non-ribbon locations the fluorescence per pixel averaged 46 ± 6% of the total fluorescence per pixel ($p < 0.001$). The result indicates that the primary sites of compensatory endocytosis are located near ribbon-type active zones.

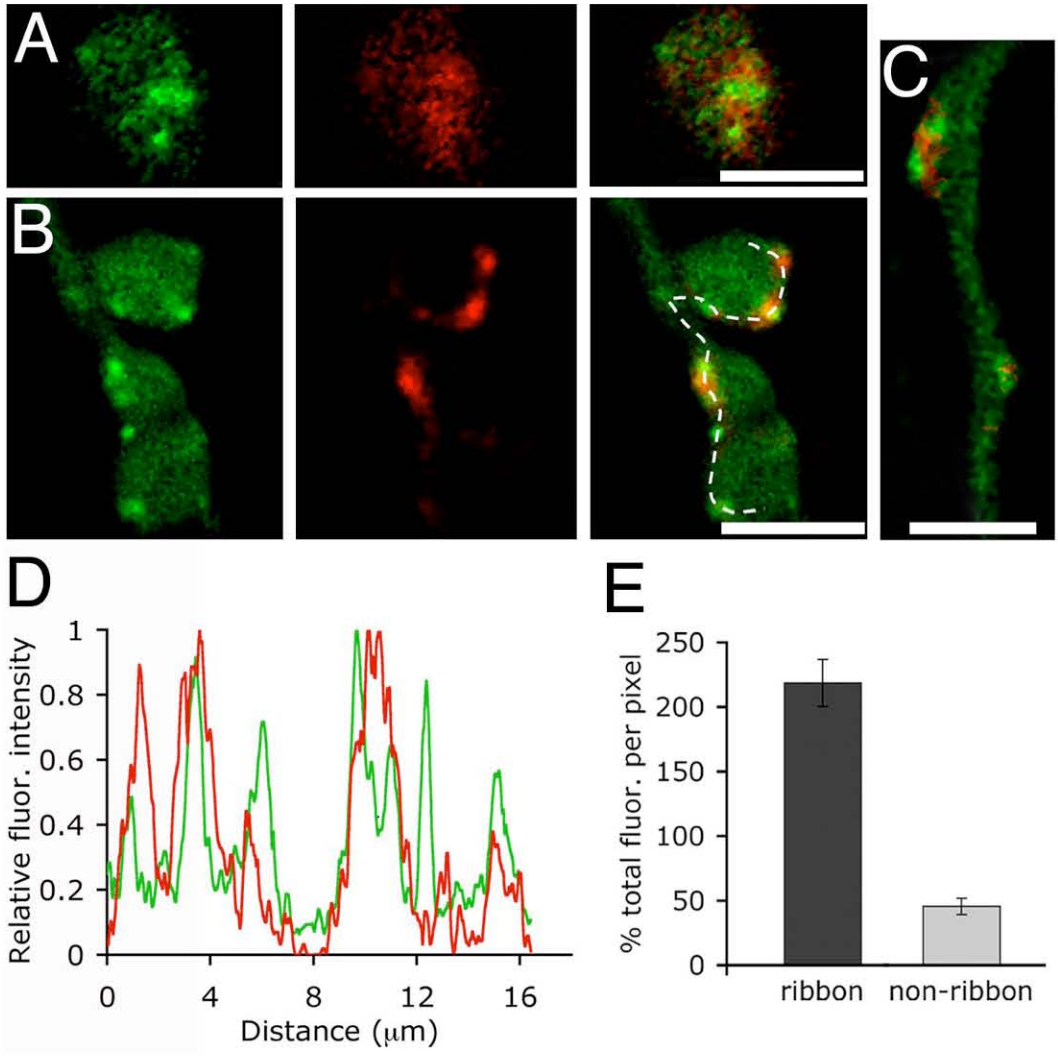

Figure 22. Sites of endocytosis correlate with the position of synaptic ribbons in the axon and terminals. A, Confocal images of a live bipolar cell loaded with FM4-64 (red) and RIBEYE-binding peptide (green). To load recycling vesicles, cells were bathed in a high K^+ solution containing 20 μM FM4-64 for 90 s and washed with Advasep-7. The last panel is an overlay of the red and green channels. Scale bar represents 2.5 μm. B, Confocal images of a different terminal loaded with RIBEYE-binding peptide (green) via a patch pipette and depolarized from a holding potential of -60 mV to 0 mV for 250 ms in the presence of FM4-64. Dye was removed after ~12 seconds, and the cell was washed with Advasep-7 to expose the location of trapped dye (middle panel). Far right panel is the overlay. Scale bar represents 5.0 μm. C, FM4-64 labeling (red) also concentrates around axonal ribbons (green). Scale bar represents 2.5 μm. D, Fluorescence intensity profile of synaptic ribbons (green) and FM4-64 (red) along the dashed line shown in B. E, Graph showing the percent total FM4-64 fluorescence per pixel at ribbon and non-ribbon locations within the axon and terminals ($p < 0.001$, n=10 cells). See text for a description of the measurement procedure.

Evidence for direct retrieval of synaptic vesicles

Following brief or sustained stimulation, compensatory endocytosis in goldfish bipolar cell terminals relies heavily on bulk-membrane retrieval (Paillart et al., 2003; Holt et al., 2003). In mouse bipolar cells however, single vesicles, not large endosomes, are most frequently labeled with FM1-43 after prolonged stimulation (LoGiudice et al., 2008). To clarify further whether membrane is retrieved in large bites or as single synaptic vesicles, we depolarized cells that were exposed to FM1-43, fixed, photoconverted, and prepared them for electron microscopy. In strongly stimulated terminals that were repetitively depolarized with local superfusions of high K^+ over the course of five minutes, the majority of photoconverted product was contained within single synaptic vesicles with a mean diameter of ~33 nm (Fig. 23A,F). In total, ~20% of vesicles were labeled after 5 minutes of repetitive stimulation with high K^+, including a subset that recycled back to synaptic ribbons (LoGiudice et al., 2008). To examine retrieval after brief stimulation, cells were patch-clamped and fixed following a single 250-ms depolarizing voltage-clamp pulse. After brief depolarization, photoconverted product also localized to structures with a size distribution equivalent to that of synaptic vesicles (Fig. 23E,F). A single 250-ms stimulus resulted in the labeling of ~5% of the total vesicle population, and even with such brief stimulation, a small number of labeled vesicles appeared to be associated with synaptic ribbons (Fig. 23D), suggesting immediate entry of at least some recently recycled vesicles into the releasable pool.

The immediate appearance of labeled synaptic vesicles in the releasable pool argues for direct production of vesicles during endocytosis, rather than bulk membrane retrieval of large endosomes that later give rise to synaptic vesicles, as was described in goldfish bipolar neurons (Paillart et al., 2003; LoGiudice and Matthews, 2007). To examine this in more detail, we depolarized cells with superfusion of high K^+ and then fixed during the stimulus to capture the early phases of membrane retrieval. By EM, the plasma membrane of these neurons was crenellated, with numerous omega-shaped invaginations that are similar in size to synaptic vesicles (Fig. 23B, C). Large invaginations were not observed budding from the plasma membrane and labeled cytosolic structures were equivalent in size to synaptic vesicles. The results suggest that

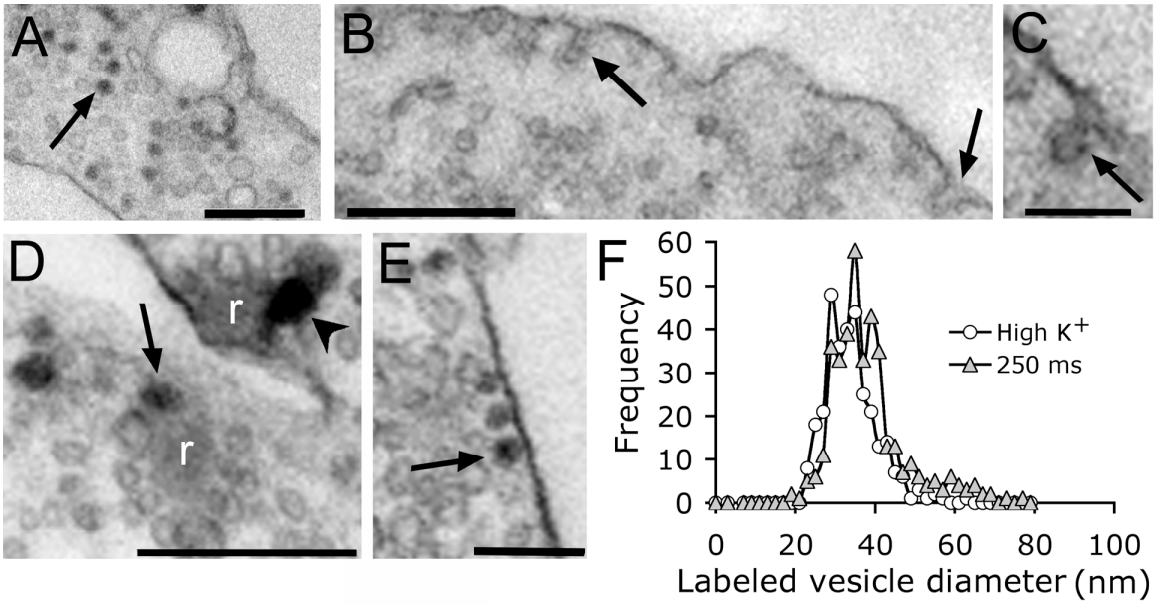

Figure 23. EM analysis of photoconverted FM1-43 reveals that single synaptic vesicles are retrieved in response to brief and prolonged stimulation. A, EM image of a mouse bipolar cell synaptic terminal loaded with FM1-43 in the presence of high K^+. Cells were fixed and then photoconverted. Sections were not stained with uranyl acetate or lead citrate in order to preserve the native contrast between photoconverted and unlabeled vesicles. Dark spots indicate vesicles filled with FM1-43 (e.g., arrow). Scale bar represents 0.5 μm. B and C, Cell was fixed before removing high K^+ from the bath. B, The plasma membrane appears crenellated with omega-shaped invaginations (arrows). Scale bar represents 0.25 μm. C, High magnification image of a budding vesicle. Scale bar represents 0.1 μm. D, EM image of two synaptic ribbons (r) in a cell that was patch clamped and then stimulated with a single 250-ms depolarization. The cell was fixed shortly thereafter and photoconverted. Arrow points to a synaptic vesicle that appears to have recycled back to the ribbon. Scale bar represents 0.25 μm. A larger structure appears adjacent to the other ribbon (arrow head). E, Three labeled synaptic vesicles docked at the membrane (arrow). Scale bar represents 0.125 μm. F, Size distribution of labeled vesicles in cells stimulated with high K^+ (triangles) and a 250-ms depolarizing stimulus (circles). Mean diameter is ~33 nm. Vesicle size was measured in NIH Image.

under both strong and weak stimulus conditions, the principal mechanism of endocytosis in mouse bipolar neurons involves the retrieval of single synaptic vesicles rather than large endosomes.

Evidence for clathrin-mediated retrieval

A candidate mechanism for such direct retrieval of synaptic vesicles is clathrin-mediated endocytosis, which involves the formation of coated pits and coated vesicles that can be recognized in EM images. However, in the experiments using photoconverted FM dye to label vesicles, presented above, we omitted staining of sections with uranyl acetate and lead citrate in order to preserve the contrast between labeled and unlabeled vesicles. As a result, the low contrast of the unstained sections made it difficult to detect clathrin coats on nascent endocytic profiles in stimulated terminals. Therefore, to better distinguish clathrin cages, we fixed cells in the absence of FM dye and changed our EM protocol to include uranyl acetate and lead citrate staining of the EM sections. In this material, coated pits and coated vesicles were commonplace in stimulated terminals and were frequently detected near synaptic ribbons (Fig. 24). From this, we conclude that clathrin is involved in the initial stages of retrieval in mouse bipolar neurons, similar to synaptic vesicle recycling at conventional synapses.

The GTPase dynamin is thought to play a crucial role in the pinching off of clathrin-coated pits from the plasma membrane to form internalized coated vesicles (Koenig and Ikeda, 1989; Takei et al., 1998; Sweitzer and Hinshaw, 1998; Henley et al., 1999). To determine if dynamin is enriched in synaptic terminals of mouse bipolar cells, we immunolabeled isolated cells using an antibody against dynamin-1. We found intense dynamin immunostaining specifically in the synaptic terminals (Fig. 25A), which is consistent with our EM evidence suggesting an important role for clathrin-mediated endocytosis in membrane retrieval after bouts of exocytosis. To obtain functional evidence that the high level of dynamin at the mouse bipolar cell synapse is important for synaptic vesicle endocytosis, we used the dynamin inhibitor dynasore (Macia et al., 2006), which has previously been shown to strongly block endocytosis at synapses of

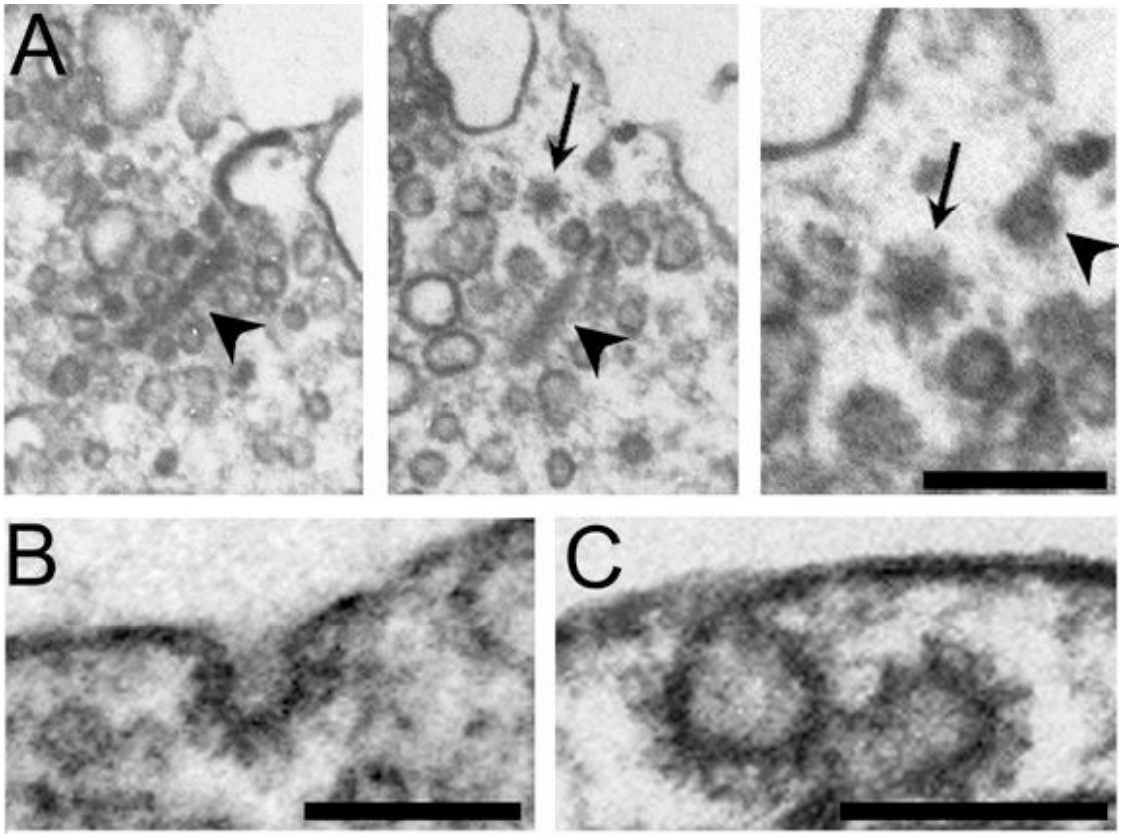

Figure 24. Clathrin-coated vesicles in mouse bipolar neurons. A, Serial EM sections of a cell that was patch-clamped and held at –60 mV, then fixed ~30s after the patch pipette was removed. The left panel shows a synaptic ribbon (arrow head). The middle panel is the next section in the series and shows a cytoplasmic clathrin-coated vesicle (arrow) adjacent to the synaptic ribbon (arrow head). The panel on the right is a higher-magnification view of the coated vesicle in the middle panel. Another structure, also visible in the left and middle panels, seems to be budding from the membrane (arrow head). B, EM image of a clathrin-coated vesicle budding from the plasma membrane. The cell was stimulated with high K^+ for ~30 s and fixed before removing high K^+ from the bath. C, EM image of multiple clathrin coated vesicles in the process of budding. Same cell as in A. Scale bars in A-C represent 0.125 μm.

cultured hippocampal neurons (Newton et al., 2006). In bipolar cell terminals that were exposed to 80 μM dynasore prior to and during stimulation, FM4-64 fluorescence remained associated with the plasma membrane of the terminal (Fig. 25B), whereas control cells from the same preparation showed the normal pattern of dye internalization (Fig. 25C). This is consistent with inhibition by dynasore of the scission stage of endocytosis. Curiously, however, the plasma membrane of dynasore-treated terminals continued to fluoresce 8-10 min after removing the dye from the bath (Fig. 25B). By contrast, unstimulated control terminals treated similarly lost plasma fluorescence within seconds after removing external FM dye, as expected from the rapid exit of the dye from the external membrane leaflet. The fact that dynasore-treated terminals did not similarly destain indicates that the FM dye was trapped in an internalized compartment, yet remained close to the plasma membrane.

To identify the basis of the trapped, membrane-associated fluorescence, cells that were stimulated in the presence of AM1-43 and dynasore were fixed and photoconverted approximately three minutes after stimulation, and then prepared for EM. Ultrastructural inspection uncovered a likely explanation for the unusual dye retention near the plasma membrane. Much of the AM1-43 photoproduct was contained within membrane-bound structures that appeared to be arrested in the budding phase of retrieval (Fig. 25D) and often remained connected to the plasma membrane via a thin neck (examples are shown in the inset of Fig. 25D). No similar labeled structures were observed in the cell body of stimulated, dynasore-treated bipolar neurons (Fig. 25E) or in the axon (not shown), which indicates that the membrane-associated structures are specifically related to membrane retrieval at the synapse. In dynasore-treated terminals fixed 3 minutes after stimulation, there were 0.71 ± 0.10 labeled vesicles per μm of terminal perimeter that were attached to the plasma membrane (mean ± s.e.m.; 15 terminals in 6 thin sections from 2 cells), but in control cells exposed only to DMSO, the average number of labeled vesicles associated with the membrane was 0.1 ± 0.04 vesicles per μm of terminal perimeter (mean ± s.e.m.; 7 terminals in 5 thin sections from 2 cells; $p<0.005$). Therefore, dynasore inhibits the complete internalization of vesicles during compensatory endocytosis at the synapse, but apparently at a stage *after* the interior of the endocytosed vesicle is no longer connected

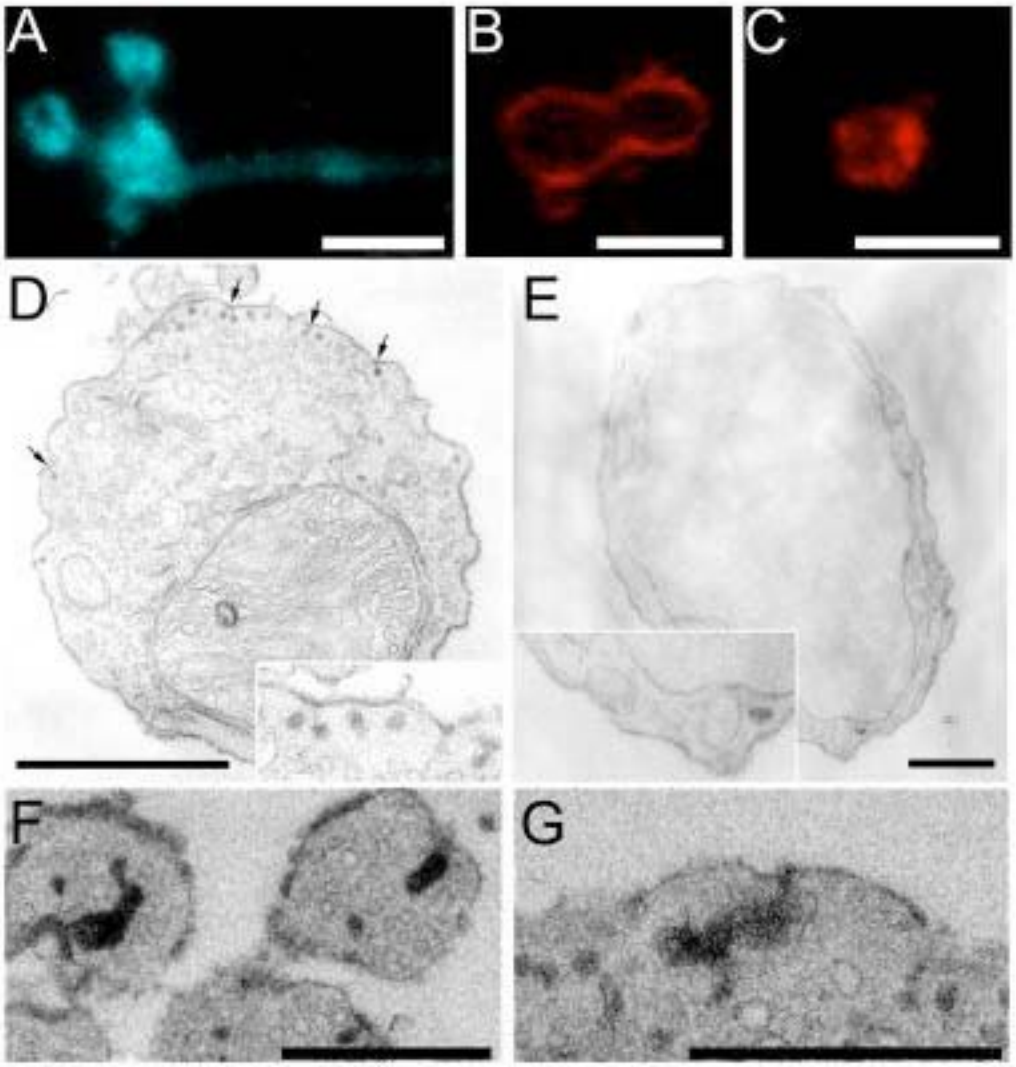

Figure 25. Membrane retrieval is modified when dynamin GTPase is inhibited by dynasore. A, Confocal image of an isolated mouse bipolar cell terminal immunolabeled with an antibody against dynamin-1. B, C, Confocal images of terminals briefly stimulated by high K^+ in the presence of FM4-64. Control cells were bathed in buffer containing 0.16% DMSO (C) and experimental cells were bathed in buffer containing 80 μM dynasore dissolved in 0.16% DMSO (B). Images were taken ~5.5 min after stimulation. Dye appears to be trapped at the membrane in cells exposed to dynasore, while control cells internalized the dye. Scale bars in A-C represent 5.0 μm. D, EM image of a cell exposed to 80 μM dynasore and stimulated with a 3-s puff of high K^+ in the presence of AM1-43. Cell was fixed ~ 3.0 min after stimulation and subsequently photoconverted. Synaptic vesicles containing photoconverted AM1-43 appear "stuck" on the membrane (arrows). Scale bar represents 1 μm. Inset shows a higher-magnification view of some of the labeled structures. E, The cell body of the same bipolar neurons shown in A lacks structures containing photoconverted AM1-43. Scale bar = 1 μm. F, G, Large structures containing photoconverted AM1-43 appear to be attached to the plasma membrane. Scale bars represent 0.5 μm.

to the extracellular space. Otherwise, the dye would not have been trapped, and the vesicles would not have been marked with dark photoproduct.

In addition to the synaptic vesicle-like structures attached to the membrane, larger endocytic structures were also observed to be associated with the membrane in dynasore-treated terminals. Figures 25F and 25G show EM images of terminals that were stimulated in the presence of AM1-43 and dynasore, and then fixed and photoconverted 3 minutes later. Larger, irregular structures appeared near the membrane in dynasore-treated terminals, and these complex structures also contained photoproduct from AM dye that did not destain during the 3 min interval between dye removal and fixation. In stimulated terminals exposed to dynasore, the density of large labeled endosomes (>100 nm in the longest dimension) was $0.59 \pm 0.13/\mu m^2$ (15 terminals in 6 thin sections from 2 cells), compared with $0.09 \pm 0.09/\mu m^2$ in DMSO control cells (7 terminals in 5 thin sections from 2 cells; $p<0.05$). The formation of these large endosomes may also reflect inhibition by dynasore of the normal process of budding and pinching off membrane in bites the size of synaptic vesicles. The overall density of labeled endosomes of all sizes was not significantly different in dynasore-treated and control terminals (control: $8.4 \pm 2.5/\mu m^2$; dynasore: $13.4 \pm 1.9/\mu m^2$). Therefore, dynasore does not block endocytosis *per se* in mouse bipolar cell synapses, but seems to arrest the process of complete separation from the plasma membrane and release of newly formed vesicles.

Discussion

Direct recycling vs. bulk endocytosis

We have found that mouse bipolar cell terminals retrieve the membrane added during neurotransmitter release by direct recovery of small synaptic vesicles. This scheme contrasts with goldfish bipolar cells and frog saccular hair cells, where membrane is primarily recovered by means of large endosomes (Lenzi et al., 2002, Holt et al., 2003, Paillart et al., 2003), which later give rise to synaptic vesicles (LoGiudice and Matthews, 2007). Thus, compensatory endocytosis in mouse bipolar cells more closely resembles endocytosis in neurons containing conventional active zones, such as retinal amacrine

cells (Paillart et al., 2003; LoGiudice and Matthews, 2007). Furthermore, recently recycled vesicles were found to be associated with synaptic ribbons, even after brief stimulation, which indicates that at least some newly retrieved vesicles are reused quickly in mouse bipolar cells.

What accounts for the different endocytic mechanisms used in terminals of goldfish vs. mouse bipolar neurons? Perhaps the key is simply the relative volume of the synaptic terminals, and hence the size of the pool of preformed synaptic vesicles held in reserve. For comparison, Figure 26 shows examples of isolated mouse and goldfish bipolar neurons, filled with fluorescent RBP to reveal cell shape and mark ribbons in the terminals. In agreement with reconstructions of bipolar neurons from EM images of serial sections of mouse retina (Tsukamoto et al., 2001), dissociated mouse bipolar cell somata are ~5 μm in diameter, and their synaptic endings consist of a spray of small boutons 1.5-2.5 μm in diameter (Figs. 26A and 26C). In contrast, goldfish bipolar cell bodies are >10 μm in diameter, and their bulbous terminals are 10-14 μm across (Figs. 26B and 26D). The giant terminals of goldfish bipolar neurons contain up to 900,000 synaptic vesicles (von Gersdorff et al., 1996), which is >100-fold more than in single terminals of mouse bipolar cells. Therefore, mouse bipolar cells depend more strongly on immediate resupply of new synaptic vesicles to maintain the pool of releasable vesicles, while goldfish bipolar cells can rely on their large pool of pre-existing vesicles to replenish the releasable pool.

Comparison of the degree of labeling of the total vesicle population after stimulation of the two cell types supports this interpretation. We found here that even a single 250-ms depolarization under voltage clamp labels ~5% of the total vesicle population in mouse bipolar cell terminals, but in goldfish terminals, repetitive stimulation for >10 min with dozens of calcium action potentials—each lasting ~200 ms (Zenisek and Matthews, 1998)—caused labeling of only ~10% of the total vesicle pool (Paillart et al., 2003). This demonstrates directly that immediate recycling of synaptic vesicles is more significant for the small terminals of mouse bipolar cells than the large terminals of goldfish bipolar cells.

Immediate recycling of synaptic vesicles, without bulk retrieval, also occurs in ribbon synapses of cone photoreceptors from lizard retina (Rea et al., 2004), even though

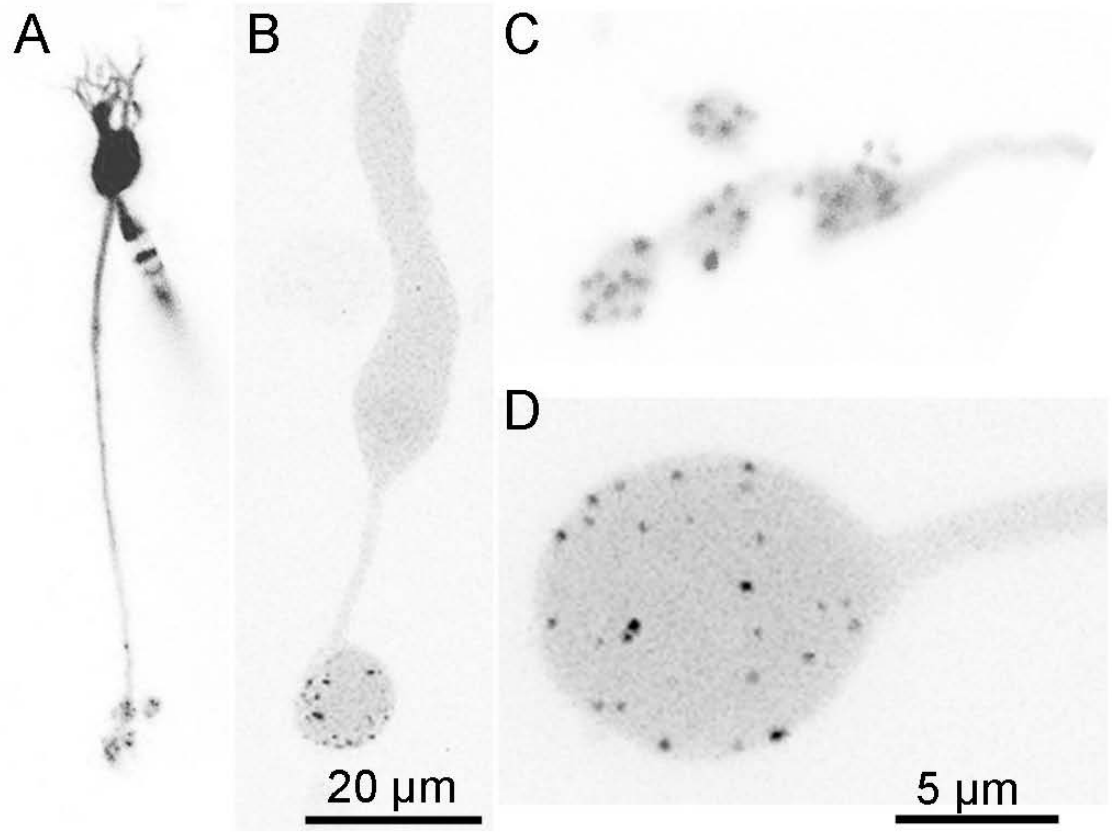

Figure 26. Comparison of synaptic terminals of living bipolar neurons isolated from mouse and goldfish retina. Cells were filled via a whole-cell patch pipette with fluorescein-conjugated RBP and imaged using confocal microscopy. Images are z-axis projections of optical sections through the entire cell. A, An isolated mouse bipolar neuron. The patch pipette is visible, attached to the cell body. B, An isolated goldfish bipolar neuron at the same magnification as A. The patch pipette was removed in this instance prior to imaging. Scale bar applies to A and B. C, Mouse bipolar cell terminal boutons at higher magnification. Different cell from A. D, Goldfish bipolar cell terminal at the same magnification as C. Different cell from B. Scale bar in D applies to C.

these terminals contain large numbers of vesicles (~250,000; Rea et al., 2004), much like goldfish bipolar cell terminals. Why, then, do cones not use the more leisurely approach to vesicle retrieval that appears to be used in goldfish bipolar neurons? In darkness, cones are depolarized and have a high rate of ongoing vesicle release, which is reduced in a graded manner to encode light intensity during illumination (Choi et al., 2005). However, ON-type bipolar cells, like the giant-terminal cells of goldfish, produce a transient burst of release at the onset of depolarization, followed by slower sustained release (von Gersdorff et al., 1998; Singer and Diamond, 2003). Therefore, cones have unusually high demand for vesicle resupply compared to bipolar cells, and their synaptic terminals are specialized in a number of ways to ensure that high release rates can be sustained in darkness. For example, synaptic ribbons in photoreceptors are much larger than in bipolar neurons (Sterling and Matthews, 2005), and they tether many more immediately releasable vesicles. In addition, cones have only a small reserve pool of vesicles, and nearly all of their large stock of vesicles are rapidly mobile and participate in the vesicle cycle (Rea et al., 2004). So, we suggest that in addition to terminal size, the requirements for continuous release can also dictate the use of an immediate recycling scheme in ribbon synapses.

Clathrin-mediated endocytosis

Retrieval of single synaptic vesicles is mediated by a clathrin-dependent pathway in conventional synapses (Heuser and Lennon, 1973, Takei et al., 1996, Shupliakov et al., 1997, Granseth et al., 2006), and in keeping with this mechanism, we frequently observed clathrin-coated vesicles budding from the plasma membrane in mouse bipolar cell terminals following stimulation. Also, we found that the dynamin inhibitor, dynasore, modified the endocytotic process. Ultrastructural examination of dynasore-treated terminals revealed AM1-43-labeled structures the size of synaptic vesicles that were suspended in the budding phase of endocytosis, indicating a role for dynamin in the recovery of membrane added during synaptic exocytosis. In addition, some labeled vesicles that were fully internalized were also observed in terminals exposed to dynasore, which may indicate that block of dynamin by dynasore was incomplete in our

experiments. Alternatively, the fully internalized vesicles in the presence of dynasore may reflect a dynamin-independent form of endocytosis operating in parallel, such as the mechanism described at the rat calyx of Held by Xu et al. (2008).

The incidence of large pleiomorphic invaginations attached to the membrane also increased significantly in cells exposed to dynasore. What process might give rise to these structures? One possibility is that they reflect a GTP-dependent form of bulk retrieval that occurs normally but is too rapid to be caught using standard chemical fixation, but is revealed when dynamin is inhibited by dynasore. However, any such large endosomes formed by bulk retrieval in the normal endocytic process would also need to be very rapidly broken up into synaptic vesicles, since our photoconversion experiments detected label only in objects the size of synaptic vesicles, even under conditions of brief stimulation and rapid fixation (Fig. 23F). It seems unlikely, then, that the large structures observed in the presence of dynasore represent a normally occurring process. An alternative explanation is that excess membrane that is unable to pinch off when dynamin is inhibited accumulates in some instances beneath the surface, resulting in the formation of large invaginations.

Endocytosis occurs at hot spots near ribbons

In addition to the mechanism of membrane retrieval, we have addressed several questions about the location of compensatory endocytosis in mouse bipolar cells. First, compensatory membrane retrieval, visualized with FM4-64, occurs at discrete locations within axons and synaptic terminals. By optically tracking FM dye over time, we showed that recaptured membrane remains concentrated near retrieval sites over the course of several minutes. Moreover, sites of membrane retrieval were consistent over multiple rounds of endocytosis, indicative of endocytotic “hot spots” in mouse bipolar cell synaptic terminals.

Second, the hot spots of compensatory retrieval are spatially correlated with the position of synaptic ribbons, a structural hallmark of exocytotic active zones in bipolar neurons (LoGiudice et al., 2008, Zenisek et al., 2008). Previously, EM images in photoreceptor cells and hair cells supported the idea that excess membrane inserted during fusion is locally recycled near synaptic ribbons. In cone and rod photoreceptors,

retrieved vesicles appeared to form on the membrane lateral to synaptic ribbons (Gray and Pease, 1971; Sterling and Matthews, 2005), and in frog hair cells, elongated omega profiles and clathrin-coated pits were observed adjacent to synaptic bodies (Lenzi et al., 1999). However, the sites of membrane retrieval had not been directly visualized in living ribbon synapses. By concurrently visualizing fluorescently labeled synaptic ribbons and FM4-64 uptake in living neurons, we have shown that sites of endocytosis are indeed related to synaptic ribbon locations and hence, active zones. This is analogous to the layout of retrieval sites in the frog neuromuscular junction, where sites of vesicle fusion and endocytosis are closely associated in space (Heuser, 1983; Roos, 1999; Teng et al., 1999; Teng and Wilkinson, 2000). Thus, local recycling at active zones is a shared feature of conventional and ribbon-type synapses.

Chapter VI
Conclusion

Synaptic vesicles in ribbon-containing neurons are continuously released and retrieved. In this dissertation, I have explored the dynamic processes influencing vesicle exocytosis and endocytosis at ribbon-type synapses in mouse bipolar neurons. In particular, I have discussed the calcium channels that drive release at active zones, the mobility and turnover of vesicles with respect to synaptic ribbons, and the sites and mechanisms of compensatory retrieval in the nerve terminal.

Glutamate release in ribbon-containing neurons is driven by calcium influx through L-type calcium channels with unusual activation and inactivation kinetic profiles for L-type channels. These features, attributed to specific channels including the $Ca_v1.3$ isoforms expressed in goldfish bipolar neurons (LoGiudice et al., 2006), allow the L-type channels to rapidly modulate sustained neurotransmitter release (von Gersdorff and Matthews 1996; Mennerick and Matthews 1998). These channels cluster just beneath the synaptic ribbon, in close proximity to the release machinery (Roberts, Jacobs et al. 1990; Heidelberger and Matthews 1992; Issa and Hudspeth 1994; Llobet, Beaumont et al. 2003; Zenisek, Davila et al. 2003) and as a result, docked, ribbon-associated vesicles are poised for rapid release when calcium channels open. Thus, it is likely that synaptic ribbons immobilize a pool of vesicles for calcium-triggered release.

The idea that synaptic ribbons enhance the size and accessibility of the readily releasable pool of vesicles has long been assumed though the ribbon's precise function remains unresolved. We sought to determine if the synaptic vesicles attached to ribbons are indeed immobilized in the resting neuron and then released by stimulation. Our results demonstrate that in mouse bipolar cell terminals, synaptic vesicles associate stably with ribbons and remain immobile until stimulus-triggered released. By directly visualizing the stimulus-induced turnover of ribbon-associated vesicles, we have shown that the vesicles tethered to the ribbon contribute a major fraction of the readily releasable

pool (LoGiudice et al., 2008). Only a portion of the total immobile fraction was released in response to stimulation; therefore, we cannot definitively conclude that all of the vesicles on the ribbon are releasable.

Since synaptic ribbons are found in cells that release neurotransmitter tonically, it has long been assumed that the ribbon provides a steady supply of synaptic vesicles to the active zone to allow for continuous release of transmitter quanta. Consistent with this view, the size of ribbons and the number of ribbon-associated vesicles correlate across cell types with the physiological needs of the synapse. For example, in the retina, rod and cone photoreceptors have the largest ribbons, in keeping with their high need for ongoing exocytosis at a rapid rate. Also, there is a tonotopic map of ribbon surface area in the cochlea, with hair cells in high-frequency regions having larger ribbons that tether more vesicles. It is surprising, then, that recent work points to greater importance of ribbons for transient, synchronous release than for the sustained release that is, after all, the hallmark of ribbon-containing synapses. There is at present no satisfactory resolution to this contradiction, but to us, it seems unlikely that the large pools of ribbon-tethered vesicles are just bystanders to synaptic transmission, with the real work of continuous release being carried out elsewhere. This issue aside, one thing that does seem reasonably clear is that the ribbon facilitates synchronous fusion of multiple synaptic vesicles, and it will also be interesting to see if this high throughput is achieved via vesicle-vesicle fusion or by coordinated exocytosis of two or more separate vesicles. Fortunately, optical tools are at hand that may soon allow ribbon researchers to settle these questions regarding the important role of the ribbon and its tethered vesicles at sensory synapses.

The next phase of the vesicle cycle, membrane retrieval, is necessary to counterbalance release from ribbon locations. Given that compensatory endocytosis has a significant impact on neuronal function, it is perhaps not surprising that synapses may use more than one mechanism of retrieval. This is also true of ribbon synapses, where compensatory endocytosis at photoreceptors, hair cells, and retinal bipolar cells seems to rely on different mixes of CME and alternative pathways. For example, the endocytotic mechanisms utilized by bipolar cells differs across species. Goldfish bipolar neurons predominately rely on bulk endocytosis to retrieve excess membrane inserted during

fusion yet we have found that mouse bipolar cells retrieve single vesicles via a clathrin-mediated pathway, not large endosomes.

Why are different endocytotic pathways utilized? Goldfish bipolar cell synapses can keep up with quantal demand using their large stock of reserve vesicles (>600,000 per terminal in goldfish bipolar cells, see von Gersdorff et al., 1996), which can be replenished using a recycling pathway that starts with bulk retrieval. Compared to goldfish bipolar cells, mouse bipolar terminals have a small volume and about 100x less synaptic vesicles. Therefore, mouse bipolar cells may require immediate resupply of new vesicles to replenish the pool of releasable vesicles. Our work also indicates that endocytosis of single vesicles occurs at locations that correlate with sites of ribbon-type active zones in mouse bipolar cells. Perhaps this local recycling is a safeguard to ensure fast refilling of the releasable pool.

Evidently, ribbon-synapses form the hub of synaptic vesicle recycling in ribbon-containing sensory and second order neurons. Furthermore, vesicle dynamics are directly influenced by the presence of synaptic ribbons, the structural hallmark of active zones in these cell types. Taken together, our work demonstrates that synaptic ribbons mark “hot spots” of vesicle exocytosis and endocytosis.

Bibliography

Allwardt, B. A., A. B. Lall, et al. (2001). "Synapse formation is arrested in retinal photoreceptors of the zebrafish nrc mutant." J Neurosci 21(7): 2330-42.

Balkema, G. W. (1991). "A synaptic antigen (B16) is localized in retinal synaptic ribbons." J Comp Neurol 312(4): 573-83.

Bech-Hansen, N. T., M. J. Naylor, et al. (1998). "Loss-of-function mutations in a calcium-channel alpha1-subunit gene in Xp11.23 cause incomplete X-linked congenital stationary night blindness." Nat Genet 19(3): 264-7.

Berglund, K., M. Midorikawa, et al. (2002). "Increase in the pool size of releasable synaptic vesicles by the activation of protein kinase C in goldfish retinal bipolar cells." J Neurosci 22(12): 4776-85.

Betz, W. J. and G. S. Bewick (1993). "Optical monitoring of transmitter release and synaptic vesicle recycling at the frog neuromuscular junction." J Physiol 460: 287-309.

Bourinet, E., P. Charnet, et al. (1994). "Voltage-dependent facilitation of a neuronal alpha 1C L-type calcium channel." Embo J 13(21): 5032-9.

Brandstatter, J. H., E. L. Fletcher, et al. (1999). "Differential expression of the presynaptic cytomatrix protein bassoon among ribbon synapses in the mammalian retina." Eur J Neurosci 11(10): 3683-93.

Brandstatter, J. H., P. Koulen, et al. (1996). "Compartmental localization of a metabotropic glutamate receptor (mGluR7): two different active sites at a retinal synapse." J Neurosci 16(15): 4749-56.

Brandstatter, J. H., P. Koulen, et al. (1997). "Selective synaptic distribution of kainate receptor subunits in the two plexiform layers of the rat retina." J Neurosci 17(23): 9298-307.

Brandt, A., D. Khimich, et al. (2005). "Few $Ca_V1.3$ channels regulate the exocytosis of a synaptic vesicle at the hair cell ribbon synapse." J Neurosci 25(50): 11577-85.

Brandt, A., J. Striessnig, et al. (2003). "$Ca_V1.3$ channels are essential for development and presynaptic activity of cochlear inner hair cells." J Neurosci 23(34): 10832-40.

Brumback, A. C., J. L. Lieber, et al. (2004). "Using FM1-43 to study neuropeptide granule dynamics and exocytosis." Methods 33(4): 287-94.

Burrone, J., G. Neves, et al. (2002). "Endogenous calcium buffers regulate fast exocytosis in the synaptic terminal of retinal bipolar cells." Neuron 33(1): 101-12.

Catterall, W. A., E. Perez-Reyes, et al. (2005). "International Union of Pharmacology. XLVIII. Nomenclature and structure-function relationships of voltage-gated calcium channels." Pharmacol Rev 57(4): 411-25.

Charnet, P., E. Bourinet, et al. (1994). "Calcium currents recorded from a neuronal alpha 1C L-type calcium channel in Xenopus oocytes." FEBS Lett 344(1): 87-90.

Chen, S. and J. S. Diamond (2002). "Synaptically released glutamate activates extrasynaptic NMDA receptors on cells in the ganglion cell layer of rat retina." J Neurosci 22(6): 2165-73.

Coggins, M. R., C. P. Grabner, et al. (2007). "Stimulated exocytosis of endosomes in goldfish retinal bipolar neurons." J Physiol 584(Pt 3): 853-65.

Cooper, N. G. and B. J. McLaughlin (1983). "Tracer uptake by photoreceptor synaptic terminals. I. Dark-mediated effects." J Ultrastruct Res 84(3): 252-67.
Deguchi-Tawarada, M., E. Inoue, et al. (2006). "Active zone protein CAST is a component of conventional and ribbon synapses in mouse retina." J Comp Neurol 495(4): 480-96.
Dick, O., S. tom Dieck, et al. (2003). "The presynaptic active zone protein bassoon is essential for photoreceptor ribbon synapse formation in the retina." Neuron 37(5): 775-86.
Edmonds, B. W., F. D. Gregory, et al. (2004). "Evidence that fast exocytosis can be predominantly mediated by vesicles not docked at active zones in frog saccular hair cells." J Physiol 560(Pt 2): 439-50.
Ertel, E. A., K. P. Campbell, et al. (2000). "Nomenclature of voltage-gated calcium channels." Neuron 25(3): 533-5.
Gaffield, M. A., S. O. Rizzoli, et al. (2006). "Mobility of synaptic vesicles in different pools in resting and stimulated frog motor nerve terminals." Neuron 51(3): 317-25.
Ghosh, K. K., S. Bujan, et al. (2004). "Types of bipolar cells in the mouse retina." J Comp Neurol 469(1): 70-82.
Ghosh, K. K., S. Haverkamp, et al. (2001). "Glutamate receptors in the rod pathway of the mammalian retina." J Neurosci 21(21): 8636-47.
Glowatzki, E. and P. A. Fuchs (2002). "Transmitter release at the hair cell ribbon synapse." Nat Neurosci 5(2): 147-54.
Granseth, B., B. Odermatt, et al. (2006). "Clathrin-mediated endocytosis is the dominant mechanism of vesicle retrieval at hippocampal synapses." Neuron 51(6): 773-86.
Gray, E. G. and H. L. Pease (1971). "On understanding the organisation of the retinal receptor synapses." Brain Res 35(1): 1-15.
Hama, K. and K. Saito (1977). "Fine structure of the afferent synapse of the hair cells in the saccular macula of the goldfish, with special reference to the anastomosing tubules." J Neurocytol 6(4): 361-73.
Harata, N., T. A. Ryan, et al. (2001). "Visualizing recycling synaptic vesicles in hippocampal neurons by FM 1-43 photoconversion." Proc Natl Acad Sci U S A 98(22): 12748-53.
Heidelberger, R. (2001). "ATP is required at an early step in compensatory endocytosis in synaptic terminals." J Neurosci 21(17): 6467-74.
Heidelberger, R., C. Heinemann, et al. (1994). "Calcium dependence of the rate of exocytosis in a synaptic terminal." Nature 371(6497): 513-5.
Heidelberger, R. and G. Matthews (1992). "Calcium influx and calcium current in single synaptic terminals of goldfish retinal bipolar neurons." J Physiol 447: 235-56.
Heidelberger, R., P. Sterling, et al. (2002). "Roles of ATP in depletion and replenishment of the releasable pool of synaptic vesicles." J Neurophysiol 88(1): 98-106.
Henkel, A. W., L. L. Simpson, et al. (1996). "Synaptic vesicle movements monitored by fluorescence recovery after photobleaching in nerve terminals stained with FM1-43." J Neurosci 16(12): 3960-7.
Henley, J. R., H. Cao, et al. (1999). "Participation of dynamin in the biogenesis of cytoplasmic vesicles." Faseb J 13 Suppl 2: S243-7.

Heuser, J. and A. M. Lennon (1973). "Morphological evidence for exocytosis of acetylcholine during formation of synaptosomes from Torpedo electric organ." J Physiol 233(1): 39P-41P.
Holt, M., A. Cooke, et al. (2004). "High mobility of vesicles supports continuous exocytosis at a ribbon synapse." Curr Biol 14(3): 173-83.
Holt, M., A. Cooke, et al. (2003). "Bulk membrane retrieval in the synaptic terminal of retinal bipolar cells." J Neurosci 23(4): 1329-39.
Hull, C., K. Studholme, et al. (2006). "Diurnal changes in exocytosis and the number of synaptic ribbons at active zones of an ON-type bipolar cell terminal." J Neurophysiol 96(4): 2025-33.
Issa, N. P. and A. J. Hudspeth (1994). "Clustering of Ca^{2+} channels and $Ca(^{2+})$-activated K^{+} channels at fluorescently labeled presynaptic active zones of hair cells." Proc Natl Acad Sci U S A 91(16): 7578-82.
Jockusch, W. J., G. J. Praefcke, et al. (2005). "Clathrin-dependent and clathrin-independent retrieval of synaptic vesicles in retinal bipolar cells." Neuron 46(6): 869-78.
Khimich, D., R. Nouvian, et al. (2005). "Hair cell synaptic ribbons are essential for synchronous auditory signalling." Nature 434(7035): 889-94.
Kollmar, R., L. G. Montgomery, et al. (1997). "Predominance of the alpha1D subunit in L-type voltage-gated Ca^{2+} channels of hair cells in the chicken's cochlea." Proc Natl Acad Sci U S A 94(26): 14883-8.
Koenig, J.H., and Ikeda, K. 1996. Synaptic vesicles have two distinct recycling pathways. J. Cell Biol. 135, 797-808.
Koschak, A., D. Reimer, et al. (2003). "Cav1.4alpha1 subunits can form slowly inactivating dihydropyridine-sensitive L-type Ca^{2+} channels lacking Ca2+-dependent inactivation." J Neurosci 23(14): 6041-9.
Lenzi, D. (2002). "Depolarization redistributes synaptic membrane and creates a gradient of vesicles on the synaptic body at a ribbon synapse." Neuron 36(4): 649-59.
Lenzi, D., J. Crum, et al. (2002). "Depolarization redistributes synaptic membrane and creates a gradient of vesicles on the synaptic body at a ribbon synapse." Neuron 36(4): 649-59.
Lenzi, D., J. W. Runyeon, et al. (1999). "Synaptic vesicle populations in saccular hair cells reconstructed by electron tomography." J Neurosci 19(1): 119-32.
Lipscombe, D., T. D. Helton, et al. (2004). "L-type calcium channels: the low down." J Neurophysiol 92(5): 2633-41.
Llobet, A., V. Beaumont, et al. (2003). "Real-time measurement of exocytosis and endocytosis using interference of light." Neuron 40(6): 1075-86.
Llobet, A., A. Cooke, et al. (2003). "Exocytosis at the ribbon synapse of retinal bipolar cells studied in patches of presynaptic membrane." J Neurosci 23(7): 2706-14.
LoGiudice, L., D. Henry, et al. (2006). "Identification of calcium channel alpha1 subunit mRNA expressed in retinal bipolar neurons." Mol Vis 12: 184-9.
LoGiudice, L. and G. Matthews (2007). "Endocytosis at ribbon synapses." Traffic 8(9): 1123-8.
LoGiudice, L., P. Sterling, et al. (2008). "Mobility and turnover of vesicles at the synaptic ribbon." J Neurosci 28(12): 3150-8.

LoGiudice, L. and G. Matthews (2009). "The Role of Ribbons at Sensory Synapses." Neuroscientist.
Macia, E., M. Ehrlich, et al. (2006). "Dynasore, a cell-permeable inhibitor of dynamin." Dev Cell 10(6): 839-50.
Magupalli, V. G., K. Schwarz, et al. (2008). "Multiple RIBEYE-RIBEYE interactions create a dynamic scaffold for the formation of synaptic ribbons." J Neurosci 28(32): 7954-67.
Martinez-Dunst, C., R. L. Michaels, et al. (1997). "Release sites and calcium channels in hair cells of the chick's cochlea." J Neurosci 17(23): 9133-44.
Matsubara, A., J. H. Laake, et al. (1996). "Organization of AMPA receptor subunits at a glutamate synapse: a quantitative immunogold analysis of hair cell synapses in the rat organ of Corti." J Neurosci 16(14): 4457-67.
Matsui, K., J. Hasegawa, et al. (2001). "Modulation of excitatory synaptic transmission by GABA(C) receptor-mediated feedback in the mouse inner retina." J Neurophysiol 86(5): 2285-98.
Matthews, G. and P. Sterling (2008). "Evidence that vesicles undergo compound fusion on the synaptic ribbon." J Neurosci 28(21): 5403-11.
McRory, J. E., J. Hamid, et al. (2004). "The CACNA1F gene encodes an L-type calcium channel with unique biophysical properties and tissue distribution." J Neurosci 24(7): 1707-18.
Meinertzhagen, I. A. (1996). "Ultrastructure and quantification of synapses in the insect nervous system." J Neurosci Methods 69(1): 59-73.
Meister, A. and M. E. Anderson (1983). "Glutathione." Annu Rev Biochem 52: 711-60.
Mennerick, S. and G. Matthews (1996). "Ultrafast exocytosis elicited by calcium current in synaptic terminals of retinal bipolar neurons." Neuron 17(6): 1241-9.
Mennerick, S. and G. Matthews (1998). "Rapid calcium-current kinetics in synaptic terminals of goldfish retinal bipolar neurons." Vis Neurosci 15(6): 1051-6.
Midorikawa, M., Y. Tsukamoto, et al. (2007). "Different roles of ribbon-associated and ribbon-free active zones in retinal bipolar cells." Nat Neurosci 10(10): 1268-76.
Minami, N., K. Berglund, et al. (1998). "Potentiation of transmitter release by protein kinase C in goldfish retinal bipolar cells." J Physiol 512 (Pt 1): 219-25.
Morgans, C. W. (1999). "Calcium channel heterogeneity among cone photoreceptors in the tree shrew retina." Eur J Neurosci 11(8): 2989-93.
Morigiwa, K. and N. Vardi (1999). "Differential expression of ionotropic glutamate receptor subunits in the outer retina." J Comp Neurol 405(2): 173-84.
Moser, T., A. Brandt, et al. (2006). "Hair cell ribbon synapses." Cell Tissue Res 326(2): 347-59.
Muresan, V., A. Lyass, et al. (1999). "The kinesin motor KIF3A is a component of the presynaptic ribbon in vertebrate photoreceptors." J Neurosci 19(3): 1027-37.
Neef, A., D. Khimich, et al. (2007). "Probing the mechanism of exocytosis at the hair cell ribbon synapse." J Neurosci 27(47): 12933-44.
Newton, A. J., T. Kirchhausen, et al. (2006). "Inhibition of dynamin completely blocks compensatory synaptic vesicle endocytosis." Proc Natl Acad Sci U S A 103(47): 17955-60.
Nguyen, T. H. and G. W. Balkema (1999). "Antigenic epitopes of the photoreceptor synaptic ribbon." J Comp Neurol 413(2): 209-18.

Nordstrom, K., T. A. Larsson, et al. (2004). "Extensive duplications of phototransduction genes in early vertebrate evolution correlate with block (chromosome) duplications." Genomics 83(5): 852-72.
Paillart, C., J. Li, et al. (2003). "Endocytosis and vesicle recycling at a ribbon synapse." J Neurosci 23(10): 4092-9.
Parsons, T. D. and P. Sterling (2003). "Synaptic ribbon. Conveyor belt or safety belt?" Neuron 37(3): 379-82.
Platzer, J., J. Engel, et al. (2000). "Congenital deafness and sinoatrial node dysfunction in mice lacking class D L-type Ca^{2+} channels." Cell 102(1): 89-97.
Prokop, A. and I. A. Meinertzhagen (2006). "Development and structure of synaptic contacts in Drosophila." Semin Cell Dev Biol 17(1): 20-30.
Qin, P. and R. G. Pourcho (1999). "Localization of AMPA-selective glutamate receptor subunits in the cat retina: a light- and electron-microscopic study." Vis Neurosci 16(1): 169-77.
Rao-Mirotznik, R., A. B. Harkins, et al. (1995). "Mammalian rod terminal: architecture of a binary synapse." Neuron 14(3): 561-9.
Rea, R., J. Li, et al. (2004). "Streamlined synaptic vesicle cycle in cone photoreceptor terminals." Neuron 41(5): 755-66.
Richards, D. A., C. Guatimosim, et al. (2000). "Two endocytic recycling routes selectively fill two vesicle pools in frog motor nerve terminals." Neuron 27(3): 551-9.
Roberts, W. M., R. A. Jacobs, et al. (1990). "Colocalization of ion channels involved in frequency selectivity and synaptic transmission at presynaptic active zones of hair cells." J Neurosci 10(11): 3664-84.
Roos, J. and R. B. Kelly (1999). "The endocytic machinery in nerve terminals surrounds sites of exocytosis." Curr Biol 9(23): 1411-4.
Schmitz, F., A. Konigstorfer, et al. (2000). "RIBEYE, a component of synaptic ribbons: a protein's journey through evolution provides insight into synaptic ribbon function." Neuron 28(3): 857-72.
Sherry, D. M. and R. Heidelberger (2005). "Distribution of proteins associated with synaptic vesicle endocytosis in the mouse and goldfish retina." J Comp Neurol 484(4): 440-57.
Shupliakov, O., P. Low, et al. (1997). "Synaptic vesicle endocytosis impaired by disruption of dynamin-SH3 domain interactions." Science 276(5310): 259-63.
Sidi, S., E. Busch-Nentwich, et al. (2004). "gemini encodes a zebrafish L-type calcium channel that localizes at sensory hair cell ribbon synapses." J Neurosci 24(17): 4213-23.
Singer, J. H. and J. S. Diamond (2006). "Vesicle depletion and synaptic depression at a mammalian ribbon synapse." J Neurophysiol 95(5): 3191-8.
Singer, J. H., L. Lassova, et al. (2004). "Coordinated multivesicular release at a mammalian ribbon synapse." Nat Neurosci 7(8): 826-33.
Spassova, M. A., M. Avissar, et al. (2004). "Evidence that rapid vesicle replenishment of the synaptic ribbon mediates recovery from short-term adaptation at the hair cell afferent synapse." J Assoc Res Otolaryngol 5(4): 376-90.
Sterling, P. and G. Matthews (2005). "Structure and function of ribbon synapses." Trends Neurosci 28(1): 20-9.

Strom, T. M., G. Nyakatura, et al. (1998). "An L-type calcium-channel gene mutated in incomplete X-linked congenital stationary night blindness." Nat Genet 19(3): 260-3.
Sweitzer, S. M. and J. E. Hinshaw (1998). "Dynamin undergoes a GTP-dependent conformational change causing vesiculation." Cell 93(6): 1021-9.
Takei, K., V. Haucke, et al. (1998). "Generation of coated intermediates of clathrin-mediated endocytosis on protein-free liposomes." Cell 94(1): 131-41.
Takei, K., O. Mundigl, et al. (1996). "The synaptic vesicle cycle: a single vesicle budding step involving clathrin and dynamin." J Cell Biol 133(6): 1237-50.
Teng, H., J. C. Cole, et al. (1999). "Endocytic active zones: hot spots for endocytosis in vertebrate neuromuscular terminals." J Neurosci 19(12): 4855-66.
Teng, H. and R. S. Wilkinson (2000). "Clathrin-mediated endocytosis near active zones in snake motor boutons." J Neurosci 20(21): 7986-93.
Thoreson, W. B., K. Rabl, et al. (2004). "A highly Ca2+-sensitive pool of vesicles contributes to linearity at the rod photoreceptor ribbon synapse." Neuron 42(4): 595-605.
tom Dieck, S., W. D. Altrock, et al. (2005). "Molecular dissection of the photoreceptor ribbon synapse: physical interaction of Bassoon and RIBEYE is essential for the assembly of the ribbon complex." J Cell Biol 168(5): 825-36.
Tsukamoto, Y., K. Morigiwa, et al. (2001). "Microcircuits for night vision in mouse retina." J Neurosci 21(21): 8616-23.
Ullrich, B. and T. C. Sudhof (1994). "Distribution of synaptic markers in the retina: implications for synaptic vesicle traffic in ribbon synapses." J Physiol Paris 88(4): 249-57.
Van Epps, H. A., M. Hayashi, et al. (2004). "The zebrafish nrc mutant reveals a role for the polyphosphoinositide phosphatase synaptojanin 1 in cone photoreceptor ribbon anchoring." J Neurosci 24(40): 8641-50.
von Gersdorff, H. and G. Matthews (1996). "Calcium-dependent inactivation of calcium current in synaptic terminals of retinal bipolar neurons." J Neurosci 16(1): 115-22.
von Gersdorff, H., E. Vardi, et al. (1996). "Evidence that vesicles on the synaptic ribbon of retinal bipolar neurons can be rapidly released." Neuron 16(6): 1221-7.
Von Kriegstein, K., F. Schmitz, et al. (1999). "Distribution of synaptic vesicle proteins in the mammalian retina identifies obligatory and facultative components of ribbon synapses." Eur J Neurosci 11(4): 1335-48.
Wan, Q. F., A. Vila, et al. (2008). "Synaptic vesicle dynamics in mouse rod bipolar cells." Vis Neurosci 25(4): 523-33.
Xu, J., B. McNeil, et al. (2008). "GTP-independent rapid and slow endocytosis at a central synapse." Nat Neurosci 11(1): 45-53.
Xu, W. and D. Lipscombe (2001). "Neuronal Ca(V)1.3alpha(1) L-type channels activate at relatively hyperpolarized membrane potentials and are incompletely inhibited by dihydropyridines." J Neurosci 21(16): 5944-51.
Zanazzi, G. and G. Matthews (2009). "The molecular architecture of ribbon presynaptic terminals." Mol Neurobiol 39(2): 130-48.
Zenisek, D. (2008). "Vesicle association and exocytosis at ribbon and extraribbon sites in retinal bipolar cell presynaptic terminals." Proc Natl Acad Sci U S A 105(12): 4922-7.

Zenisek, D., V. Davila, et al. (2003). "Imaging calcium entry sites and ribbon structures in two presynaptic cells." J Neurosci 23(7): 2538-48.
Zenisek, D., N. K. Horst, et al. (2004). "Visualizing synaptic ribbons in the living cell." J Neurosci 24(44): 9752-9.
Zenisek, D. and G. Matthews (1998). "Calcium action potentials in retinal bipolar neurons." Vis Neurosci 15(1): 69-75.
Zenisek, D., J. A. Steyer, et al. (2000). "Transport, capture and exocytosis of single synaptic vesicles at active zones." Nature 406(6798): 849-54.
Zhang, J. and J. S. Diamond (2006). "Distinct perisynaptic and synaptic localization of NMDA and AMPA receptors on ganglion cells in rat retina." J Comp Neurol 498(6): 810-20.
Zhang, J. F., A. D. Randall, et al. (1993). "Distinctive pharmacology and kinetics of cloned neuronal Ca2+ channels and their possible counterparts in mammalian CNS neurons." Neuropharmacology 32(11): 1075-88.
Zhou, C. and R. F. Dacheux (2004). "All amacrine cells in the rabbit retina possess AMPA-, NMDA-, GABA-, and glycine-activated currents." Vis Neurosci 21(2): 181-8.
Zhou, Z. Y., Q. F. Wan, et al. (2006). "Capacitance measurements in the mouse rod bipolar cell identify a pool of releasable synaptic vesicles." J Neurophysiol 96(5): 2539-48.